ISSN number 0971 - 9709

The Journal of Indian Geophysical Union

VOLUME 22, ISSUE 4 I JULY 2018

AN OPEN ACCESS BIMONTHLY JOURNAL OF IGU

EDITORIAL OFFICE

Indian Geophysical Union, NGRI Campus, Uppal Road, Hyderabad- 500 007
Telephone: +91 -40-27012799; 27012734; Telefax:+91-04-27171564
E. mail: jigu1963@gmail.com, website: www.j-igu.in

The Open Access Journal with six issues in a year publishes articles covering
Solid Earth Geosciences; Marine Geosciences; and Atmospheric, Space and Planetary Sciences.

Annual Subscription

Individual ₹ 1000 per issue and Institutional ₹ 5000 for six issues

Payments should be sent by DD drawn in favour of "The Treasurer, Indian Geophysical Union", payable at Hyderabad, Money Transfer/NEFT/RTGS (Inter-Bank Transfer), Treasurer, Indian Geophysical Union, State Bank of India, Habsiguda Branch, Habsiguda, Uppal Road, Hyderabad- 500 007
A/C: 52191021424, IFSC Code: SBIN0020087, MICR Code: 500002318, SWIFT Code: SBININBBHO9.

For correspondence, please contact, Hon. Secretary, Indian Geophysical Union, NGRI Campus, Uppal Road, Hyderabad - 500 007, India; Email: igu123@gmail.com; Ph: 040 27012799, 272012734

ISSN: 0257-7968 (Clarivate Analytics)
ISSN: 0971-9709 (NISCAIR)
Approved as bimonthly ESCI journal by Clarivate Analytics
Cited in Indian Citation Index (ICI), New Delhi
Evaluated by NISCAIR, New Delhi

CONTENTS

Editorial

The Journal of Indian Geophysical Union (JIGU) is a multidisciplinary geoscientific journal, published bi-monthly by Indian Geohysical Union since 1997. Dr. P.R. Reddy has been associated with this journal since its inception and nurtured this journal as his own baby. He took utmost care in converting the journal from quarterly to bi-monthly and insured publication on time. He was ably supported by a team of learned editorial members. With his continued efforts, it is envisaged that the journal may get the SCI accreditation soon. As per Clarivate Analytics, the JIGU is covered in the Emerging Sources Citation Index, which means all articles published in the journal are indexed in Web of Science at the time of publication. The journal is full-fledged cited by Indian Citation Index. Since Dr. Reddy wished to be relieved, I formally took the charge as the Chief Editor of JIGU from April, 2018. I consider it a great honour and therefore like to express my sincere gratitude to the IGU Executive Council for reposing faith in me. I am sure, with the active support of IGU and fellow geoscientists, the journal would be able to play a major role in disseminating rapidly growing inter-disciplinary scientific information to earth scientific community, in a shortest possible time.

I am fully aware that the editorship comes with lots of responsibilities, like dealing different set of authors and their writings and publishing them on time after peer reviews. Our first job therefore is to inculcate a new culture of editing and peer review process that would require balance between a well written paper and its technical contents. I believe, responsible reviews can provide significant information and input to improve the quality of papers, thus choice of finding appropriate reviewers becomes critical,specially so, when our journal receives a good number of articles from young researchers from the universities and research institutes.

Therefore, to facilitate this process, I have attempted to reconstitute the editorial board, by accommodating as much as possible, some well-known researchers having scientific background in diversified disciplines. This would help to discharge my duties as an editor, towards the author, as well as the readers of the journal, which will ultimately shape the future of this journal. Basically, I have been a bench researcher myself, working on the diversified topics in geosciences and allied fields for almost 47 years. So, I am fully aware about the intricacies involved in bringing out quality publication of international standard. Only time will tell how far I succeeded in this endeavour. We plan to introduce soon a new tutorial section on specified topics, written by the invited experts. The current issue contains 10 research papers and hopefully, readers would like them. Suggestions to improve the journal are always welcome.

O.P. Pandey
Chief Editor

J. Ind. Geophys. Union (July 2018)
v.22, no.4, pp: 371-378

On robust estimation of derivative of noisy dataset: Application on temperature gradient of ocean water column

Indrajit G. Roy
Spaceage Geoconsulting, 5 Bick Place, Banks, ACT 2906, Australia
Email: spaceage.geocon@gmail.com

ABSTRACT
We propose a simple technique of robust estimation of first order derivative of a discrete set of noisy measurements. The proposed technique uses conventional numerical tools, such as the first order finite difference and the natural cubic spline on evenly spaced noisy dataset and provides robust estimation of the first order derivative. We also propose simple techniques in estimating noise level in the measured data. This allows designing the estimated derivative dependent on the noise level in the measured data. We conducted numerical experiments using the proposed technique on synthetic data contaminated with random noise. Results from numerical experiment demonstrate applicability of the technique to the data contaminated with a moderate level of noise. We validate the proposed technique in estimating the temperature gradient of a water column from a set of noisy measurements of temperature versus depth at the northern Gulf of Mexico.

Key words: Finite difference, Cubic spline, Robust, Derivative

INTRODUCTION

Derivative analysis often becomes an essential exercise in various disciplines of earth sciences. The difficulty, one often faces, is lack in robustness in estimating derivative due to the presence of noise in the measured data. To circumvent such difficulty there, in fact, are many numerical methods which claim not only to provide improving precision (Lyness and Molar, 1967; Lele, 1992; Qu, 1996; Shirashi et al., 2007), but also to provide the robustness in the estimating derivative (Anderssen and Bloomfeld, 1974; Cullum, 1971; Wei and Hon, 2005; Chartrand, 2011; Roy, 2015, 2017). Majority of those schemes, as mentioned in the cited literature, have been presented excellently with a full mathematical rigor, but unfortunately such presentations are inconsequential for the researchers, who are not strongly mathematically inclined. On the other hand, a large section of researchers, widely across many scientific fields, are comfortable with the use of a simple difference equation, and the interpolation technique while estimating derivative. The major motivation of the present work is to reduce the communication gap between an excellent theoretician and an avid practitioner in understanding the issue of computational instability in derivative estimation and to provide the necessary remedial measure.

We demonstrate, in this paper, that an appropriate use of a difference equation and selection of an appropriate interpolation technique could be the only two simple elements required in the robust estimation of evenly spaced (mild to moderate level) noisy data. We also demonstrate how the ordeal that an unassuming researcher often faces while estimating the derivative of evenly spaced measured data, using a simple difference scheme. We conducted numerical tests using the proposed scheme on noise contaminated synthetic data in order to demonstrate the applicability of the scheme in estimating derivative of a set of evenly spaced noisy measurements. We next apply the proposed technique in delineating temperature gradient of an ocean water column from northern Gulf of Mexico.

THEORETICAL BACKGROUND

In an exercise of estimating derivative the premise that we rely on is that the measured data is actually the sample values of a continuous and regular function which is continuously differentiable. Suppose that $f(x)$, defined within an interval $[a,b]$, is one such function such that within a small neighborhood around x the function $f(x)$ can be, decomposed via Taylor series, written as

$$f(x+h) = f(x) + hf^{(1)}(x) + \frac{h^2}{2!}f^{(2)}(x) + \frac{h^3}{3!}f^{(3)}(x) + \cdots, \quad (1)$$

$$f(x-h) = f(x) - hf^{(1)}(x) + \frac{h^2}{2!}f^{(2)}(x) - \frac{h^3}{3!}f^{(3)}(x) + \cdots, \quad (2)$$

where h is a small perturbation in x, $f^{(1)}$, $f^{(2)}$ and $f^{(3)}$ are the first, second and the third order derivatives of the function $f(x)$ respectively. Using equations (1) and (2) following three difference schemes can be designed to estimate the first order derivative $f^{(1)}$.

Forward difference (I):

$$f^{(1)} = D_h^F[f(x)] = \frac{f(x+h) - f(x)}{h} + O(h) \quad (3)$$

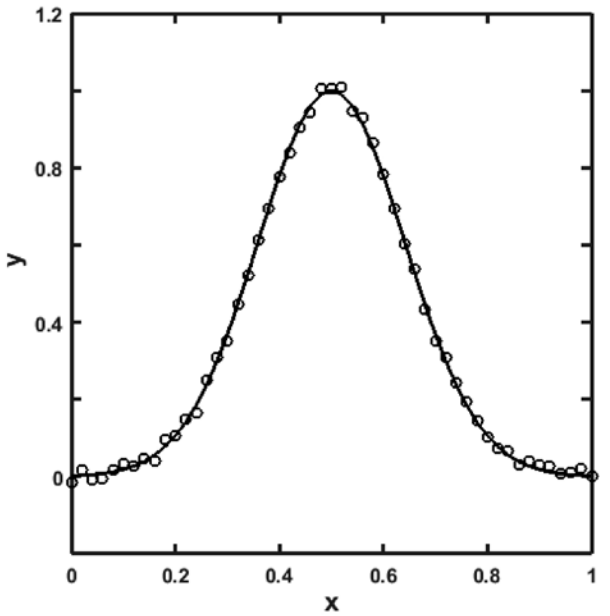

Figure 1. Plot of synthetic response (solid line) and the 2% (uniform deviate) random noise contaminated data (open circle). Sampling interval is 0.02.

Backward difference (II):

$$f^{(1)} = D_h^B\left[f(x)\right] = \frac{f(x) - f(x-h)}{h} + O(h) \tag{4}$$

Central difference (III):

$$f^{(1)} = D_h^C\left[f(x)\right] = \frac{f(x+h) - f(x-h)}{2h} + O(h^2), \tag{5}$$

where the symbol 'Big O' in the right hand side of the above three schemes indicates that the error in the precision of estimating derivative is proportional to either h or h^2; D_h^F, D_h^B and D_h^C denote the forward, backward and central difference operator respectively. If h is small, say a fraction lies between 0 and 1, then the approximation error for the central difference scheme is much smaller compared to the other two schemes, as stated. Note that these are not the only difference schemes in estimating the first order derivatives. There are higher order schemes as well, which offer even much smaller approximation error. One would be tempted enough, in the light of equations (3) to (5), to carrying out measurements as closely as possible; or in other words, maintaining a small data interval, in order to achieve a high level of accuracy in estimating derivative. One would even argue that the smaller the sampling interval in the measurements, larger will be the frequency bandwidth in the measured signal, and hence one should expect a better outcome in estimating derivative of finely sampled data. Such an expectation remains achievable if the set of measurements is completely noise free. Situation, however, changes dramatically the moment a small amount of random noise is incorporated in the measured data. To elucidate it, suppose that the true sampled data $f(x_i)$; $i=1,2,\ldots,n$ contain random noise $e(x_i)$ with the noise amplitude (in terms of r.m.s value) δ during measurement. Denote the noise contaminated data as $f^\delta(x_i)$ which is equal to $f(x_i) + e(x_i)$, where $e(x_i)$ corresponds to the noise part. The index i denotes the i-th instance. Any of the difference operators, as mentioned above, can be used to estimate the derivative. Suppose that the operator D_h^C is used in estimating derivative. Then

$$D_h^C\left[f^\delta(x)\right] = D_h^C\left[f(x) + e(x)\right] = D_h^C\left[f(x)\right] + D_h^C\left[e(x)\right] \tag{6}$$

On what follows, the error in estimating the derivative is now the sum of two components; one is the loss of precision due to the choice of difference operator, which is often termed as consistency error and the other is due to the noise part, commonly called as perturbation error. The noise in data can be realized as wiggles overlain the otherwise smooth data and, supposedly, describe a bounded variation. In the light of equations (3) – (5) the consistency error can be expressed as a non-decreasing function $\varphi(h)$, such that $0 = \varphi(0) < \varphi(h)$ (Lu and Pereverzev, 2006). The perturbation error which arises due to the noise part is, however, proportional to δ/h. Therefore, as the data interval h is becoming small the approximation error due to the loss of precision falls off, but the perturbation error increases in a faster rate. To visualize the effect we give a numerical example, considering a bell-shaped function $\exp[-(x-\mu)^2/2\sigma^2]$, with $\mu=0.5$ and $\sigma=0.02$, defined within an interval $[0,1]$. The analytical expression of the first order derivative of the bell-shaped (or Gaussian) function is given as $-(x-\mu)^2/2\sigma^2 \exp[-(x-\mu)^2/2\sigma^2]$. The bell-shaped function is digitized with different sampling intervals,

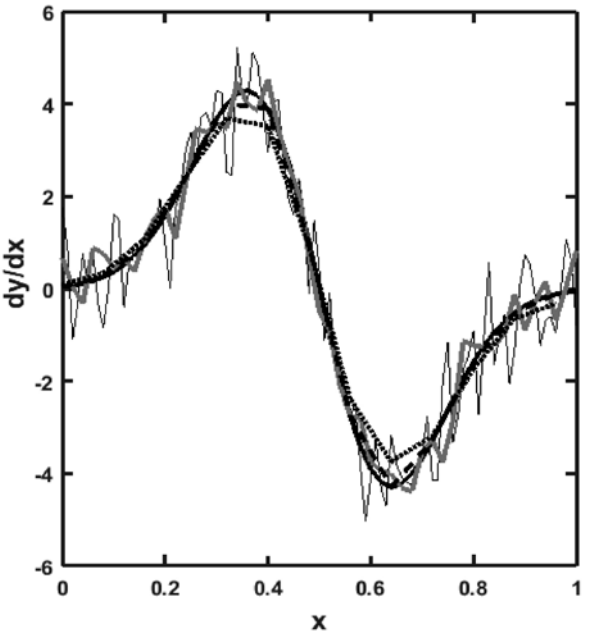

Figure 2. Plot of the analytical first order derivative (thick solid line) of synthetic response (Figure 1) and the estimated ones using finite difference schemes for various sampling intervals 0.01 (thin black solid line), 0.02 (thick gray solid line), 0.03 (thick black broken line) and 0.04 (black dotted line).

such as 0.01, 0.02, 0.03 and 0.04, and the digitized data are contaminated with uniformly distributed random noise with a standard deviation (*s*) of 0.02. However, for the sake of clarity only the noise contaminated data (open circle) corresponding to the sampling interval 0.02 and the theoretical response (solid line) and are presented in Figure 1. The figure clearly depicts a realistic situation of measured noisy data. The estimated first order derivative using the difference schemes (I and II for the end points and III for all other points) and the analytical response of derivatives corresponding to three different sampling intervals, as mentioned in the foregoing text, are presented in Figure 2. Consideration of the central difference scheme, except at the end points, for derivative estimation is prompted by the fact that it provides an accurate estimation of derivative than the forward and the backward difference method as truncation error falls of in the power of 2 with respect to the data interval. Note that with the decreasing sample interval, especially at 0.01, the error due to noise component dominates substantially.

However, noise exaggeration is not significant corresponding to the relatively coarse sampling interval (0.04). On the other hand, loss of precision due to coarsening becomes prominent. Results from the numerical experiment with noise contaminated synthetic data corresponding to four distinct sampling intervals clearly suggest that the instability issue in the derivative estimation using a difference scheme can be addressed by increasing the sampling interval or in other words by coarsening the grid while discarding some of the measured data. If such a coarsening can be controlled using the noise level in data (Groetsch, 1991; Ramm and Smirnova, 2001; Lu and Pereverzev, 2006) then a sense of regularization is implied in estimating derivative.

Groetsch (1991) establishes that the regularization in derivative estimation using forward and backward difference schemes is possible if the data spacing h is proportional to $\sqrt{\delta}$. Ramm and Smirnova (2001) suggest that the sampling interval h should be proportional to δ^{γ}, where $0<\gamma<1$ in order to ensure regularization in a difference scheme to estimate the first order derivative. Lu and Pereverzev (2006), however, propose a strategy in determining an optimal data spacing in the finite difference based derivative estimation, which is somewhat complicated and computationally involving. According to Lu and Pereverzev (2006) an optimal data spacing, say h_*, would be the one which satisfies following condition

Condition: Suppose that $\{h_j\}$ for all $j=1,2...$ is a sequence of spacings of a difference grid. A spacing h_* would be an optimal spacing if it is the maximum of all h_j in the sequence so that the discrepancy between the estimated derivative (using any difference scheme) corresponding to h_j and all other estimated derivative previous to the j-th one must be less than or (at least) equal to $2a_l\,\delta(1/h_j+1/h_i)$ for $i=1,2,...,j$, where a_l is the absolute sum of the coefficients of an l-th order difference equation, such as $a_l=\sum_{j=-l}^{l}|c_j|$. For example, with the first order difference scheme $l=1$, and the coefficients are c_{-1},c_0,c_1.

However, Hanke and Scherzer (2001) argue against regularizing computational regime by means of a coarse

discretisation with a view point that discarding data in a grid, in fact, causes loss of information. They also point out that the finite difference approximation essentially renders to the use of piecewise linear or constant functions. They propose to take the route of determining a smoothing function which satisfies the constraint of minimization of an error function, defined in terms of Lagrange's multiplier (or regularization parameter) λ, and is given as.

$$S[f]=\frac{1}{n-1}\sum_{i=1}^{n}\left(f^{\delta}(x_i)-f(x_i)\right)^2+\lambda\left(\int_0^1\left[f^{(2)}(x)\right]^2 dx\right) \quad (7)$$

Once an optimally smoothed function is obtained the robust derivative can be estimated readily. Note that the function which satisfies equation (7) is nothing but a smoothing spline. However, Hanke and Scherzer (2001) demonstrate that as long as the sampling interval $h>\sqrt{\delta/f^{(2)}}$, where $f^{(2)}$ denotes the second order derivative of a smooth and continuously differentiable function, the error bound obtained by a finite difference method and that of the method of the smoothing spline is same. In addition, they also demonstrate that the smoothing functional, thus obtained, satisfying the constraint equation, is actually a natural cubic spline over the grid of sampling points.

PROPOSED METHOD

In the light of the aforementioned discussion in the earlier section we propose in the following a simple methodology for robust estimation of the first order derivative, given a set of discrete measurements. Instead of providing a garb of mathematical treatment we give a sequential algorithmic pattern (or a work flow).

Work flow

Get the evenly spaced measured data in a grid Δ with a known sampling interval h.

Get an a priori estimate of the noise level δ in the measured data.

Piecewise interpolate the measured data using a spline interpolator.

Get the interpolated value at the grid points x_j separated with a grid interval $h_*=c\sqrt{\delta}$, where $c\in(0,1]$. The suffix j is used to denote the node corresponding to the new 'coarse' difference grid.

Piecewise interpolate the interpolated values corresponding to the new grid points x_j to the original data grid points.

Compute derivative using a difference schemes (I and II for end points) and III (for all other points).

Natural spline interpolation

A spline interpolator is actually the major tool of the proposed algorithm in estimating derivative via difference scheme for noisy data. Note that smoothness or regularity is the ultimate attribute of a continuous function to control the wild oscillations what we, generally, observe in estimating derivative of a noisy data. A spline interpolator, which is essentially a piecewise polynomial function demonstrates both the local and the global properties. Locally such a function satisfies every data points while globally, it maintains the regularity condition. A natural cubic spline which possesses the property of continuous second order derivative is widely used spline interpolator and is readily available as a software tool or subroutine function in publicly available open access software, such as Python, Octave, Julia or as a Fortran and C libraries.

Noise estimation

An a priori knowledge of the noise level in the noise contaminated data is an essential element of the proposed algorithm. Having an a priori knowledge of the noise level in data, in many occasions, especially in earth sciences, is a non-trivial task. This is because, in many occasions, one is forced to have a single set of measurements and hence statistical methods, as available, in the standard text book on statistics, are not applicable in estimating the noise variance in data. For the sake of ease, let us assume that the contaminated noise in data is random and stationary in nature, which means that the noise variance remains fixed for the entire data set. Such assumption, by and large, acceptable in general, although the author agrees that a comprehensive knowledge of noise characteristics requires more elaborate studies. We propose a simple approach in estimating the noise level in a single set of measured data, although such approach does not guarantee providing a precise estimate of the noise level. Presence of random noise causes wiggles in otherwise smooth curve. The smoothest part of a curve is the portion of the curve attaining saturation or becoming flat. In the portion of flat or low slope region the signal-to-noise ratio (SNR) will be very small causing the noise component more prominent. This is the major rationale behind choosing such portion of the curve. The estimated noise variance corresponding to the homogeneous (or nearly homogeneous) regions would lead to estimate the noise level in the data. Following two strategies are proposed:

Strategy I:

Plot the measured data in X-Y frame and identify the flat or nearly flat portion(s) where the plotted curve would attain saturations. One may use any generic spreadsheet (including open access) software to plot and select a portion of data which corresponds to a nearly flat (or low slope) part of the curve.

If the selected portion of the data is suspected to be reasonably flat then the mean of the selected data would

approximately approaches the true value. If the selected data are normalized and the noise, as perceived, is random in nature then the estimated mean would approach the zero value. The estimated variance would then suggest the noise level in data.

If several flat regions in the plotted data are identified then the aforementioned procedure should be continued separately and the average of all estimated noise variance is considered as the best estimated noise variance.

Strategy II:

If flat or nearly flat region of the plotted data is not identified then choose the portion of the data which seems to be monotonic and corresponds to have mild to moderate slope. Note that the number of data points of the selected region should be at least more than 7 in order to get a reasonable accuracy in the estimation.

Choose a median window of size 3 or 5 and do median filtering by sliding the window every data point and replacing it with the median value. The choice of window size is somewhat ad-hoc, but the guiding principle in selecting an appropriate window size should depend on the noise level in data. The small widow-size works well for data with a low noise level. If the noise level in data is high, a bigger window may be required. For 1D data with the geophysical anomaly the size of the window of a median filter between 3 and 5 is sufficient. The median filter is a sliding window technique where the center of the window should correspond to the data point. The rationale in considering median filter is that it is robust in handling occasional large excursion of data within the selected patch effectively.

We, however, suggest using iterated median filtering on the selected portion of the data set. The pseudo-codes are given below:

Algorithm on iterated median filtering

Set: $\mathbf{d}^{\text{old}} = \mathbf{d}^{\delta}$

Compute: $\mathbf{d}^{\text{new}}$ = medianfilter ($\mathbf{d}^{\text{old}}$)

Do until: $\sum_{i=1}^{ns} |d_i^{\text{old}} - d_i^{\text{new}}| / ns \leq \epsilon$, a threshold value $\epsilon \sim 10^{-3}$

Set: $\mathbf{d}^{\text{old}} = \mathbf{d}^{\text{new}}$

Compute: $\mathbf{d}^{\text{new}}$ = medianfilter ($\mathbf{d}^{\text{old}}$)

End Do

Estimate: $\delta \sim \|\mathbf{d}^{\delta} - \mathbf{d}^{\text{new}}\|_{L_2}$.

NUMERICAL TESTS

Synthetic data

We conducted numerical experiment to validate the proposed technique of robust estimation of derivative of noisy set of data. For that, we considered synthetically generated data using bell-shaped function. The evenly spaced data ranging within the interval [0,1] are the discrete values of bell-shaped function contaminated with random noise with standard deviation 0.02 are presented in Figure 1. The sampling interval of the digitized data is 0.02. We first attempted to estimate the noise level d in data in order to validate the noise estimation algorithm. The value of the estimated noise level using the Strategy-I for selected data at the left flank of the curve (Figure 3) turns out to be 0.0171, a slight underestimation. The value of the estimated noise level using the Strategy-II on the selected data at the right flank of the curve is 0.0295, a slight overestimation. The average estimated noise level turns out to be 0.0233. The noisy data are piecewise interpolated using natural cubic spline interpolator. We then selected the grid interval $h_*(=c\sqrt{\delta})$ as 0.1202 which corresponds to a set of new spline knots (as presented by large bullets in Figure 3). The knot values are computed using the spline parameters which are already estimated during piecewise interpolation. We then spline fit the estimated data corresponding to the coarse grid interval h_* and get the interpolated data values at the original sampling interval. This gives a smooth estimate of the noisy data. The interpolated curve (solid line) is shown in Figure 3.

To estimate the first order derivative we then used the finite difference schemes, I, II (for the end points) and III (for all other points) corresponding to the original sampling grid. The estimated first order derivative using the proposed algorithm and the synthetic response of the first order derivative are shown in Figure 4.

The estimated mean squared error is given as 0.03267, which suggests a sufficiently robust estimation of the first order derivative of data contaminated with random noise.

Validation of the method: an example of ocean temperature profile from Gulf of Mexico

The variation of temperature within a column of ocean water plays significant roles in climate research, meteorology and ocean circulation both locally and globally (Helland-Hansen, 1930; Munk, 1966; Stewart, 2008; Williams et al., 2010; Hieronymous et al., 2014). The robust estimate of vertical gradient of temperature depth profile is a key in understanding the movement of water parcel (Stewart, 2008), analyzing the variability of meridional gradient with depth (Roden, 1979), and in making an account of change in temperature due to vertical movement of density surface (Bindoff and McDougall, 1994, Yaremchuk et al., 2001).

We implement the proposed algorithm in estimating the temperature gradient from measured temperature versus depth profile. We chose temperature profile data of a water column at the northern Gulf of Mexico, which is publicly available by US National Ocean and Atmospheric Administration (NOAA). Forrest et al. (2005) compiled and processed 70,000 measurements of mean annual temperature versus depth from 3495 profiles taking an

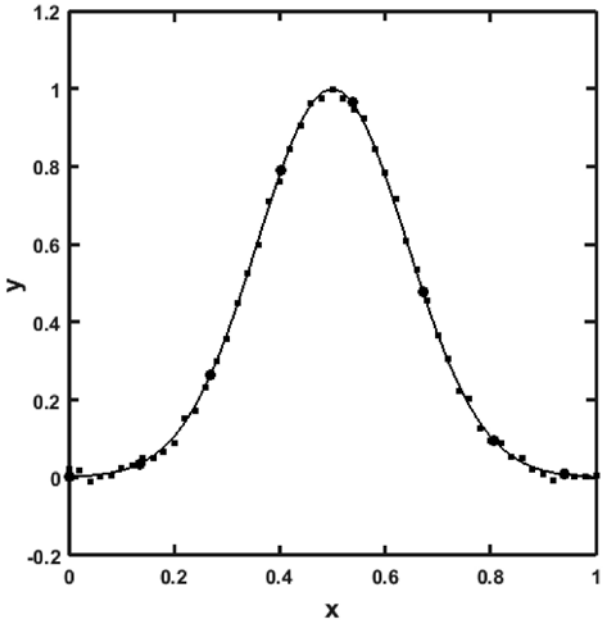

Figure 3. Plot of evenly spaced noisy data values (small bullet), interpolated values correspond to coarse grid (large bullet) and final interpolated curve (solid line).

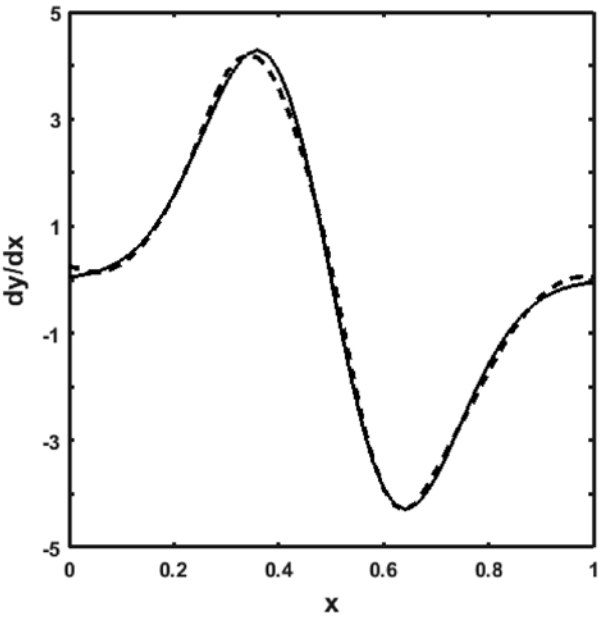

Figure 4. Plot of the estimated first order derivative using the proposed algorithm (solid line) and the synthetic response of the first order derivative (broken line).

average from near to ocean surface up to the depth of 5000 feet with a depth interval of 100 ft. We redraw the Figure 3 of Forrest et al., (2005) and digitized it. The original temperature versus depth data are in the units of degree Fahrenheit and foot. We first converted the data into degree Celsius and meter.

The water temperature versus depth profile clearly suggests monotonous decrease in temperature. However, beyond the depth of 1200 meter of the water column such decrease slows down and the curve almost reaches to a flat homogeneous region. We considered a small data sample from the homogeneous region and used the Strategy-I in estimating the noise level in the data. The estimated value of the noise level in data turns out to be 0.0283. We also used Strategy-II in the noise estimation as well. The estimated value of the noise level using Strategy-II is

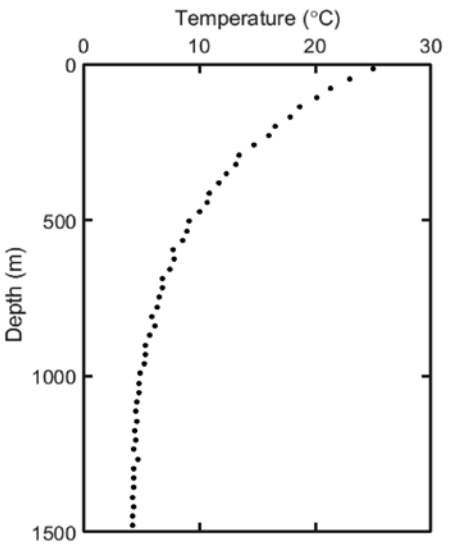

Figure 5. Temperature versus depth profile of a water column form the northern Gulf of Mexico, U.S.A.

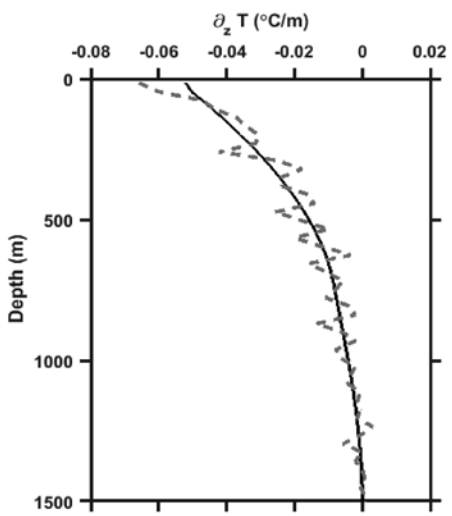

Figure 6. Estimated temperature gradient versus depth plot using the proposed (solid line) and the finite difference (gray broken line) scheme on the original data.

0.0274. The average of these two values is 0.02785. The first order derivative which is the temperature gradient $(\partial_z T)$ with depth estimated by the proposed scheme (solid line) and the one estimated using the standard procedure (the finite difference scheme as mentioned in the paper) on the original noisy data (broken line) are presented in Figure 6.

Note that even when the discrete data set contains a moderate level of noise the conventional difference scheme in estimating the first order derivative lacks in robustness. On the other hand, the proposed technique demonstrates sufficient robustness in estimating the first order derivative of a set of evenly spaced noisy measurements. The temperature gradient steadily increases up to a depth of 650 m and attains a plateau there after.

CONCLUSIONS

The estimation of the first order derivative of a set of measurements is an important exercise to be carried out almost routinely in every field of science including geosciences. A simple technique for robust estimation of derivative of noisy evenly spaced measured data is proposed. The proposed technique which is based on the conventional first order finite difference scheme and cubic spline interpolation technique, demonstrates sufficient robustness in estimating the first order derivative of random noise contaminated synthetic data. A simple strategy (with a workflow) of making an approximate estimate of the noise level in data is discussed. The applicability of

the method in estimating the temperature gradient, using temperature versus depth profile data from the northern Gulf of Mexico, is also demonstrated. Most importantly, the proposed technique is so simple that a limited knowledge on numerical methods and an access to the public domain software, such as Python, Octave and Julia is suffice to implement it without much difficulty.

ACKNOWLEDGEMENT

The author gratefully acknowledges the reviewer, Dr. Simanchal Padhy, for illuminating review which helps significantly in improving the manuscript. The current research is supported by Spaceage Geoconsulting, a research oriented consulting firm.

Compliance with Ethical Standards

The author declares that he has no conflict of interest and adheres to copyright norms.

REFERENCES

Anderssen, R.S. and Bloomfield, P., 1974. A time series approach to numerical differentiation, Technometrics, 16, 69-75.

Bindoff, N.L. and McDougall, T.J., 1994. Diagnosing climate change and ocean ventilation using hydrographic data, J. Phy. Ocean., 24, 1137-1152.

Chartrand, R., 2011. Numerical differentiation of noisy non-smooth data, ISRN Appl. Math., Article ID: 164564, DOI: 10.5402/2011/164564.

Cullum, J., 1971. Numerical differentiation and regularization, SIAM J. Num. Anal., 8, 254-265.

Forrest, J., Marcucci, E. and Scott, P., 2005. Geothermal gradients and subsurface temperatures in northern Gulf of Mexico, Trans. GCAGS, 55, 233-248.

Groetsch, C.W., 1991. Differentiation of approximately specified functions. Am. Math. Mon., 98, 847-850.

Hanke, M. and Scherzer, O., 2001. Inverse problems light: Numerical differentiation, Am. Math. Mon., 108, 512-521.

Helland-Hansen, B., 1930. Physical oceanography and meteorology: Results of the Michael Sars North Atlantic Deep-Sea Expedition, 1910, Bergen Museum.

Hieronymous, M., Nilsson, J. and Nycander, J., 2014. Water-mass transformation in salinity-temperature space, J. Phys. Ocean., 44, 2547-2568.

Lele, S., 1992. Compact finite difference schemes with spectral like resolution, J. Comp. Phys., 103, 16-42.

Lu, S. and Pereverzev, S.V., 2006. Numerical differentiation from a viewpoint of regularization theory, Math. Comp., 75, 1853-1870.

Lyness, J.N. and Moler, C.B., 1967. Numerical differentiation of analytic functions, SIAM J. Num. Anal., 4, 202-210.

Munk, W.H., 1966. Abyssal recipes, Deep-Sea Res. Oceanogr. Abstr., 13, 707-730, DOI: 10.1016/0011-7471(66)90602-4.

Qu, R., 1996. A new approach to numerical differentiation and integration. Math. Comp. Modl., 24, 55-68.

Ramm, A.G. and Smirnova, A.B., 2001. On stable numerical differentiation, Math. Comp., 70, 1131-1153.

Roden, G.I., 1979. The depth variability of meridional gradients of temperature, salinity and sound velocity in the Western North Pacific, J. Phys. Ocean., 9, 756-767.

Roy, I.G., 2015. On computing first and second order derivative spectra, J. Comp. Phys., 295, 307-321.

Roy, I.G., 2017. Interpreting potential field anomaly of an isolated source of regular geometry revisited. Geophysics, 82 (5), IM41-IM48.

Stewart, R.H., 2008. Introduction to physical oceanography, Open text book downloaded from https://open.umn.edu/opentextbooks/BookDetail.aspx?bookId=20.

Wei, T. and Hon, Y.C., 2005. Numerical derivatives from one-dimensional scattered noisy data. J. Phys. Conf. Ser., 12, 171-179.

Williams, P.D., Guiliardi, E., Madec, G., Gualdi, S. and Scoccimarro, E., 2010. The role of mean ocean salinity on climate, Dyn. Atmos. Oceans., 49, 108-123.

Yaremchuk, M., Bindoff, N.L., Schroter, J., Nechaev, D. and Rintoul, S.R., 2001. On the zonal and meridional circulation and ocean transports between Tasmania and Antactica, J. Geophy, Res., 106, 2795-2814.

Received on: 18.2.18; Revised on: 30.4.18; Accepted on: 1.5.18

J. Ind. Geophys. Union (July 2018)
v.22, no.4, pp: 379-388

Geophysical investigation for base metal mineralization in Karoi-Rajpura area, Bhilwara district, Rajasthan

D.C. Naskar*[1], A.V. Kulkarni[2], and M. Lakshmana[1]

*[1] Southern Region, Geological Survey of India, Bandlaguda, Hyderabad-500068
[2] Central Region, Geological Survey of India, Seminary Hills, Nagpur-440006
*Corresponding Author: dcnaskar@yahoo.com

ABSTRACT

Today, there is a challenge before geoscientists to discover new mineral deposits by an exploration technique, which should have low risk, consume less time and also cost effective. Towards reaching this goal, Geophysical methods with the phenomenal improvement in the design and development of equipment, methods and precision of data acquisition, processing and interpretation, play an indispensable role. A combination of SP, IP, Resistivity and Magnetic methods was attempted in Karoi-Rajpura area of Bhilwara District of Rajasthan for locating base metal occurrence. The integrated interpretation of the geophysical response of the different geophysical methods, revealed more precise information about the subsurface configuration and mineral distribution in the prospect area. Strong geophysical anomalies were observed in the northern, southern, central and eastern parts of the study area. The low resistivity zones (200 Ohm-m) and high chargeability zones (>24 mV/V) are situated in the southern and eastern parts of the investigated area. However, to strengthen the reliability of the results, the resistivity map is compared with chargeability map; those who have intersection area between low resistivity and high chargeability (> 24 mV/V), are considered to be the prospective zones of base metal mineralization. However, these low resistivity zones may have been influenced by the presence of clay or weathered soil. In this case, the high chargeability zones will help in confirming the prospective zones caused by base metal mineralization. Recent deep drilling by Hindustan Zinc Limited (HZL) in this area has intersected rich ore lodes, thereby confirming depth wise continuity of ore zones at some places.

Key words: Aravalli craton, Bhilwara Super Group, Polymetallic sulphide belt, Rajpura-Dariba Group.

INTRODUCTION

Rajasthan is endowed with a continuous geological sequence of rocks from the oldest Archaeans represented by Bhilwara Super Group (Bundelkhand gneiss and the banded gneissic complex) to sub-recent, that are exposed chiefly in the central plains, existing between the Aravalli and Vindhyan range (Yadav and Avadich, 2010). The sedimentary rock includes the rocks of Aravalli Super Group, Delhi Super Group and Upper Vindhyan Super Group. The south-eastern extremity of the state is occupied by a pile of basaltic flows of Deccan traps. Several mineral deposits of economic importance occur in association with the above rock units. In Rajasthan, the base metal mineralization is found to be confined to the three successive geological time domains, which are identified as the three geo-synclinal basins namely, Bhilwara basin, Aravalli basin and Delhi basin (Ametha and Sharma, 2008). The area exhibits three phases of deformation, giving rise to complicated structural geometry to the lithology and mineralized zones. The rocks exposed in the study area shows surface indication of mineralization in the form of malachite staining and presence of primary copper minerals. Old workings in South Rajasthan (Bhilwara district) by M/S Hindustan Zinc Ltd. (HZL) include:

Aravalli Supergroup Udaipur Group	Zawar lead-zinc belt.
Bhilwara Supergroup Rajpura Group	Rajpura-Dariba-Bethumni belt. Pur-Banera lead-zinc-copper belt.

Base-metal potential recognition criteria in study area is based on knowledge-driven and data-driven Fuzzy models for predictive mineral potential mapping (Porwal et al., 2003a) as well as tectonostratigraphy and base-metal mineralization controls (Porwal et al., 2006b). These findings prompted to conduct geophysical survey in small patch e.g. Karoi-Rajpura area, Bhilwara district to assess the mineralization. Integrated geophysical surveys comprising Self Potential (SP), Induced Polarization (IP) cum resistivity and magnetic surveys have been carried out in Karoi-Rajpura area, Bhilwara district, Rajasthan for delineating the mineralized zones (Figure 1).

GEOLOGY OF THE STUDY AREA

The NE-SW trending Proterozoic Pur-Banera metasedimentary belt in south-east Rajasthan is metallogenetically important. The Karoi-Rajpura area forms a part of the Pur-Banera belt in Bhilwara district, Rajasthan. Regionally, the Karoi-Rajpura area forms a

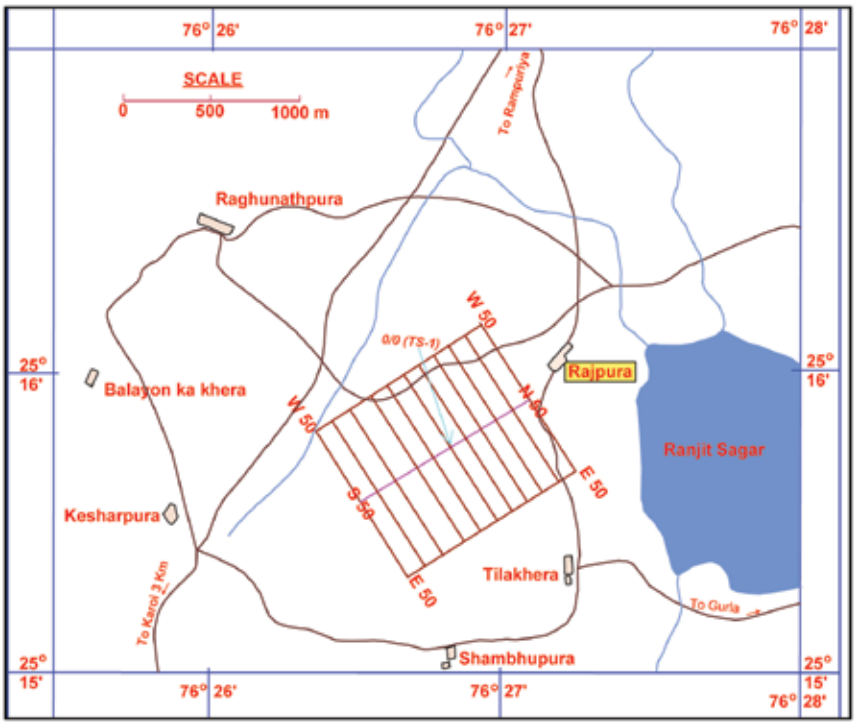

Figure 1. Location Map of the Karoi-Rajpura area, Bhilwara Districts, Rajasthan. 0/0 indicates traverse 1 (TS-1).

part of the western limb of the Pur-Syncline and all the rocks of the area have a generalized NE-SW to NNE-SSW trend (Fig. 2). The main rock types exposed in the area belong to Mangalwar Complex of Bhilwara Supergroup and metasediments of Pur-Banera Group. The rocks of Mangalwar Complex are represented by biotite + garnet + staurolite + kyanite schist along with arenaceous and amphibolite bands. Schist, quartzite, conglomerate, calc-silicate and metavolcanic represent the rocks of Pur-Banera Group. Profuse malachite staining and primary chalcopyrite, pyrrhotites are observed in the western part of the area. Sulphide mineralization has been observed at several locations and the host rock for the mineralization is mostly calc-silicate dolomite and graphite mica schist of Rajpura-Dariba Group (Ametha and Sharma, 2008; Haldar, 2001; Haldar and Deb, 2001). The lead-zinc mineralization occurs in the form of galena and sphalarite (Mishra, 2000). Structures associated with mineralization such as folds, faults, veins and shear zones highlight the importance of a changing history of brittle and ductile deformation for economic mineralization. The Dariba-Rajpura part of the area show very narrow basin elongated for a strike length of 3 km. In this part, the mineralized loads are concentrated along two faults. These two faults are parallel to each other and the regional strike of the area, thus almost N-S. Among two faults, eastern fault has accumulated metals to form a load called east load. In the western fault there are two loads, named north load and south load. It is very clear that the mineralization is faulting controlled (Nawal, 2017). Stratigraphy of the study area (Gandhi, 2001) is given below:

Intrusive	Quartz vein Granite
Rajpura-Dariba Group	*Upper Unit:* Interbanded quartzite and mica-schist/ash bed/ tuffaceous mica-schist/graphite mica-schist. *Middle Unit:* Limonitised graphite mica-schist, silicified/ gossanised ferruginous chert breccia. Garnetiferous-magnetite quartzite. Graphite±garnet±staurolite±kyanite±a ndalusite, mica-schist, micaceous cherty dolomite, acid-basic volcanics, tuffaceous/ carbonaceous/mica-schist. *Lower Unit:* Marble, amphibolite, metamarl, quartzite and conglomerate.
Unconformity	
Mangalwar Complex	Migmatites Gneisses and schist.

MINERALIZATION

India has a geological and metallogenic history similar to the mineral-rich shield areas of Antarctica, Australia, South Africa and South America. Its geological domains are well endowed with mineral resources; however, they are yet to

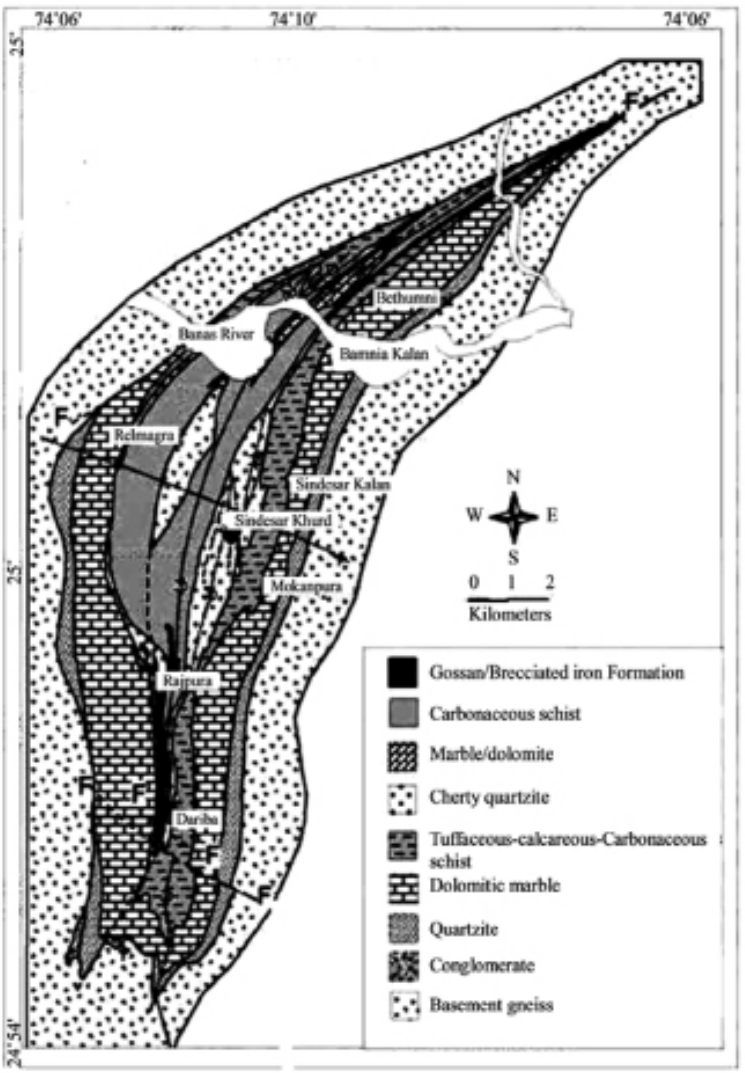

Figure 2. Geological map of the study area (after Ametha et al., 1999).

be fully explored, assessed and exploited. Interestingly, the Proterozoic Aravalli-Delhi orogenic complex hosts a large number of economically important strata bound base metal sulphide deposits. Rock samples taken from Outcrop and Underground mines of Sindeskar Kalan, Vedanta Group, Rajpura-Dariba-Bethumni Belt have been petrographicaly by Juned Alam et al., (2015). The chief litho-units of the group which were identified contain sulfide-bearing calc-silicate and graphite mica schist, dolomite marble, calc-biotite schist and quartzite. Important ore minerals like galena and sphalerite, which have been reported in association with the buffer minerals like pyrite and pyrrhotite, occurred in these host rocks (Juned Alam and Farhat Nasim Siddiquie, 2015). Keeping in mind the importance of mineral exploration, geophysical surveys employing SP, magnetic (VF) and IP cum resistivity, were carried out in the study area for delineating sulphide mineralization.

Geophysical Instruments and Survey Layout

The IP unit used in the present survey consists of an 8 HP petrol engine generator, 3 KW transmitters (TSQ-3) and IPR-10A receiver of Scintrex make. The SP measurements were made using NGRI, India, make digital potentiometer. A vertical field conventional Fluxgate Magnetometer was used for magnetic survey. Sensitivity of potentiometer used for SP survey was ± 1 mV, for magnetometer was 10 nT and for IP receiver was ±0.5 mV/V.

Geophysical surveys were carried out with base line trending in N60°E direction. A total of 11 regular traverses (N50, N40……S50), each 1000 m in length were laid orthogonal to base line at 100 m interval and 20 m station interval. All the observations were taken in 100 m X 20 m grid pattern. The unit of distance was kept 10 m for traverses as well as for stations also.

RESULTS AND DISCUSSION

Results of geophysical surveys comprising SP, magnetic, IP chargeability and resistivity methods have been presented in the form of contour maps to identify the significant anomaly zones, which might reveal mineralization. Structures associated with mineralization such as folds, faults, fissures and shear zones highlight the importance of a changing history of brittle and ductile deformation for economic mineralization. The Dariba-Rajpura part of the area show very narrow basin elongated for a strike length of 3 km. In this part, the mineralized loads are concentrated along two faults, which are parallel to each other and the regional strike of the area, thus run almost N-S. Among the two faults, eastern fault has accumulated metals to form a load called east load. In the western fault, there are two loads named north load and south load. Thus it is very clear that the mineralization in this area is fault controlled (Nawal, 2017).

Self Potential (SP) survey

This method makes use of small currents which are naturally produced beneath the Earth's surface. SP method is mainly used for exploration of massive sulphide ore bodies, finding leaks in canal embankments, defining zones and plumes of contaminants, etc. The data in the study area has been presented in the form of contour map as shown in Figure 3. SP value in the surveyed area varies from + 20 to – 50 mV. The map has indicated SP low anomaly zone of about 100 m width, bounded by – 10 mV contour trending in E-W direction. The highest magnitude of SP anomaly is about – 15 mV. This anomaly extends from '0' (traverse 1; TS-1) in the north to traverse S10 in south as indicated in the contour map. The dimension of anomaly zone is about 100 m X 100 m. Another SP low anomaly zone of about 200 m width, bounded by – 5 mV contour trending in N-S direction has the peak anomaly of – 10 mV. This anomaly extends from N15/E40 in the north to traverse S10 in the south. The dimension of this anomaly zone is 200 m X 200 m. The continuous E-W trending SP anomaly zone in the north-east corner beyond north of traverse N40 is indicative of litho contact in the surveyed area.

Magnetic (VF) survey

In the present study area, the magnetic base was chosen at a non-magnetic point and the magnetic observations were taken in 100 m X 20 m grid pattern. All the magnetic data were processed with respect to base and results are shown Figure 4. The magnetic value varies from – 300 nT to + 700 nT in the area. The magnetic survey has delineated few isolated magnetic high anomaly zones of the order of about 500 nT in the north-west part of the area. In this zone, there are five isolated peaks of the order of 650 nT that may be due to the presence of some ferruginous magnetic material. High magnetic responses observed in western part compared to eastern part may be due to the lithological contacts in the area apart from picking up a few dipolar-nature anomalies. These high amplitude dipolar anomalies suggest either emplacement of basic bodies along some fault planes, or the faults/fractures, along which concentration of magnetite is a natural phenomenon.

Induced Polarization (IP) survey

IP survey was carried out in the area using dipole-dipole array with a = 20 m and n = 3, where 'a' is array spacing and 'n' is represented by separation parameter between the current and potential electrode pair (Kearey et al., 2003). Dipole-dipole array was used in the field measurement by considering that even though it has low vertical resolution, it is very sensitive to deeper lateral variations, making it suitable for deeper sounding (Reynolds, 1997). Chargeability and resistivity values were measured at an interval of 20 m. The results of IP chargeability have been presented as a contour map (Figure 5), which revealed four anomaly zones that are favorable for mineralization, as discussed below. These anomaly zones are trending almost in N-S and NE-SW directions. The peak magnitude in these fair anomaly zones is varying from 20-28 mV/V. The chargeability anomaly zones may be due to base metal sulphide mineralization.

Zone-I: This zone is reflected by an anomaly having a peak magnitude of 28 mV/V over background of 14 mV/V. This anomaly zone is trending almost in a NE-SW direction and is occurring between traverses S15 in north and S45 in the south. The extent of this anomaly zone is about 200 m and width is about 50 m (between E5 and E10). This zone has indicated two isolated anomalies of 2 to 6 mV/V near station E5 on traverse S20, and E10 on traverse S40 respectively.

Zone-II: This zone is trending almost in a NE-SW direction having peak magnitude 20 mV/V over a background of 14 mV/V, which is localized in nature near station E35 on traverse '0' (TS-1). The background contour 14 mV/V extends over wider area and is open towards north and is still continuing as reflected from contour map. The extent of this anomaly zone is about 150 m. This zone is also supported by the occurrence of SP anomaly.

Zone-III: This zone is characterized by an anomaly of the order 20 mV/V over a 14 mV/V background. This zone is trending almost in a NE-SW direction and is occurring between traverses N50 in the north and N40 in the south.

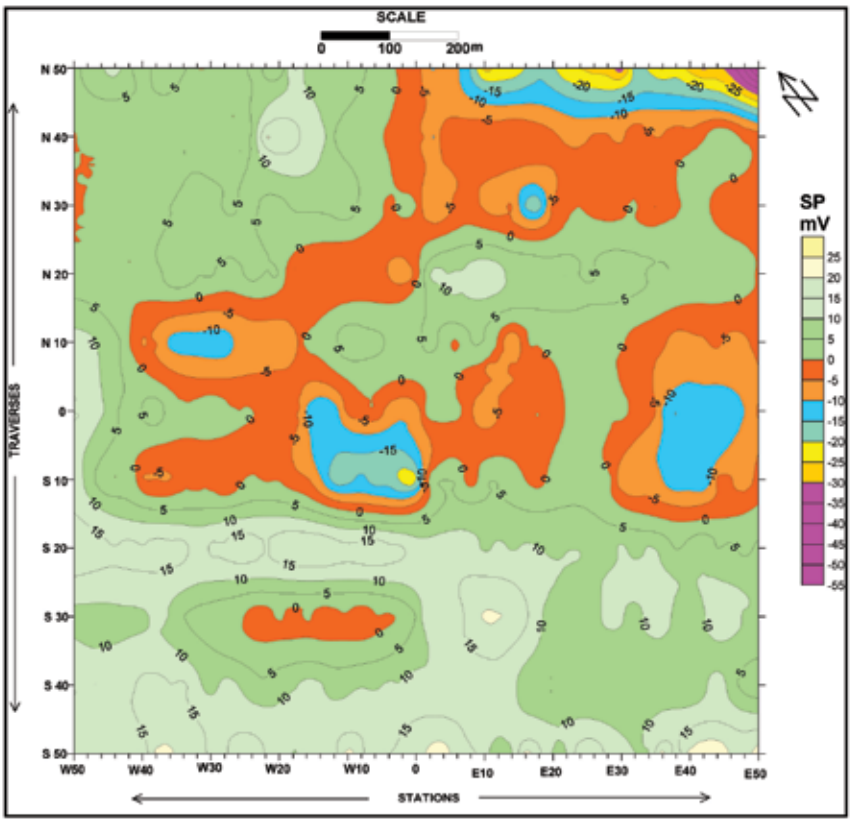

Figure 3. SP contour map of Karoi-Rajpura area, Bhilwara district, Rajasthan. '0' indicates traverse 1 (TS-1).

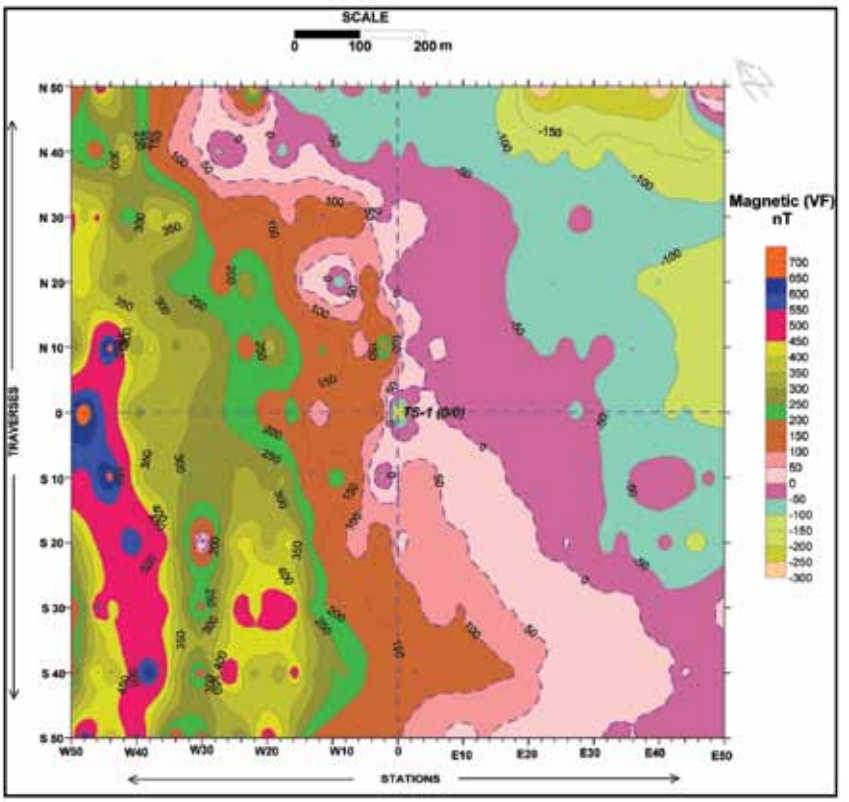

Figure 4. Magnetic (VF) contour map of Karoi-Rajpura area, Bhilwara district, Rajasthan.

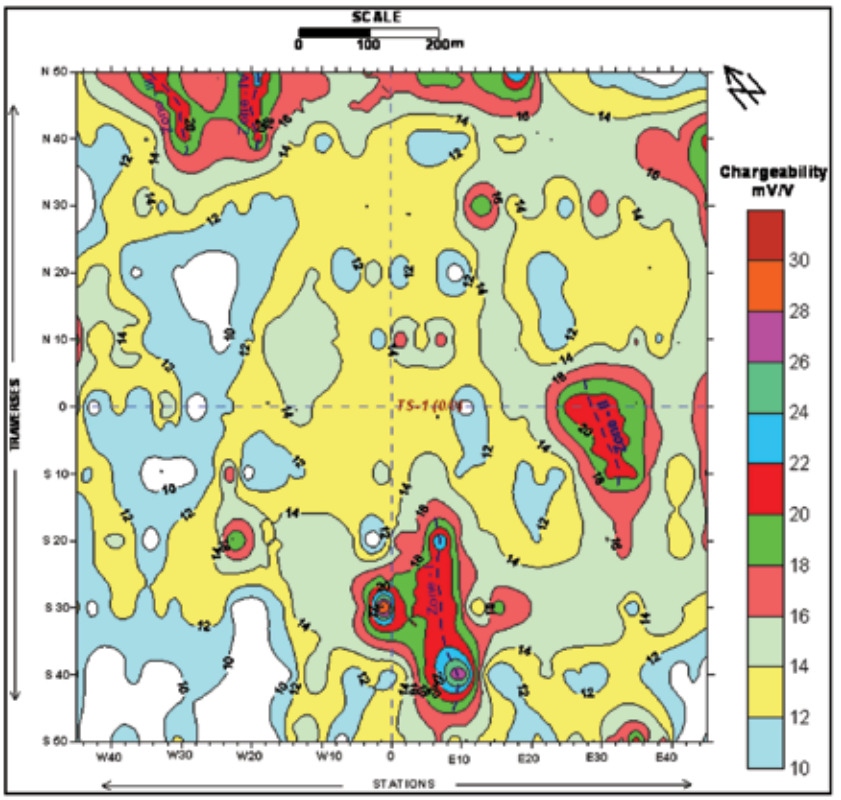

Figure 5. Chargeability contour map (a=20m & n=3) of Karoi-Rajpura area, Bhilwara district, Rajasthan.

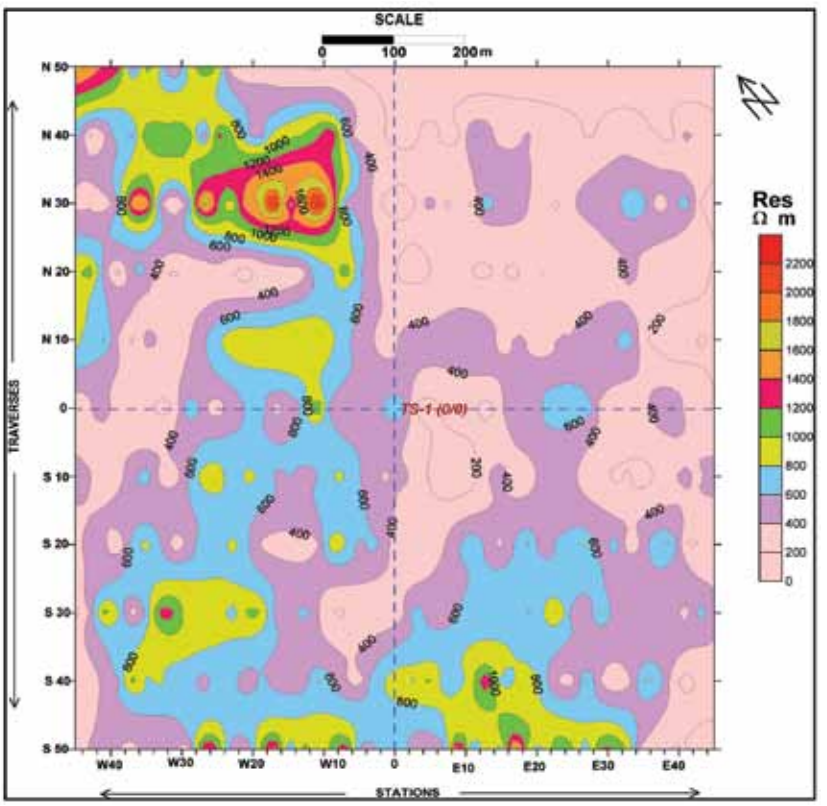

Figure 6. Resistivity contour map (a=20m and n=3) of Karoi-Rajpura area, Bhilwara district, Rajasthan.

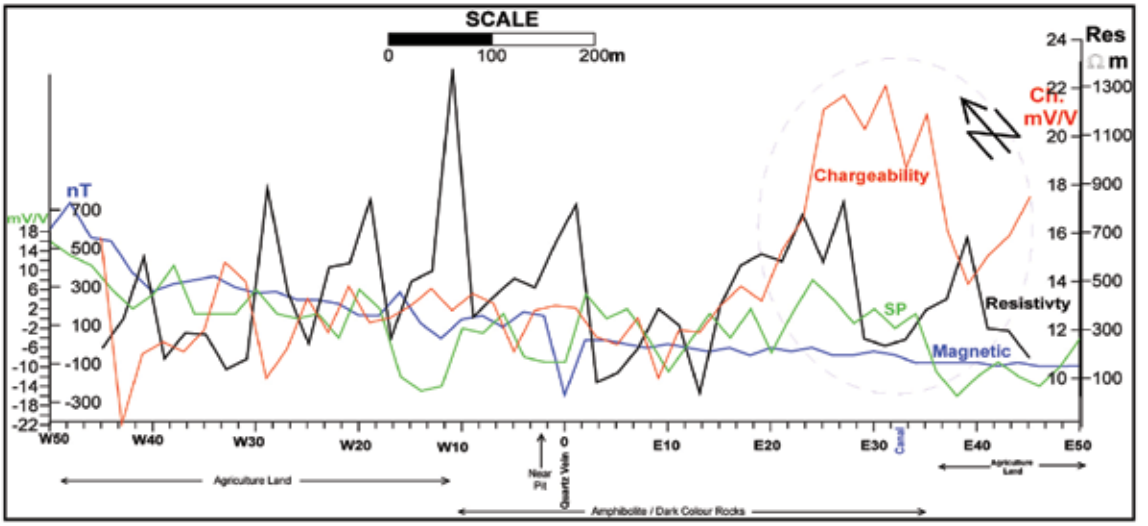

Figure 7a. SP, magnetic, IP cum resistivity profiles along traverse '0' (TS-1) of Karoi-Rajpura area, Bhilwara district, Rajasthan.

The extent of this anomaly zone is about 100 m and width about 40 m (between W35 and W30).

Zone-IV: This zone is characterized by an anomaly of the order 20 mV/V over a 14 mV/V background and is trending almost in a N-S direction. This zone is occurring between traverses N50 in north and N40 in the south like in Zone-III. The extent of this anomaly zone is about 100 m and width is about 50 m (between stations W25 and W30). The continuous high chargeability value between stations W10 to E25 of traverses N45 and N50 corroborated with low SP trend has been recorded in the surveyed area.

Resistivity survey

The result of resistivity survey has been presented in the form of a contour map (Figure 6). Almost throughout the map, resistivity values range between 200 and 400 Ohm-m, which is considerably low from overall perspective. This feature may be attributed to the presence of base metal mineralization and/or clay matrix or rocks with low bulk resistivity. The rocks with mineralization content are interpreted to have resistivity < 600 Ohm-m. However, to strengthen the reliability of the results, the resistivity sections are compared with chargeability sections, those who have intersection area between low resistivity and high chargeability (> 24 mV/V) are considered to be the prospective zones of mineralization. The low resistivity closure in the central and eastern portion of the surveyed area is corroborated with high chargeability zone. These zones may strongly correlate to the presence of base metal mineralization. These low resistivity zones may have been influenced by the presence of clay or weathered soil. In this case, the high chargeability zones will help in confirming the prospective zones caused by sulphide mineralization. However, several isolated zone of high resistivity of the order of 800 Ohm-m have been picked on traverse S50. This anomaly may be due to presence of hard rock in subsurface.

Representative profile

Representative anomaly profiles 0 (Figure 7a), N50 (Figure 7b), S30 (Figure 7c) and S40 (Figure 7d) are presented in order to quick look of described anomalous zones in the study area.

Representative anomaly profile '0' (traverse-1; TS-1) has been shown for easy comprehension. High chargeability value of magnitude 22 mV/V is corroborated with low resistivity value (300 Ohm-m) with a flat magnetic response at station E30 (Figure 7a). Another geophysical anomaly having low SP of – 16 mV, is well corroborated with high chargeability (18 mV/V) and low resistivity (200 Ohm-m) along with high magnetic response (300 nT) at station W32.

Representative anomaly profile 'N50' has shown high chargeability value of 30 mV/V (Fig. 7b) is associated with low resistivity, flat magnetic response and high SP values around station -60 (60 m towards west from center). Another high chargeability value of 25 mV/v is observed around station 200 (200 m towards east from center) which is associated with low resistivity, low magnetic and low SP values. In between station, -60 to 200 moderate chargeability values have been observed. High amplitude magnetic response is observed around station -220, (220 m towards west from center) which is, associated with high chargeability values (22 mV/V).

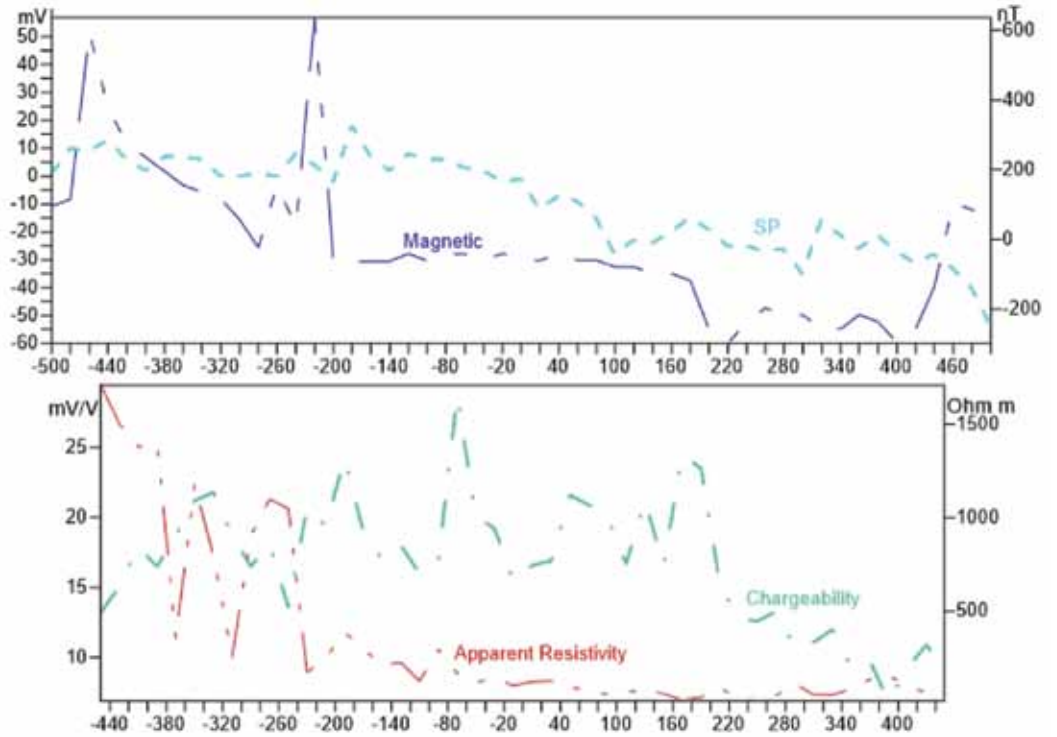

Figure 7b. SP, magnetic, IP cum resistivity profiles along traverse N50 of Karoi-Rajpura area, Bhilwara district, Rajasthan.

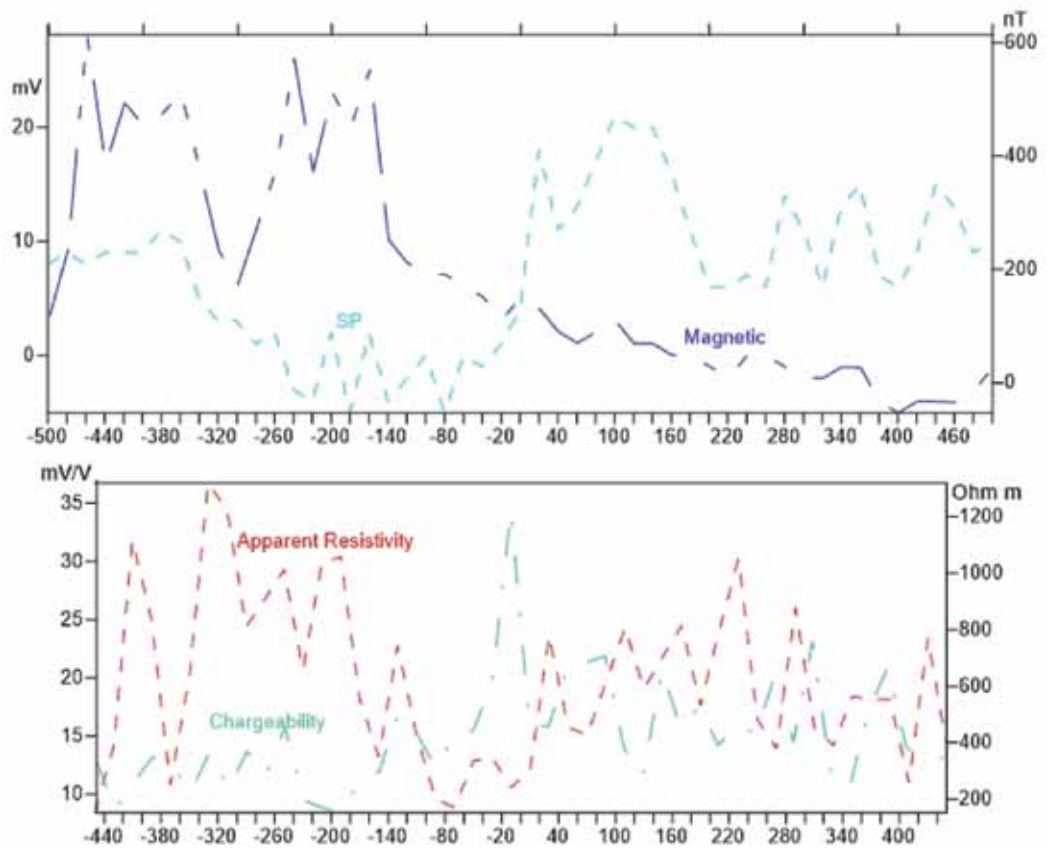

Figure 7c. SP, magnetic, IP cum resistivity profiles along traverse S30 of Karoi-Rajpura area, Bhilwara district, Rajasthan.

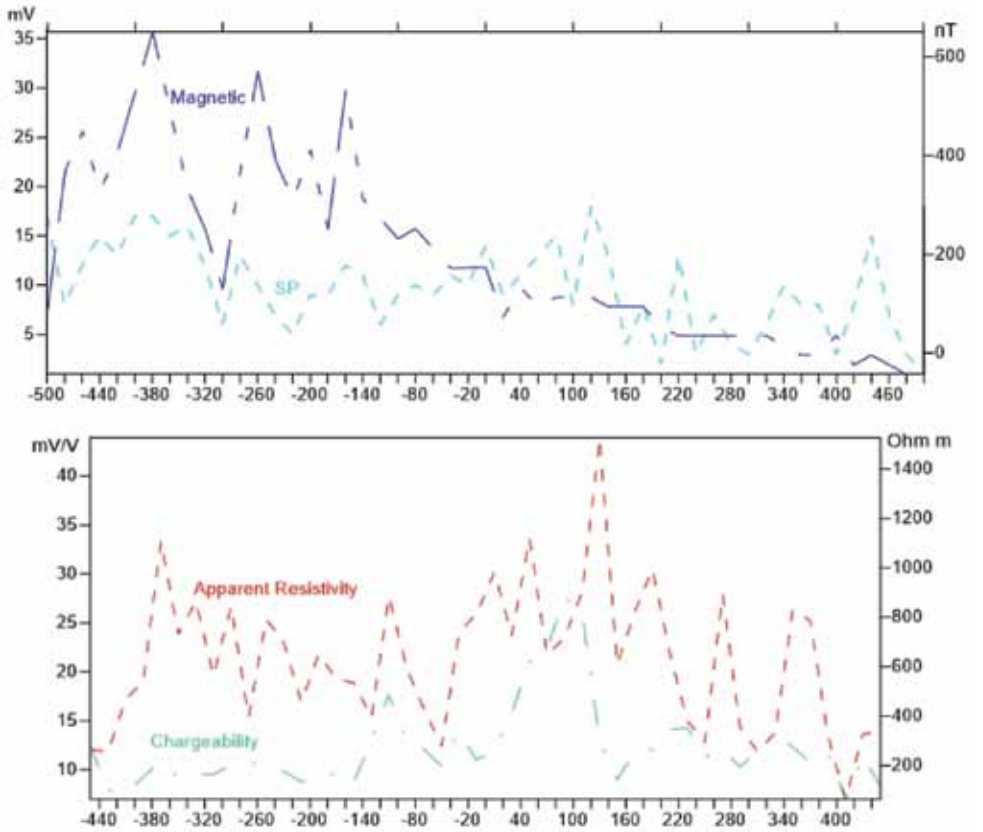

Figure 7d. SP, magnetic, IP cum resistivity profiles along traverse S40 of Karoi-Rajpura area, Bhilwara district, Rajasthan.

Apart from these fluctuating responses are observed throughout the profile.

Representative anomaly profile 'S30' has shown intermediate chargeability value of 15 mV/V, which is associated with high resistivity (Figure 7c), low SP and high amplitude magnetic responses around station in between -140 to -360 (140 m to 360 m towards west from center). High SP value of 20 mV is observed around station in between 80 to 160 (80 m to 160 m towards east from center) and is associated with low magnetic, high resistivity and low chargeability values. Gradual decrease in magnetic response is observed in between station -140 to 500 (140 m from west to 500 m east).

Representative anomaly profile 'S40' has shown high chargeability value of 27 mV/V which is associated with low resistivity, low magnetic and low SP values (Fig. 7d) around station 80 (80 m towards east from center). High resistivity values are corroborated with low chargeability values throughout the profile. High amplitude (300-600 nT) magnetic values are observed in between station -140 to -260 (140 m to 260 m towards west from center), which is associated with low SP values.

EXPLORATION AND DEVELOPMENT

The details of exploration activities conducted by GSI during 2012-13 have been given below:
Agency: GSI; Mineral: Base metal; District: Bhilwara
Location: Karoi & Rajpura
Drilling: No. of boreholes = 8 and Meterage = 1224
Remarks: Reserves/Resources estimated
Prospecting stage investigation (G-3) was carried out for base metals in areas in Pur-Banera belt, to assess the base metal potential of the area. Based on field evidences and ore microscopic studies, it is established that the mineralization is strata bound and evidences of remobilization has been identified. The sulphide mineralization occurs as fracture filling in the form of stringers and veins. The investigation was supplemented by drilling to test the presence of sub surface copper mineralization in this area. The different units intersected in the boreholes are biotite bearing banded calc silicate rock, amphibole bearing banded calc silicate rock and garnet bearing banded calc silicate rock. The sulphide mineralization intersected in the boreholes are in the form of disseminations, stringers and veins of chalcopyrite, bornite, covellite, pyrite and pyrrhotite.

Analytical results of borehole BH-1 have been received. One mineralized zone is intersected in this borehole between depths of 3.00 m and 8.70 m with 0.28 % Cu.

CONCLUSIONS

Geophysical surveys in the area have delineated four anomaly zones favorable for the occurrence of sulphide mineralization. IP survey has brought out four chargeability zones trending N-S and NE-SW directions. Zone-I in NE-SW direction falling in the southern part of the area has moderate order of anomaly. This anomaly zone seems to be favorable for sulphide mineralization and has a dimension of about 200 m X 50 m. Zone-II aligning in NE-SW direction falling in the central portion of surveyed area has a strike length of 150 m. This zone is well corroborated with low SP anomaly. Zone-III trending in N-S and NE-SW directions is lying in northern corner of the area and is extending for 100 m. The opening of 20 mV/V chargeability anomaly contour has indicated its further extension in northern side of surveyed area. Zone-IV aligning in N-S and NE-SW directions is open towards northern side. This zone has strike length of 100 m. The magnetic and SP surveys have picked up lithological variation as well as structural features. State-of-the-art modeling workflows can lead to a better structural insight in already developed and explored mine settings (Vollgger et al., 2015). It may be concluded that the most potential zone of possible mineralization is concentrated in the base metal sulphide deposits and the host rock for the mineralization is mostly calc-silicate dolomite and graphite mica schist of Rajpura-Dariba Group. Based on the present studies structural and lithological controls of base metal mineralization have been recorded and guides for searching new areas and exploration strategy has been suggested here.

ACKNOWLEDGEMENT

Authors thank Dr. B.V.S. Murty for objective evaluation and useful suggestions. Thanks are due to Chief Editor for final refinement and apt editing of the manuscript.

Compliance with Ethical Standards

The authors declare that they have no conflict of interest and adhere to copyright norms.

REFERENCES

Alam, J. and Siddiquie, F.N., 2015. Melt inclusion studies of Pb-Zn ore deposits of Rajpura-Dariba-Bethumni belt in district Udaipur (Rajasthan), India. Int. J. Geosci., 6(6), 9.

Alam, J. and Siddiquie, F.N. and Shaif, M., 2015. Petrographic studies of Pb-Zn ore deposits of Rajpura-Dariba-Bethumni belt in district Udaipur (Rajasthan) India. Int. J. Geosci., 6, 402-412.

Ameta, S., Das Gupta, S. and Sharma, B.B., 1999. Geology, structure and mineralisation in dariba-Bethumni-Sura-Belt, Rajsamand Dist., Rajasthan records of the Geol. Surv. India, 129, 22-24.

Ametha, S.S. and Sharma, B.B., 2008. Geology, structure and mineralization in Rajpura-Dariba-Surawa belt, Sindesar-Khurd area, Rajasmand district, Rajasthan. J. Geol. Soc. India, 72, 381-391.

Gandhi, S.M., 2001. The Ancient Mining and Metallurgy in Rajasthan. Hindustan zinc limited, 4, 2-13.

Haldar, S.K., 2001. Grade-tonnage model for lead-zinc deposits of Rajasthan, India, in Deb, M., and Goodfellow, W.D., compilers, Sediment-hosted lead-zinc sulfide deposits in the northwestern Indian shield: Delhi-Udaipur, India. Proceedings of an Int. Workshop, IUGS-UNESCO Deposit Modeling Program, 153-160.

Haldar, S.K. and Deb, M., 2001. Geology and mineralization of Rajpura-Dariba lead-zinc belt, Rajasthan, in Deb, M., and Goodfellow, W.D., compilers, Sediment-hosted lead-zinc sulfide deposits in the northwestern Indian shield: Delhi-Udaipur, India. Proc. Int. Workshop, IUGS-UNESCO Deposit Modeling Program, 177-187.

Kearey, P., Brooks, M., and Hill, I., 2003. An introduction to geophysical exploration. Geophys. J. Int., 152(2), 506

Mishra, B., 2000. Evolution of the Rajpura-Dariba sulphide deposit: constraints from sulphide-sulphosalt phase equilibria and fluid inclusion studies, in Deb, M., ed., Crustal evolution and metallogeny in the northwestern Indian shield: New Delhi, Narosa Publishing House, 307-328.

Nawal, S., 2017. Geology of Malikhera-Mokanpura area of Dariba-Rajpura-Bethunmi Polymetallic sulphide belt Rajasthan. Int. J. of Adv. Res. Sci. Eng., 6(8), 836-854.

Porwal, A., Carranza, E.J.M. and Hale, M., 2003a. Knowledge-driven and data-driven fuzzy models for predictive mineral potential mapping. Nat. Resources Res., 12(1), 1-25.

Porwal, A., Carranza, E.J.M. and Hale, M., 2006b. Tectonostratigraphy and base-metal mineralization controls, Aravalli province (Western India): new interpretations from geophysical data. Ore Geology Reviews.

Reynolds, J.M., 1997. An Introduction to applied and environmental geophysics, John Wiley Sons Ltd.

Vollgger, S.A., Alexander Cruden, R., Laurent Ailleres, E. and Cowan, J., 2015. Regional dome evolution and its control on ore-grade distribution: Insights from 3D implicit modelling of the Navachab gold deposit, Namibia. Elsevier, Ore geology Reviews, 69, 268-284.

Received on: 15.12.17; Revised on: 19.2.18; Re revised on: 15.4.18; Accepted on: 3.5.18

J. Ind. Geophys. Union (July 2018)
v.22, no.4, pp: 389-398

Probabilistic Seismic Hazard Analysis for Jabalpur area, Madhya Pradesh, India

G. Dhanunjaya Naidu*, S. Selvan, G.R.Tripathy and L.R.Pattanur
Central Water and Power Research Station, Khadakwasla, Pune-411024
*Corresponding Author: dhanugeo@gmail.com

ABSTRACT
The Jabalpur city, situated in seismically active Central Indian Tectonic Zone (CITZ), witnessed a major earthquake of M_w 5.8 on 21st May, 1997. It caused significant damage to the structures and loss of human lives in Jabalpur city and surrounding areas. This necessitated the estimation and quantification of future ground motion in the Jabalpur area for protecting the buildings, life line and other sensitive structures. State-of-art probabilistic seismic hazard analysis study was carried out, covering the Jabalpur city on a grid size of 0.01° x 0.01° to develop seismic hazard maps of the city. Suitable Ground Motion Prediction Equation (GMPE) is used for reliable estimation of seismic hazard by considering the effects of all the earthquakes of different magnitudes and their spatial distribution. Seismic events of different magnitudes within the radius of 300 km from the Jabalpur city as center are considered for analysis. Peak Ground Acceleration (PGA) and spectral amplitudes at 0.2 sec and 1sec are estimated at each grid point, thereby, generating seismic hazard maps for Jabalpur city for the return periods of 2475 (~2500) and 475 (~500) years with 5% damping. The results highlight the surface level seismic hazard within the city.

Key words: Seismic hazard, probabilistic seismic hazard analysis, attenuation, Peak ground acceleration, ground motion prediction equation.

INTRODUCTION

It is well known that most of the earthquakes in the continents occur along the tectonic plate boundaries. However, it is also widely accepted that some of the significant seismic events occur within the rigid tectonic plate or stable continental region (Sykes, 1978). The peninsular India is considered to be seismically stable continental region, away from the seismically active Himalayan belt. However, several parts of the Peninsular India have witnessed significant seismic activity in the recent past (Khan, 2009). For instance, 1938 Satpura earthquake, 1967 Koyna earthquake, 1993 Killari earthquake, 1970 Broach earthquake, 1997 Jabalpur earthquake, and the 2001 Bhuj earthquake are some of the major devastating earthquakes that occurred in the so-called stable continental crust. Indian region is seismically divided into four zones based on intensity of the past earthquakes i.e. Zone- II, III, IV, V (IS:1893(2002). Urban areas, which are located in seismically active zones, are more vulnerable to seismic hazards due to poor land use, improper planning, lack of awareness on seismic hazard, dense population and substandard construction practices.

Jabalpur city in Madhya Pradesh is one of the major cities of India, located in seismically active Central Indian Tectonic Zone (CITZ). It lies in seismic zone-III (IS:1893(2002). Narmada South fault (NSF), which is considered to be one of the active faults in CITZ, passes close to Jabalpur city and it was assumed to be the causative source of 1997 Jabalpur earthquake with M_w 5.8 (Mandal et al., 2000). Jabalpur earthquake, apart from other earthquakes in peninsular India, has left many lessons, which are essential to be learnt in planning and design of the important structures. During Jabalpur earthquake, no strong motion records were available in the nearby affected area. The strong motion records obtained from Bhopal, about 275 km away from the earthquake affected area, are inadequate for the ground motion characterization in the Jabalpur area (EERI Special Earthquake Report, 1997). Hence, it is essential to estimate the future ground motion of the forthcoming earthquake events to mitigate the seismic risk. In the present study, the Maximum Credible Earthquake (MCE) and Design Basis Earthquake (DBE) level of ground motions, are estimated using suitable Ground Motion Prediction Equation (GMPE).

Many researchers have studied the occurrence of Jabalpur earthquake and its consequences. A study, soon after the Jabalpur earthquake by Gupta et al. (1997), revealed that it is a thrust type faulting along ENE-WSW trending by focal mechanism solutions and isoseismal map. A multi-disciplinary project on seismic microzonation study of Jabalpur urban area was initiated by Department of Science and Technology (DST). Several national nodal agencies viz. Geological survey of India (GSI), Central Region Nagpur, Indian Meteorology Department (IMD), New Delhi, CSIR-National Geophysical Research Institute, Hyderabad, Central Building Research Institute (CBRI), Roorkee and Government Engineering College, Jabalpur were involved in carrying out this study to prepare a seismic microzonation map of Jabalpur city (PCRSMJUA, 2005).

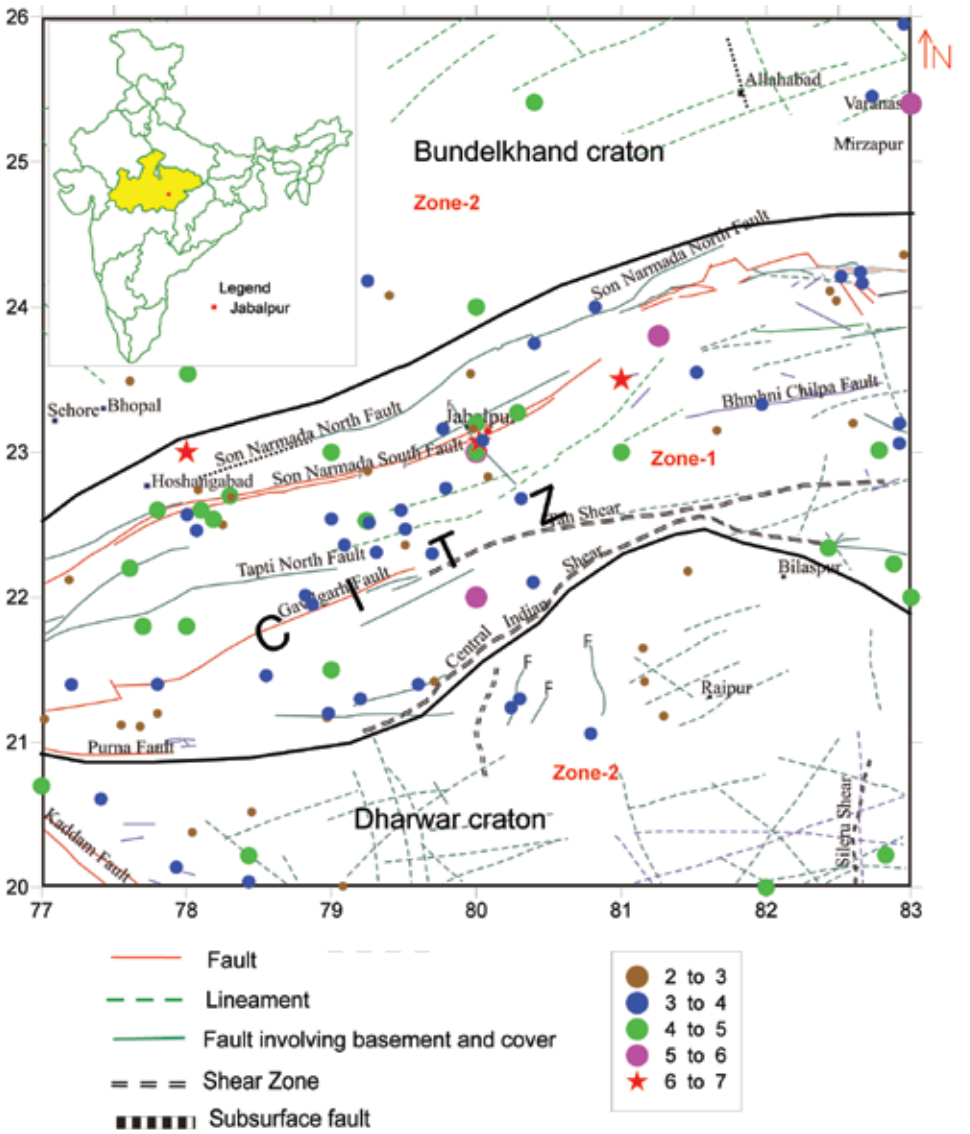

Figure 1. Seismotectonic map of Jabalpur and its surrounding area (modified after GSI, 2000) with past seismic events of different magnitudes (1846-2012).

Site amplification study, carried out by Purnachandra Rao et al. (2011) using Nakamura technique, has provided the site amplification values over different geological formations in the Jabalpur city. Another study by Grover et al., 2013 estimated the Peak ground acceleration of 0.15g for Jabalpur city. Probabilistic seismic hazard analysis study was also carried for whole India by National Disaster Management Authority (NDMA), Govt. of India (2010) and reported the Peak Ground Acceleration (PGA) values for major cities in India for different return periods. The PGA values reported from this study are 0.18 and 0.08 for Jabalpur city with 2500 and 500 return periods respectively for rock site.

The present study has an advantage of estimation of site specific seismic hazard at very close interval within the Jabalpur city. The Jabalpur city area is divided into 384 grid points with an interval of 0.01°x0.01° and assumed each corner of the grid as a site. Spectral amplitude values are computed at each grid point and thereby, seismic hazard contour maps are generated for Jabalpur city at selected periods by considering both rock and soil site conditions.

SEISMOTECTONIC SETTING AND GEOLOGY

Jabalpur earthquake epicenter lies in the ENE-WSW trending CITZ. CITZ is a mega geo-fracture of about 1200 km long extending from west to east in central India. This feature separates the Bundelkhand protocontinent towards north and Dharwar protocontinent towards south (Roy and Bandopadhyay, 1990) (Figure 1). Tectonically, CITZ is highly disturbed and reactivation is believed to

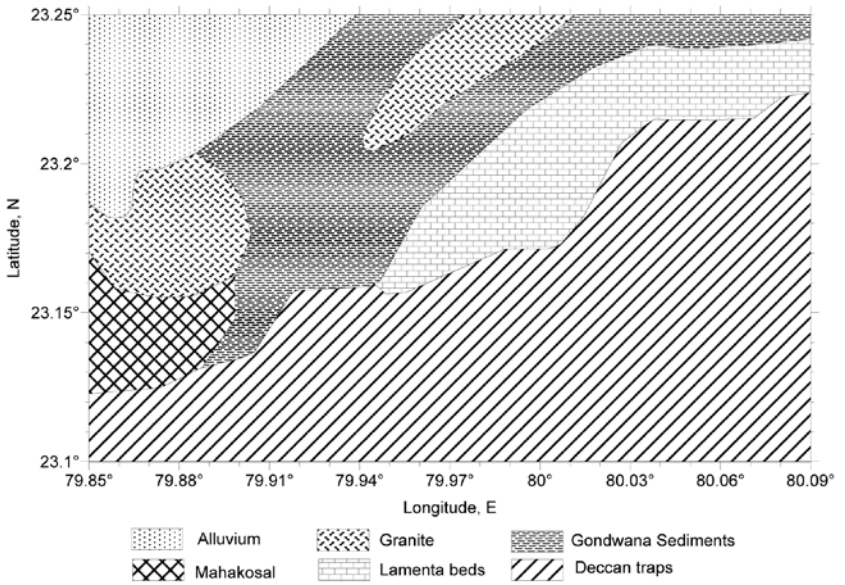

Figure 2. Geological map of the Jabalpur area consisting of various surface geological formations (modified after GSI, 2000).

be due to collision of Indian and Eurasian plates (Jain et al., 1984). Reactivation of CITZ took place throughout its evolution in different phases (Fermor, 1936; Auden, 1949; West, 1962). A total of ~25 earthquakes have occurred in Peninsular India with M>5.0 and intensity >VII (MM scale) (Purnachandra Rao et al., 2011). Out of twenty five, six are along the CITZ, indicates the level of seismic activity in this region. Jabalpur earthquake (1997) is one of them with M_w5.8.

Geologically, Jabalpur city and its surrounding region comprises a wide variety of rocks of different age ranging from Archean-Proterozoic to Tertiary-Quaternary (Matley, 1921; Jha et al., 1984). Jabalpur area mainly consists of Alluvium, Deccan traps, Vindhyan sediments, Gondwana sediments, Mahakoshal group and Madanmahal granites of different age (see Figure 2). The exposed Deccan traps in the region are considered one of the largest volcanic lava flows in the world belongs to Paleocene-Cretaceous boundary age. The Mahakosal group of rocks in the region are the oldest exposed rocks of Archean to Paleoproterozoic age. The NW of Jabalpur area is characterized by a thick layer of alluvial sediments of Tertiary and Quaternary age (Fermor, 1936; Auden, 1949; West, 1962).

These sediments are more vulnerable and cause seismic hazard during earthquake due to site amplification. Lameta group rocks of upper Cretaceous age are found towards NE of Jabalpur in the study region. These are basically sedimentary rocks overlying the Gondwana rocks. There is an abundance of Gondwana rocks found towards North and Northeast of Jabalpur. These sedimentary rocks consists of sandstones, shales and clays. In addition, there are intrusives of Madanmahal granites of late Proterozoic age at places within the Mahakoshal group.

SEISMICITY

CITZ in central India is seismically second most active tectonic zone after the Himalayas. This region had witnessed six seismic events of M>5. Out of these, two seismic events namely 1938 Satpura earthquake and 1997 Jabalpur earthquake, have occurred at lower crustal depths at 40km and 35 km depth respectively. The seismicity is mainly concentrated along the CITZ belt and also along some of the transverse features, which have been activated from time to time, as a result of the stresses accumulated by NNE movement of the Indian plate. Seismicity map has been prepared from the data on past earthquakes in a region of 6° Lat. × 6° Long. around the Jabalpur city, as compiled by different published sources. In order to study the seismicity of the region, a total of 112 earthquakes for the period from 1846 to 2012, with magnitudes greater than or equal to 2.0, are considered in the present study.

The epicenters of past earthquakes are plotted in seismotectonic map to decipher the association of past earthquakes with various tectonic features in the region (Figure 1). Though, the epicenters are seen to be dispersed widely, definite clustering along the CITZ longitudinal trend and along some of the transverse features is discernible. Epicentral concentrations are seen to occur along the Narmada South Fault, Narmada North Fault and lineaments and faults within the CITZ. Low level of seismicity observed in the Bundelkhand craton in the north and Dharwar craton in the south of CITZ may be related to the various lineaments/subsurface tectonic features. The earthquakes with magnitude M>4.0, and their epicenters are seen to be concentrated within the CITZ. The observed distribution of epicenters within the CITZ is explained

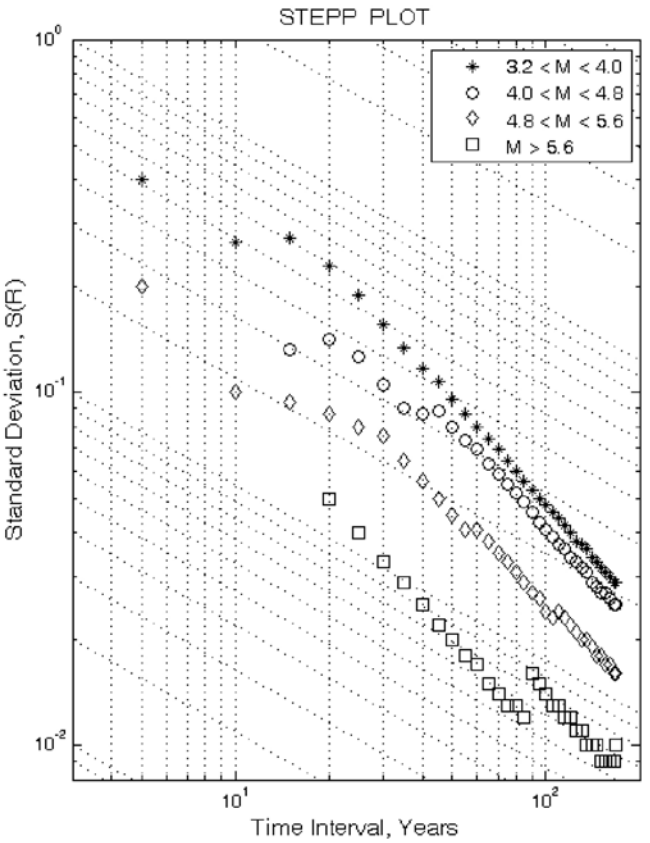

Figure 3. Stepp's completeness plot for the standard deviation S(R) as a function of time interval (T) for zone-1.

by reactivation of the crustal blocks due to subduction and collision tectonics along the Mesoproterozoic suture (Naganjaneyulu and Santosh, 2010b). This indicates neo-tectonic activity in this region. The recent seismicity in the CITZ reveals that reactivation process is still going on and suggests that this region is associated with mantle reaching faults (deep seated faults) since Precambrian to early Quaternary age (Mall et al., 2005; Mall and Sharma 2009; Choubey, 1971).

The study area is divided into two seismic source zones based on the trend of lineaments/faults and location of the past earthquake epicenters in the study region (Figure 1). Majority of the seismic events have been found to occur in the seismic source zone-1 i.e. CITZ and remaining events have occurred on either side of it, which is considered as seismic source zone-2. A total of 79 earthquake events have been observed in seismic zone-1with a maximum observed magnitude (M_{obs}) of M_w 6.5, where as 33 events were found in zone-2 with a maximum observed magnitude (M_{obs}) of M_w 5.5. The data completeness and annual recurrence rate of earthquakes using Gutenberg-Richter (G-R) recurrence relation are estimated for each zone in the following section.

Data completeness and G-R recurrence relationship

Based on available past earthquake data, the seismic activity of each source zone is characterized by the following recurrence relationship, as suggested by Gutenberg and Richter (1944).

$$Log_{10}N\,(M) = a - bM \qquad \text{..... (1)}$$

where, N is number of earthquakes with magnitude M or greater per year and 'a' and 'b' are statistical parameters estimated by least square analysis of past earthquake data. Parameter 'a' indicates the number of events per year with M=0. The value of 'b' is close to 1 and is tectonic parameter. A higher 'b' value indicates the large number of smaller magnitude seismic events in the catalogue whereas, lower 'b' value implies the small number of large magnitude seismic events in the catalogue (Tsapanos, 1990). The seismic hazard at any seismic zone is controlled by these two parameters. The annual recurrence rate of earthquakes can be assessed correctly from analysis of past seismic data, only when the available earthquake data are complete. However, in most of the cases data on past earthquakes are incomplete due to various reasons.

Table 1. The period of completeness of different magnitude intervals for seismic zone-1 and zone-2.

S.no	Earthquake magnitude interval	Period of completeness	Earthquake magnitude interval	Period of completeness
		Zone-1		Zone-2
1	$3.2 \leq M_w \leq 4.4$	20	$3.2 \leq M_w \leq 4.4$	20
2	$4.4 \leq M_w \leq 4.8$	50	$4.4 \leq M_w \leq 4.8$	50
3	≥ 4.8	160	$4.8 \leq M_w \leq 5.6$	110
4	--	--	≥ 5.6	170

Table 2. The seismic parameters a, b and observed and assigned upper bound magnitudes (M_{obs} and M_{max}) for source zone 1 and zone-2.

S. No.	Seismic Source zone	***a***	***b***	M_{obs}	M_{max}
1.	Zone -1	2.56	0.75	6.5	7.0
2.	Zone-2	1.55	0.59	5.5	6.2

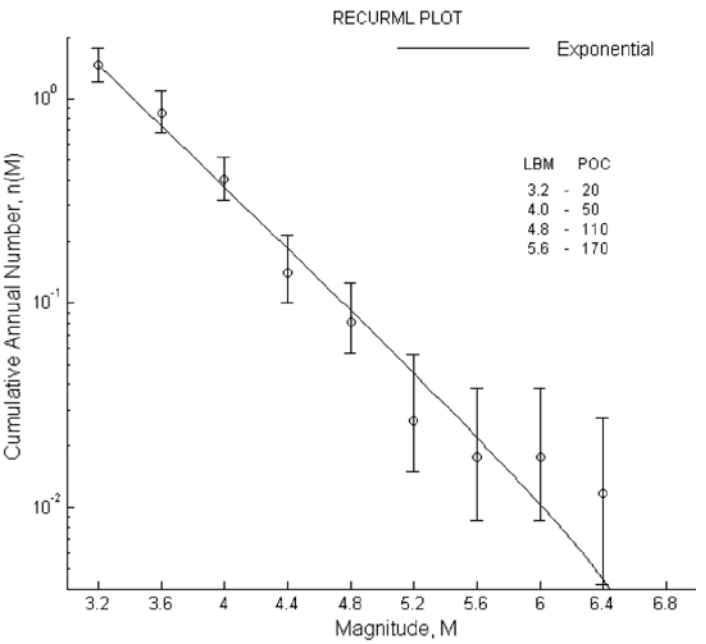

Figure 4. A typical exponential decay curve for annual recurrence rate versus magnitude for the source zone-1.

The effect of incompleteness in the available data set can be minimized by adopting statistical method suggested by Stepp (1972). In this method, the available earthquake catalogue is grouped into magnitude intervals with a time interval of about 5-10 years to calculate the completeness period. The completeness plot for the standard deviation S(R) as a function of time interval (T) is plotted in Figure 3 for zone-1. The estimated completeness period for source zones 1 and 2 are given in Table-1. The parameters 'a' and 'b' are evaluated by maximum likelihood method (Weichert, 1980) and given in Table-2.

The exponential decay of the recurrence relation using the parameters β, M_{min} and M_{max} is described by Cornell and VanMarcke (1969) as below.

$$N(M) = N(M_{min}) \frac{\exp(-\beta(M - M_{min})) - \exp(-\beta(M_{max} - M_{min}))}{1 - \exp(-\beta(M_{max} - M_{min}))} \quad \text{.....(2)}$$

In the above expression, threshold magnitude (M_{min}) is taken as 3.8 for the present study. The upper bound magnitude (M_{max}) used for each source zone is given in the Table 2. The upper bound magnitude (M_{max}) is obtained by incremental approach by adding some increment to the observed magnitude. The maximum magnitude (M_{max}), by definition, is no earthquakes are possible with magnitude exceeding M_{max} (Kijko, 2003). When the available data is lacking to apply a formal method for estimation of M_{max}, the observed magnitude is enhanced by a suitable amount (0.5 to 1 units), depending on the available largest magnitude and expected regional potential of the study

area. The estimation of M_{max} in probabilistic procedures is merely depends on seismological history of the area such as using seismic event catalogs and appropriate statistical estimation procedures (Kijko, 2003). The most commonly used probabilistic procedure for estimation of M_{max}, based on extrapolation of the classic, log-linear, frequency-magnitude Gutenberg-Richter relation, was developed in late sixties (Kijko, 2003). The incremental method of M_{max} has also been estimated by conventional approach of M_{obs} with an increment of 0.5, which considers Gutenberg-Richter b-value (Wheeler, 2009). This method may be used according to the regional b-value since 0.5 increment equals to one increment of equal intensity value. An increment value of 0.5 is used to the M_{obs} when b-value is close to 1 (Anbazhagan et al., 2014). The b-value of seismic zone-I is close to 1 (i.e.0.75) compared to zone-II (i.e.0.59) in the study area. Hence, increment of 0.5 is added to the observed magnitude (M_{obs}) M.6.5 for zone-I and accordingly M_{max} is fixed as M7.0 (M_{obs} + 0.5). Whereas, 0.7 units added to zone-II conservatively as its b-value and M_{obs} are less. The parameter β is related to b-value and is expressed as β = bln10. A typical exponential decay curve for annual recurrence rate versus magnitude for the source zone-1 is shown in Figure 4. The annual occurrence rate of earthquakes with a specified magnitude interval and spatial distribution is considered in the probabilistic approach to estimate the MCE and DBE level of ground motion.

Probabilistic Seismic Hazard Analysis

The probabilistic seismic hazard analysis (PSHA) approach is used to get a reliable estimation of the seismic hazard by considering the effects of total expected seismicity with suitable spatial distribution of the site of interest. The PSHA approach provides the 5 % damped target response spectra for a given area with a specified confidence level. This will not be exceeded due to any of the earthquakes expected to occur anywhere in the region during a specified exposure time. The Maximum Credible Earthquake (MCE) level of ground motion is commonly specified with a 2% of exceedence during 50 years of exposure time for 2475 (~2500) years return period (FEMA, 2004). The composite probability distribution of the spectral amplitude at a given natural period is expressed in the PSHA approach as given below (Cornell, 1968; McGuire, 1977; Anderson and Trifunac, 1978; Gupta, 2002a).

$$P[SA(T)] = \exp\left\{-Y\sum_{i,j} q[SA(T) \mid M_j, R_i]\cdot \upsilon(M_j, R_i)\right\} \quad \text{.....(3)}$$

In the above equation, Y is the considered exposure period and $\upsilon(M_j,R_i)$ is the annual occurrence rate of earthquakes within a small magnitude range $(M_j-\delta M_j,\ M_j+\delta M_j)$ and a small distance range $(R_i-\delta R_i,\ R_i+\delta R_i)$ from the site of interest. Quantity $q[SA(T)|M_j, R_i]$ represents the probability of exceeding the spectral amplitude $SA(T)$ due to an earthquake of magnitude M_j at distance R_i. In the present study, the 5 % damped probabilistic response spectra are obtained for both MCE and DBE levels of ground motion. This is estimated by the spectral amplitudes at all the natural periods with 96 % and 81% probability of not exceeding in the exposure period of 100 years. The MCE and DBE levels of ground motion are estimated for the Jabalpur area using a suitable Ground Motion Prediction Equation (GMPEs).

Ground motion prediction equations (GMPEs)

There are several ground motion prediction equations developed by many authors (Ambrahamson and Silva, 2008; Boore and Atkinson, 2008; Campbell and Bozognia, 2008; Chiou and Youngs, 2008a; Idriss, 2008) as a part of Next Generation Attenuation (NGA) of ground motions for seismically active tectonic regions worldwide. In addition, there are several attenuation relations developed for Himalayan region by many authors (Anbazhagan et al., 2015). However, no attenuation model is developed for intra-plate regions based on recorded instrumental data as the strong motion data available for the region are sparse. Since the Jabalpur area in CITZ lies in intra-plate region and selecting the suitable ground motion prediction equation is difficult. In light of this problem, the attenuation models for seismically active regions based on only instrumental recordings are adopted to find out the suitable relation for the present study area. Except Boore and Atkinson, 2008 (BA08), the NGA relations need the exact information on fault directivity, fault rupture geometry and site effects more comprehensively, which are not available in most cases. Hence, the NGA attenuation relations cannot be used without making some subjective assumptions leading to biased results (NCSDP guidelines, 2011). Hence, three different GMPEs, AS97 (Abrahamson and Silva, 1997); LEE87 (Lee, 1987) and BA08 (Boore and Atkinson, 2008) are identified for the study region, which needs less number of fault parameters.

The seismic hazard level is specified in terms of standard response spectrum shape, which is scaled by the zone factor (Raghukanth, 2010). The zone factor in Indian Standard IS:1893 (2002) is assumed to be the expected Peak Ground Acceleration (PGA). On the other hand, Zero Period Acceleration (ZPA) value obtained from the resultant spectral amplitude values by any GMPE is also considered as PGA. In this context, the terms Zero Period Acceleration (ZPA), Peak ground acceleration (PGA) and Zone factor are considered to be same. Since AS97, LEE87 and BA08 are meant for seismically active tectonic environments and the study area falls in seismically active tectonic region too i.e. CITZ in peninsular India, these three models are adopted for comparison. The response

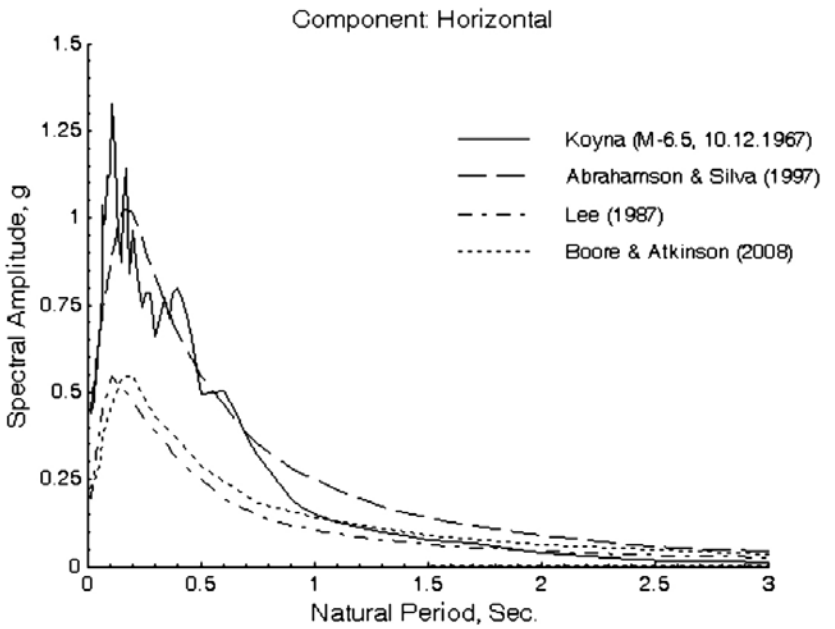

Figure 5. Comparison of mean Response spectra of two horizontal components of the accelerograms recorded from Koyna earthquake of 10 Dec, 1967 with those predicted by three selected empirical attenuation relations at bedrock level.

Table 3. The estimated ZPA/PGA values from three GMPEs (AS97, LEE87 and BA08) for both rock and soil site conditions.

S.No	Geology	Hazard parameter	GMPE		
			AS97	LEE87	BA08
1	Soil	ZPA/PGA	0.17g	0.09g	0.13g
2	Rock		0.15g	0.08g	0.07g

spectra obtained from these three GMPEs are plotted in Figure 5 for bedrock level. From the figure, it is discerned that the spectral amplitude values obtained by AS97 are found to be higher than the spectral values due to other two GMPEs for both rock and soil site conditions (table 3). To show the suitability of the AS97 attenuation relation for peninsular India, mean response spectra of two horizontal components of the Koyna earthquake of 10 December, 1967 along with the mean estimation of the predicted response spectra of other three empirical attenuation relations at bedrock level is compared. It is observed that AS97 is more compatible to the Koyna spectrum in terms of shape, amplitude and it's PGA (Figure 5). In addition, results obtained using the attenuation relations of Iyengar and Raghukanth (2004) and NDMA (2010) by Grover et al., (2003) and NDMA, 2010 for the same region, are well correlated with the values obtained in the present study. Hence, the use of GMPE of AS97 is justifiable for the study region and considered conservatively to be MCE level of target response spectra. The same has been discussed in detail in the results and discussion section. The ZPA value obtained by AS97 is also observed to be close to the zone factor value given in IS:1983(2002) i.e. 0.16 for seismic zone-III. Hence, the GMPE by AS97 is adopted for the present study to determine the spectral amplitude values for different natural periods.

The Ground motion prediction Equation (GMPE) due to Abrahamson and Silva (1997) has been used to obtain the 5 % damped acceleration response spectra for horizontal component of the ground motion.

This relation is developed using a strong motion database of 655 recordings from 58 shallow crustal events in seismically active tectonic regions worldwide. Abrahamson and Silva (1997) have presented their attenuation relation for spectral acceleration (*SA (T)*), as given below.

$$\ln Sa(g) = f_1(M,R) + F \cdot f_3(M) + HW \cdot f_4(M,R) + S \cdot f_5(a_{max}) \quad \text{.....(4)}$$

where Sa (g) is the spectral acceleration in g, *M* is moment magnitude and *R* is the closest distance to the fault rupture plane in km. Parameter *F* defines the type of faulting (1 for reverse fault, 0.5 for reverse/oblique, 0 for otherwise), *HW* is the variable, which specifies the location of site on hanging or footwall side of dipping faults (1 for hanging wall, 0 for otherwise) and *S* defines the site class (0 for rock or shallow soil, 1 for deep soil). Functions f_1, f_3, f_4 and f_5 in eqn. (2) are expressed in terms of 12 regression coefficients, $a_1(T)$, $a_2(T)$, ……, $a_{12}(T)$, evaluated by Abrahamson and

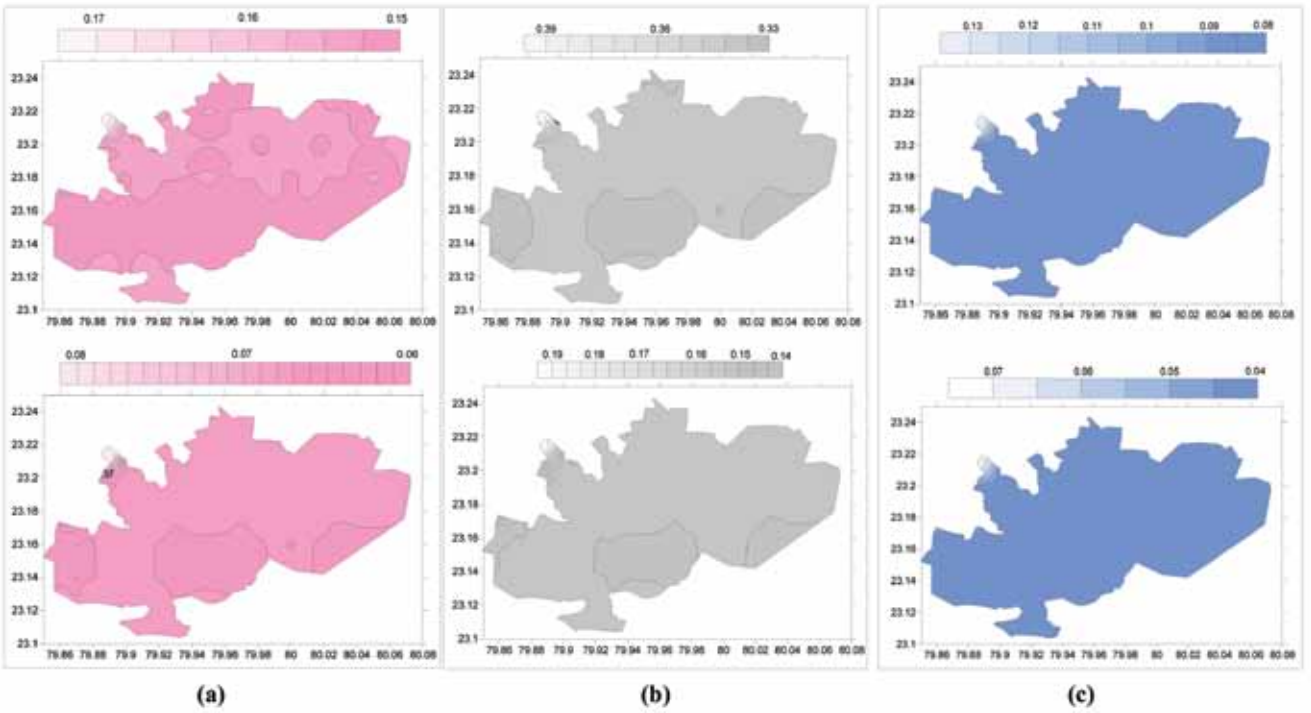

Figure 6. (a) Peak Ground Acceleration (PGA) contours for 2500 years (top) and 500 years (bottom) of return periods with an exposure period of 100 years. (b) Short period spectral acceleration values at 0.2 sec for return period of 2500 (top) and 500 (bottom) years with 5% damping for both rock and soil site conditions. (c) Long period spectral acceleration values at 1sec for return period of 2500 (top) and 500 (bottom) years with 5% damping for both rock and soil site conditions.

Silva (1997) at 28 natural periods between 0.02 sec and 5.0 sec. The expression of eqn. (2) gives the least squares median value, $\langle Sa(g) \rangle$, of the spectral amplitudes.

In this study, the seismically active Narmada South Fault (NSF) passing approximately in E-W direction and intersecting the southern part of Jabalpur city. Since this fault is southerly dipping reverse (thrust) type of fault (Mandal et al., 2000), the same is considered in the AS97 GMPE. Both hanging wall and foot wall conditions are considered based on location of the grid point, with respect to the fault line and its dip direction. Jabalpur area consists of various surface geological formations such as Basalt, Gondwana sedimemnts, lameta formation, Granite, Mahakoshal group of rocks and alluvial sediments as per Seismotectonic atlas map of India published by Geological Survey of India (GSI, 2000). However, all these rocks are broadly classified into rock and soil, based on shear wave velocities. Alluvial sediments are considered as soil, whereas all other type of rocks are considered as rock in the AS97 ground motion prediction equation. Spectral amplitudes are calculated at 28 natural periods from 0.02 sec to 5 sec.

RESULTS AND DISCUSSION

The Jabalpur city is divided into smaller grid interval of 0.01° x 0.01° (approximately 1 km x 1km) and Seismic hazard contour maps have been prepared by performing the seismic hazard computations at 384 grid points. The 5% damped spectral amplitudes are estimated at each corner of the grid for both MCE and DBE level of the ground motions. The Zero Period Acceleration (ZPA) of spectral amplitudes at each corner of the grid are assumed to be Peak ground acceleration values and plotted in contours (Figure 6a).

The PGA values are varying from 0.15g to 0.17g for MCE condition and 0.06g to 0.08g for DBE condition. In addition, Spectral amplitudes at selected natural periods of 0.2 sec and 1 sec are computed for the design response spectrum and presented in contours as shown in Figures 6 (b) and (c) respectively. The spectral amplitude values at 0.2 sec are varying between 0.33g to 0.39g for MCE condition, whereas it is varying from 0.14g to 0.19g for DBE level of ground motion. The spectral amplitude values at 1sec for MCE condition are varying from 0.08g to 0.13g and for DBE condition; it is 0.04g to 0.07g. These maps are prepared for the return period of 2500 years and 500 years with an exposure period of 100 years.

The results obtained from the study in terms of PGA for the return period of 2500 years is close to the study results carried out for Jabalpur area by several authors. A site amplification study carried out for seismic microzonation in Jabalpur area obtained the maximum site amplification in the north-western part of the Jabalpur

area (Purnachandra Rao et al., 2011) where highest PGA value of 0.17g is obtained by the present study for the return period of 2500 years as shown in Figure 6 (a) top. The maximum site amplification and higher PGA values represents the presence of thick alluvial sediments in north-western part of Jabalpur area. The highest PGA value of 0.15g obtained at bedrock level using GMPE of AS97 from the present study is well correlated with the same value i.e. 0.15g at bedrock level by Grover et al. (2003) using GMPE of Iyengar and RaghuKanth (2004, 2006). Another PSHA study carried out by National Disaster Management Authority (NDMA), Govt. of India (2010) reported the Peak Ground Acceleration (PGA) value of 0.18g at bedrock level with 2500 years return period. This value is almost close to the value obtained from the present study. Moreover, The PGA value obtained in the present study is comparable to zone factor value reported in the IS code i.e. 0.16 (IS:1893 (2002)) for seismic zone-III.

CONCLUSION

Probabilistic seismic hazard analysis is carried out for the Jabalpur city to quantify the ground motion and thereby to estimate seismic hazard for the forthcoming earthquakes. An earthquake catalogue starting from 1846 to 2010 is compiled from several resources within a radius of 300 km from the Jabalpur city. Data completeness is calculated and annual recurrence rate is estimated for available data set. Three ground motion prediction equations are tested for the study region i.e. AS97; LEE87 and BA08; and AS97 is found suitable after comparing the predicted response spectra by these three attenuation relations with the response spectra of recorded accelerogram of Koyna earthquake (10 Dec, 1967). Existing soil/rock formations, footwall/hanging wall and reverse (thrust) type of faulting are considered in the selected GMPE to determine the 5% damped spectral amplitudes for different natural periods. Seismic hazard contour maps in terms of PGA and spectral amplitudes have been generated for 2475 (~2500) and 475 (~500) years return periods, which is equal to 96% and 81% probability of not exceeding in 100 years. As per International building code IBC-2009, spectral acceleration values are also computed at 0.2 sec and 1 sec for developing the design response spectrum for any major sensitive structures/buildings in Jabalpur area. It is observed that the seismic hazard in terms of PGA is varying from 0.15g to 0.17g for MCE and 0.06 to 0.08 for DBE levels of ground motion within the Jabalpur city. The spectral acceleration and PGA values estimated from the present study are based on broad classification of site geology (Rock and soil). The maximum peak ground acceleration 0.17g is observed towards NW of Jabalpur city over the thick alluvial sediments, which is most prone for site amplifications.

ACKNOWLEDGEMENTS

Authors are thankful to Dr.M.K.Sinha, Director for providing permission to publish this work. Our sincere thanks to Shri.M.D.Kudale, Additional Director for his encouragement to carry out this study. Authors are also thankful to the anonymous reviewer for his critical comments and valuable suggestions to improve the manuscript.

Compliance with Ethical Standards

The authors declare that they have no conflict of interest and adhere to copyright norms.

REFERENCES

Abrahamson, N.A. and Silva, W.J., 1997. Empirical response spectral attenuation relations for shallow crustal earthquakes. Seism. Res. Lett., 68(1), 94–127.

Anbazhagan, P., Dutta, N., Bajaj, K., Moustafa, S.S.R. and Al-Arifi, N.S., 2014. Earthquake maximum magnitude estimation considering regional seismotectonic parameters, in ST Smith (ed.), 23rd Australasian Conference on the Mechanics of Structures and Materials (ACMSM23), Byron Bay, NSW, 9-12 December, Southern Cross University, Lismore, NSW, II, 979-984. ISBN: 9780994152008.

Anbazhagan, P., Bajaj, K. and Patel, S., 2015. Seismic hazard maps and spectrum for Patna considering region-specific seismotectonic parameters, Nat. Hazards., 78, 1163–1195.

Anderson, J.G. and Trifunac, M.D., 1978. "Uniform risk functionals for characterization of strong earthquake ground motion", Bull. Seismol. Soc. Am., 68(1), 205–218.

Auden, J.B., 1949**.** Geological discussion of the Satpura hypothesis, Proc. Natl. Inst. Sci. India., 15, 315–340.

Boore, D.M. and Atkinson, G.M., 2008. Ground-motion prediction equations for the average horizontal component of PGA, PGV and 5% damped PSA at spectral periods between 0.01 and 10.0 s, Earthq. Spectra., 24(1), 99–138.

Campbell, K.W. and Bozorgnia, Y., 2008. NGA ground motion model for the geometric mean horizontal component of PGA, PGV, PGD and 5% damped linear elastic response spectra for periods ranging from 0.01 to 10 s, Earthquake Spectra, 24, 139–171

Chiou, B.S.J. and Youngs, R.R., 2008a. An NGA model for the average horizontal component of peak ground motion and response spectra, Earthquake Spectra, 24, 173–215.

Choubey, V.D., 1971. Narmada-Son linement, India, Nature. Phys. Sci., 232, 38-40.

Cornell, C.A. and Vanmarcke, E.H., 1969. The major influences on seismic risk, Proc. Fourth World Conf. Earthq. Eng., Santiago, Chile, 1, 69–93.

Cornell, C.A., 1968. Engineering seismic risk analysis, Bull. Seism. Soc. Am., 58(5), 1583-1606.

EERI Special Earthquake Report., 1997. Some observations on engineering aspects of the Jabalpur earthquake of 22 May 1997, EERI Newsletter, 32(2).

FEMA, 2004. NEHRP recommended provisions for seismic regulations for new buildings and other structures (FEMA 450), Part 1: Provisions", 2003 Edition.

Fermor, L.L., 1936. An attempt at the correlation of the ancient schistose formation of Peninsular India, Mem. Geol. Surv. Ind., 70(I), 217.

Grover, R.K., Vishwakarma, A., Jain, R. and Mishra, K.H., 2013. Estimation of peak ground acceleration for Jabalpur city, Int. J. Eng. Res. Appl., 3(1), 1777-1780.

GSI, 2000. Seismotectonic Atlas of India and its environs, Geological Survey of India, India.

Gupta, H.K., Chadha, R.K., Rao, M.N., Narayana, B.L., Mandal, P., Ravikumar, M. and Kumar, N., 1997. The Jabalpur earthquake of May 22, 1997, J. Geol. Soc. India, 50, 85-91.

Gupta, I.D., 2002a. State of the art in seismic hazard analysis, ISET Jour. Earthq. Eng., 39(4), 311-346.

Gutenberg, B. and Richter, C.F., 1944. Frequency of earthquakes in California, Bull. Seismol. Soc. Am., 34, 185-188.

IBC, 2009. International building code, International code council.

Idriss, I.M., 2008. An NGA empirical model for estimating the horizontal spectral values generated by shallow crustal earthquakes, Earthq. Spectra, 24, 217–242.

IS:1893., 2002. Indian standard criteria for earthquake resistant design of structures, part 1-general provisions and buildings, Bureau of Indian Standards, New Delhi.

Iyengar, R.N. and Raghukanth, S.T.G., 2004. Attenuation of strong ground motion in peninsular India, Seism. Res. Lett., 79, 530 – 540.

Iyengar, R.N. and RaghuKanth, S.T.G., 2006. Seismic hazard estimation for Mumbai city, Curr. Sci., 91(11, 10), 1486-1494.

Jain, A.K., Annup, N. and Singhal, D.C., 1984. Crustal evolution of the Narmada- Son lineament and associated shear zones of the Indian lithosphere, J. Earth. Sci., CEISM Seminar, 125–148.

Jha, D.K. et al., 1984. Systematic geological mapping from Barmanghat to Tilwarghat in parts of Narsingpur and Jabalpur district of M.P GSI unpub. Report.

Khan, 2009. Why Tectonically stable Indian shield becomes seismically unstable? J. South Asia Disast. Studies, 2, 129-138.

Kijko, A., 2003. Estimation of the maximum earthquake magnitude, $M_{max.}$ Pure. Appl. Geophys., 1-29.

Mall, D.M. and Sharma, S.R., 2009. Tectonics and thermal structure of western Satpura, India, J. Asian earth sci., 34, 450-457.

Mall, D.M., Singh, A.P. and Sarkar, D., 2005. Structure and seismotectonics of Satpura central India, Curr. Sci., 88, 1621–1627.

Mandal, P., Rastogi, B.K. and Gupta, H.K., 2000. Recent Indian earthquakes, Curr. Sci., 79, 1334–1346.

Matley, C.E., 1921. Stratigraphy, fossil and of the lameta beds of Jabalpur, Geol. surv. India, 53,142-169.

McGuire, R.K., 1977. Seismic design spectra and mapping procedures using hazard analysis based directly on oscillator response, Earthq. Eng.Struct. Dyn., 5(3), 211–234.

Naganjaneyulu, K., and Santosh, M., 2010b. The central India tectonic zone: a geophysical perspective on continental amalgamation along a Mesoproterozoic suture, Gond. Res., 18, 547–564.

NDMA, 2010. National disaster management authority Govt. of India. Development of probabilistic seismic hazard map of India.

NCSDP, 2011 (revised 2014). Guidelines for preparation and submission of site specific seismic study report of river valley project.

PCRSMJUA, 2005. Project completion report of seismic microzonation of Jabalpur urban area, Department of Science and Technology, Government of India, India.2 volumes.

Purnachandra Rao et al., 2011. Site amplification studies towards seismic microzonation in Jabalpur urban area, Central India, Phys. Chem. Earth, 36, 1247-1258.

Raghukanth, S.T.G., 2010. Estimation of seismicity parameters for India, Seism. Res. Lett., 81(2), 207-217.

Roy, A., and Bandyopadhyay, B.K., 1990. Tectonic and structural pattern of the Mahakoshal belt of central India: A discussion, GSI spl. publ. no.28, workshop of Precambrian of central India, 226-240.

Stepp, J.C., 1972. Analysis of completeness of the earthquake sample in the Puget Sound area and its effect on statistical estimates of earthquake hazard, Proc. Int. conf. microzonation, 2, 897–910.

Sykes, L.R., 1978. Intraplate seismicity, reactivation of preexisting zones of weakness, alkaline magmatism, and other tectonism postdating continental fragmentation, Rev. Geophys. Space Phys., 16, 621–688.

Tsapanos, T.M., 1990. b-Values of two tectonic parts in the Circum–Pacific belt, Pure. Appl. Geophys., 134(2), 229–242.

Weichert, D.H., 1980. Estimation of the earthquake recurrence parameters for unequal observation periods for different magnitudes, Bull. Seismol. Soc. Am., 70(4), 1337–1346.

West, W.D., 1962. The line of the Narmada and Son valleys, Cur. Sci., 31, 143–144.

Wheeler, R.L., 2009. Methods of Mmax estimation east of the Rocky Mountains U.S. Geol. Surv., Open-File Report 2009-1018.

Received on: 24.1.18; Revised on: 19.2.18; Accepted on: 25.3.18

J. Ind. Geophys. Union (July 2018)
v.22, no.4, pp: 399-406

Geomorphic Expressions of Active Strike-slip faulting (Girnar Fault), Saurashtra, Western India

Tarun Solanki*[1], S. P. Prizomwala[1], and P. M. Solanki[2]

[1]Active Tectonics Group, Institute of Seismological Research, Gandhinagar, India 382009
[2]Department of Geology, M. G. Science Institute, Navrangpura, Ahmedabad 380009
* Corresponding Author: tarunsolanki86@yahoo.in

ABSTRACT

The Talala region of Saurashtra in Western India has been rocked by three moderate seismic events of Mw 4.8 (2007), Mw 5.0 (2007) and Mw 5.1 (2011). Despite several seismological observation, which hint at monsoon, triggered earthquake activity responsible for swarm type activity, the moderate events may have another causal mechanism. There is limited data available pertaining to geomorphic / surface expression of faults in the region, which is crucial for understanding the crustal deformation going on in this seismically active intraplate region. In present paper, we report the geomorphic evidences of active left-lateral strike-slip movement with presence of oblique slip component along a fault (Girnar Fault). The zone of the fault extends for about 60 km in length in NE-SW direction, nevertheless the seismological observations suggests seismicity is only restricted to a length of 40 km. The drainage network of Hiren and Shetrunji rivers show anomalous pattern inform of offset channel, deflected streams and straight channels, which are characteristic signatures of strike-slip faulting, apart from aligned drainages and linear valleys. Unpaired terraces presence in the study area indicates presence of dip slip component along the fault. Our results suggest, factors other than monsoon-triggered seismicity, are also present and active in the region, which might have played a role in causing moderate earthquakes.

Key words: Strike slip fault, Girnar Fault, Intraplate earthquake, Saurashtra, Geomorphic anomaly

INTRODUCTION

The Saurashtra region in western India (Figure 1) is considered as one of the seismically active areas experiencing high rate of intraplate seismicity (Yadav et al., 2011; Rastogi et al., 2013; Singh et al., 2013). Post 2001 Bhuj earthquake, the Saurashtra region has witnessed three moderate seismic events of Mw 4.8 (2007), Mw 5.0 (2007) and Mw 5.1 (2011) (Yadav et al., 2011; Rastogi et al., 2013; Singh et al., 2013). Apart from these moderate seismic events, the region is also experiencing swarm type activity, coincidently after heavy rains (i.e. post monsoon), which has led some to believe that the cause for this seismic activity is monsoon induced (Rastogi et al., 2013; Singh and Mishra, 2015). Yadav et al., (2011) studied the spatial-temporal properties and coulomb stress transfer assessment, where he observed the seismicity to be in NE-SW direction. Rastogi et al., (2013) studied the 2011 earthquake and reported activity along an ENE oriented 40 km long zone. On the other hand, Hainzl et al., (2015) advocated the reservoir-triggered mechanism as cause of the swarm type activity, but also cautioned that the pore pressure changes with depth were of first order approximation and there may exist other mechanisms, which may be responsible for these earthquakes. Most recently, Mahesh and Gupta (2016) studied the Vp/Vs ratios and observed the possibility of crystallized mafic magma at moderate depths that may be responsible for moderate earthquakes and these may be filling fluids to shallow depths, which might be linked to the swarm type activity. Despite these studies, there exist limited attempts or literature pertaining to surface faults and/or its expression in geomorphology (Gandhi et al., 2015). The aim of the present paper is to explore tectonically active geomorphic expression of Girnar Fault using remote sensing techniques.

GEOLOGY AND GEOMORPHOLOGY

The Saurashtra, a horst, mainly enclosed with Mesozoic and Cenozoic rocks is covered by Cretaceous rocks, followed by the Deccan Volcanics, Tertiary and Quaternary sediments (Merh, 1995). Geologically most part of the Saurashtra region covered by the Deccan traps of different phases (Merh, 1995) (Figure 1). The Mesozoic sediments are divisible in to two formations Viz., Wadhwan and Dhrangadhra Formation (Merh, 1995). These sediments are present in the NE part of the Saurashtra (Merh, 1995; Sharma et al, 2017). Tertiary sediments, Gaj and Dwarka Formations are restricted to the coastal areas in the fringed zone of Mesozoic sediments (Merh, 1995, Bhatt, 2003). Tertiary formations are mainly marine to fluvio-marine in origin, which is deposited all along the northern, south-western and southern coast (Merh, 1995). Quaternary sediments are well exposed and are deposited by marine as well as continental processes during Pleistocene and Holocene epochs (Merh, 1995; Bhatt, 2000). The middle

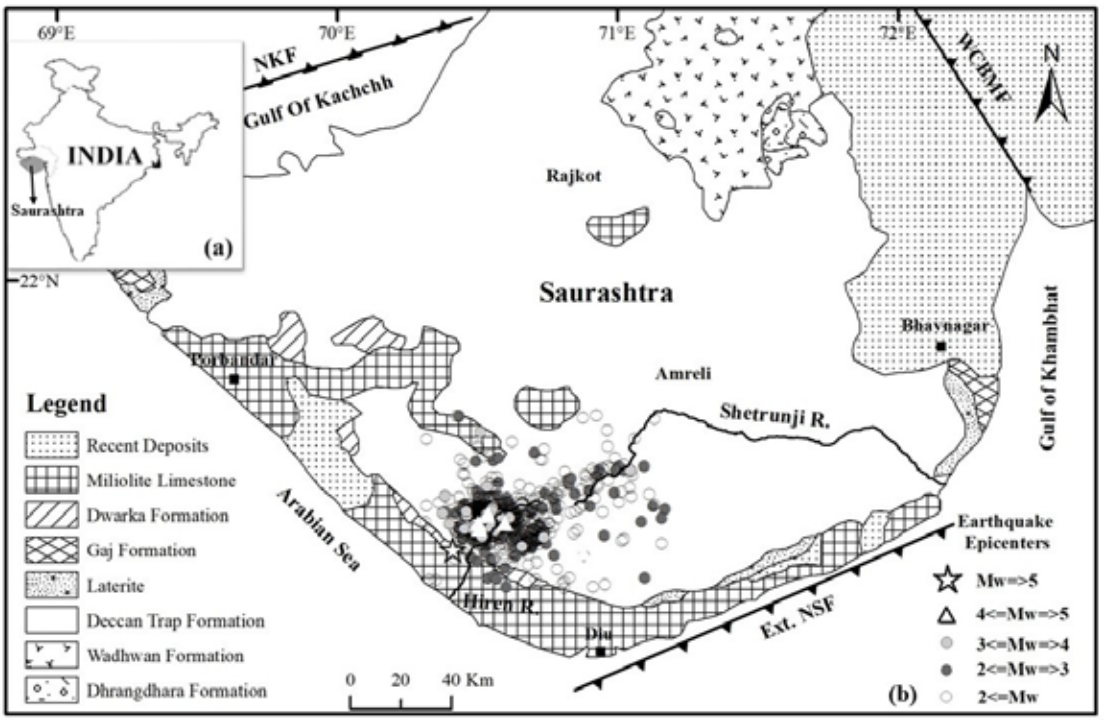

Figure 1. (a) Location map. (b) Geological map of the Saurashtra region and seismicity along Shetrunji and Hiren rivers. (ISR Catalogue 2006-2016). (Modified after Merh, 1995).

Pleistocene sediments - Miliolite Formation is the most striking deposits of Saurashtra, which is unconformably overlie the Tertiary Formations (Merh, 1995). The coastal Miliolite has both marine and aeolian origin, whereas the fluvially reworked Miliolite are found along the river channels (Merh, 1995; Bhatt, 2003). The recent deposits of Saurashtra comprise tidal-flat sediments, unconsolidated sands of present day beaches and fresh water alluvial sediments of major rivers viz., Bhadar, Ojat and Shetrunji Rivers (Merh, 1995; Sharma et al., 2017).

Geomorphologically, Saurashtra shows rocky tilted tableland, which is surrounded by the coastal plains. The centre part of the Saurashtra region shows zigzag outline and rugged topography considerably dissected by various rivers. Overall rivers of Saurashtra region flow out in all directions and exhibit radial pattern. Eastern side of the Saurashtra, which is split up from the Gujarat Mainland in the form of low-lying ground. This low-lying ground is seen as a saline wasteland, marshes and lakes (Merh, 1995). Northern boundary is marked by gulf of Kachchh and west and south boundary is marked by Arabian Sea (Figure 1) (Merh, 1995).

The present study area lies within two fluvial systems, Shetrunji River and Hiren River, where the Gir ranges act as a drainage divide between these two river systems (Figure 2). Gir Range is low mountain range present in the central part of the Saurashtra, is an extremely rugged mountain range with a steep slope towards the south and a gentle slope towards north. Shetrunji R. and Hiren R. systems are perennial and ephemeral in nature respectively. Both the river systems originate from the Dhundhi hills of Gir ranges to flow in the north-easterly and south-westerly directions respectively. The Deccan trap is dominating lithology in the upstream part of both the river systems, which is hilly terrain for both the fluvial systems. Rivers have developed piedmont surfaces along the slopes of the hills, which comprises of rocky clast of basaltic rocks. This is covered by the alluvial surfaces in the lower reaches. Alluvium surfaces are present in the form of valley fill as well as flood plain deposits along the river channels. Sandy beaches and mudflats are present at the mouth of the both the river systems.

Seismotectonics of Saurashtra

During the Late Cretaceous-Tertiary rifting of Narmada basin in the south, the second stage of Cambay rifting and tectonic inversion of Kachchh were responsible for the separation of the Saurashtra block as a horst surrounded by paleo-rifts (Biswas, 1987). These horst and graben structures were formed by reactivation of Precambrian basement trends, NNW-SSE and ENE-WSW (Naini and Kolla, 1982, Biswas, 1987). Geodynamically, the Saurashtra has considered as a seismically moderately active region of Gujarat and falls in the seismic zone III and IV of the seismic zoning map of Bureau of Indian Standards (BIS, 2002).

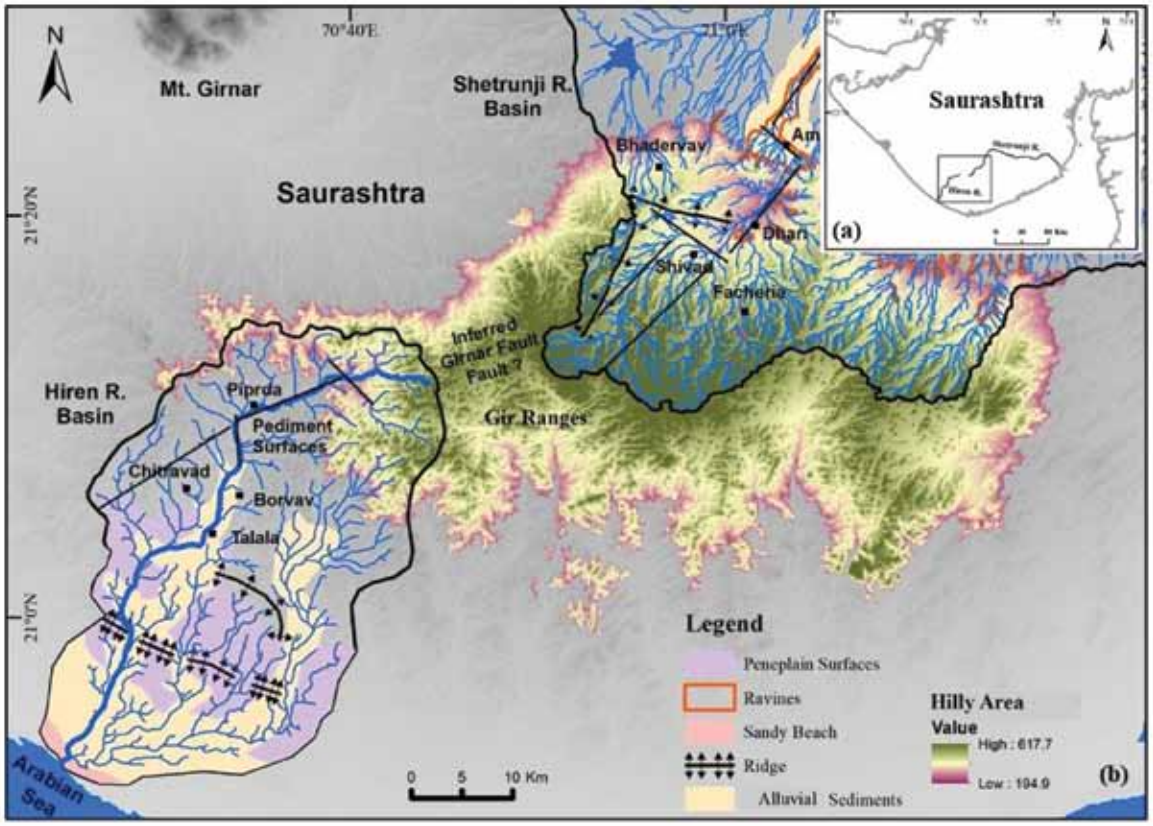

Figure 2. (a) Shows location of the study area (b) Geomorphological map of the study area with probable zone of Girnar Fault.

No major fault systems are present/have been reported, within the Saurashtra Peninsula. However, Saurashtra peninsula is bounded by the major faults namely, North Kathiawar Fault (NKF) to the north, extension of the Narmada Son Fault to the south and the West Cambay Fault System to the east (Figure 1) (Biswas, 1982). The Saurashtra region has witnessed of increasing earthquake activity in the recent past, such as 1872 Bhavnagar (M_w 5), 1883 Bhavnagar (M_w 4.4), 1886 Jamnagar (M_w 4.4), 1887 Rajkot (M_w 4.4), 1891 Amreli (M_w 4.4), 1919 Ghogha (M_w 5.7), 1938 Botad (M_w 5), 1940 Jamnagar (M_w 5), 2007 Talala (M_w 5.0) and 2011 Talala (M_w 5.1) (Bhattacharya et al., 2004, Rastogi et al., 2012; Singh et al., 2013; Mahesh and Gupta, 2016).

Several geophysical studies have been carried out in the Saurashtra region such as gravity and magnetic, which shows that NE-SW, ENE-WSW to E-W, NW-SE and N-S to NNE-SSW trends, as predominant in the entire Saurashtra region (Mishra et al., 2001). NE-SW and E-W structural trends are dominating in eastern Saurashtra (Mishra et al., 2001). Bhonde and Bhatt (2009) studied the joint pattern of the coastal landscape of Saurashtra, which suggest NE-SW pattern is most prominent and is the maximum horizontal compressive stress direction for the Indian subcontinent.

The Talala region of Saurashtra Peninsula situated in the centre part of the Hiren R. basin and 40 km SW from the Shetrunji R. basin. Talala is the main epicentral zone of 2007 (M_w 5.0, M_w 4.8) and 2011 (M_w 5.1) earthquakes. Previous study by using seismological datasets suggest that, these earthquakes occurred along the left-lateral strike-slip component (Yadav. et al., 2011, Rastogi et al., 2012). The aftershock events of 2011 earthquake at Talala region occurred along a 40 km long ENE to NE trending Girnar Fault (ISR Annual Report, 2011) and also its seismological evidence also shows left-lateral strike-slip fault which suggested that the region is neotectonically active (Singh et al., 2013) Mahesh and Gupta (2016) argued that the NNE-SSW trending faults were activated immediate after 2001 Bhuj earthquake (M_w 7.7), because of the stress perturbations.

METHODOLOGY

We used ASTER dataset having vertical resolution of 1arc second to generate a DEM of 30 m resolution. This data set was verified using Survey of India Toposheets of 1:50,000 scale (i.e. ~ 20 m resolution). The datasets were then analysed in ArcGIS 10.4 software on WGS-1984

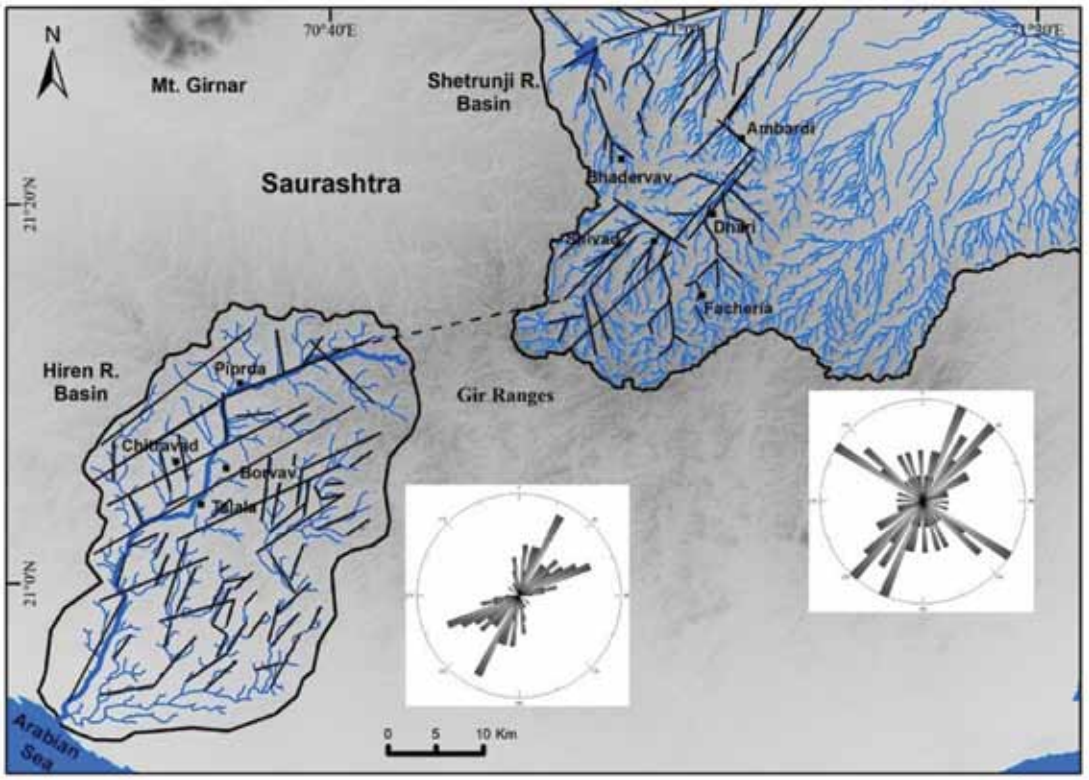

Figure 3. Lineament analysis along Shetrunji and Hiren river basins and rose diagram of those azimuthal distribution.

datum. The drainage network and contours was extracted on Global Mapper-18 for further analysis, which includes Drainage anomaly and lineament study along the probable zone of Girnar Fault.

RESULTS

Lineament Analysis

Lineament analysis of Hiren R. and Shetrunji R. basins were carried out by using ASTER DEM data in combination with Google earth imageries and Survey of India Toposheets. Lineaments were marked based on orientations of straight channel courses, offset in ridges, tonal contrast, deflection in streams and structural alignments. Azimuthal distribution of each lineament plotted as a rose diagram, the main peak of which shows the dominant orientation of lineaments in particular segment.

Girnar Fault mainly passes through the upstream part of the both the river basin, which is mostly covered by the Deccan trap rocks. Therefore, the drainage density in the upstream part is higher as compared to the lower reaches. In the Hiren R. and Shetrunji R., lineaments exhibit mainly three orientations ENE-WSW, NE-SW and NW-SE (Figure 3). Higher order streams reflect the NE-SW trend in both the river basins. Lower order streams reflect very complex orientations. Tributaries of Hiren R. shows NW-SE and NE-SW orientations in the right and left part respectively. With respect to Shetrunji R. basin, tributaries mainly reflect NE-SW orientations. E-W, ENE-WSW and N-S oriented ridges of igneous intrusive bodies are also present in the study area.

Drainage Pattern and Anomaly

Drainage pattern provides clues to *underlying* structure and to the chronology of events (Ouchi, 1985; Twidale 2004). Slope induces the formation of patterns such as parallel, radial and distributary, while structurally controlled regions produces straight, angular, trellis and annular arrangements (Twidale, 2004). Shetrunji R. and Hiren R. flow through two major lithology Deccan Trap and Quaternary sediments. Both the fluvial systems show parallel to sub-parallel and trellis drainage pattern in its upland part. Parallel drainage pattern usually develops in 1) uniform lithology in regional slope direction, 2) Parallel fault system and 3) due to presence of lineaments (Twidale, 2004; Raj, 2007), i.e. faults or fractures. In the eastern side of the Hiren R. drainage basin shows angular drainage pattern. The rivers and its tributaries adjusted with respect to slope and structure due to any catastrophic event such as climatic and tectonic, which is reflected as drainage

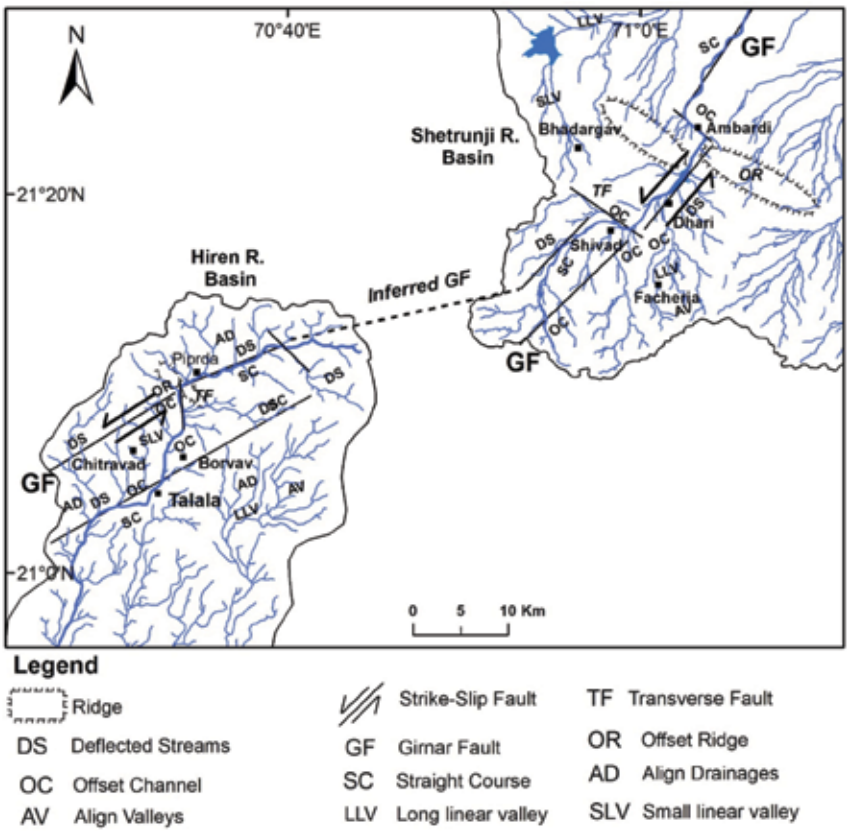

Figure 4. Drainage pattern illustrating sense of movement along the Girnar Fault.

deflection, offsetting or incision (Twidale, 2004). Such climatically governed and tectonically enhanced feature are well preserved in dry land system of western India. These landforms are Deflection Stream (DS), Offset Channel (OC), Small and Long Linear Valleys (SLV, LLV), Aligned Valley (AV), and Aligned Drainage (AD). We have analysed these landforms in study area along drainage network and extracted lineaments (Figure 4).

Hiren River as well as tributaries of all orders shows abrupt change in course along lineaments throughout along the Girnar Fault. All the drainages of Hiren R. from SW of chitravad to Piprda in NE show a deflection in streams under the influence of lineaments. Offset in channel present near Piprda, Borvav and Talala region, which is very well seen in the data along the NE-SW and NW-SE oriented lineaments. Near Bhalchhel, identified the offset in ridge due to NE-SW oriented lineaments. Straight channel courses up to few meter to kilometres is very well preserved in the river basin. Conventionally, Long Linear Valleys (LLV) are formed due to continual movement along the fault which crushes the rock and become more liable to erosion; streams try to flow along this zone of weaknesses and flow some distance along these valleys (Twidale, 2004). LLV is observed eastern side of the Talala region. SLV are observed in those regions where the bedrocks are highly fractured and weathered in nature. More specifically the strength of fractured and weathered rock is very low. However, erosive power of streams increases within the less resistive rocks, which causes river/stream to develop in linear pattern. SLV are preserved near the Chiravad village. Conventionally the AV and AD are associated with head ward erosion within the contractional overstep of a strike-slip fault (Keller, 1986; Raj, 2007). AD and AV are observed in the NW and SE part of the Hiren R. basin. Shetrunji River channel as well as tributaries up to 5th order streams show abrupt deflection (DS) along the lineaments which are lying in NE-SW direction. Major tributaries and associated streams in the upstream part flows in a NW direction and as these stream approaches towards NE-SW oriented Girnar Fault between Shivd and Dhari shows deflection. LLV are observed in the northern part where tributaries flows parallel to a NE-SW oriented lineament. Small Linear Valleys (SLV) are observed in the central part of the segment near the Bhader Gav. The north-easterly flowing streams show a prominent Offset Channel (OC) along E-W trending fault/lineament, near Ambardi village. However, small-scale offset of tributaries have been observed between Facharia and Ambardi villages along E-W and NW-SE oriented faults/lineaments. Near Facharia and Bhader Gav localities SSW oriented Align

Valleys (AV) and Align Drainages (AD) have been observed. Offset in ridge is also observed between Dhari and Ambardi due to NE-SW oriented lineament along the trunk channel.

DISCUSSION

The studies pertaining to relationship between channel orientation and tectonics are still limited. (Ciccacci et al., 1986, Lupia Palmieri et al., 1998, Beneduce et al., 2004, Hodgkinson et al., 2006, Raj, 2007; Ribolini and Spagnolo, 2008). The study area shows very well geometric relationship between drainage style and lineaments in mainly three directions, viz. NE-SW to NNE-SSE, E-W and NW-SE. The NE-SW and NNW-SSE orientations are manifestation of the Aravalli and Dharwarian trend of the Precambrian orogeny (Biswas, 1987). The Girnar Fault mainly passes through the upland part of the both basins (i.e. Shetrunji and Hiran Rivers), orientated in NE-SW trend. These basins reflect parallel to sub-parallel drainage pattern without any lithological change, most likely due to presence of fracture/liniments present in the region i.e. Girnar Fault. Tricart (1974) discussed the offsetting in river channel due to the effect of faults. Several workers used offsetting in channels, deflected streams and displaced terraces and ridges as a tectonic landform to understand strike-slip movements of the fault (Sieh and Jahns., 1984, Gaudemer et al., 1989, Hubert-Ferrari et al., 2002, Lin et al., 2002b, Raj, 2007; Singh, 2014). We have also marked lineaments (E-W, NW-SE, NNW-SSE) which cut the drainage networks and deformed their course in few centimetre scale to few kilometre scale which are discussed as OC, DS, LLV and SLV, AD and AV which clearly indicate that Girnar Fault exhibits left-lateral strike-slip movement, which is also hinted by seismological observations (Singh et al., 2013).

Offsetting in Channel (OC) and Offsetting in Ridge (OR)

The activity of the strike-slip faults can be seen in the form of the Offset Channels (OC). In OC, stream flows in a particular direction and then sudden change occurred due to influence of faults in its course. In Hiren R. basin near Borvav and Talala region biggest offset in channel observed in trunk stream which is due to NE-SW oriented Girnar Fault. Offset in ridge is also observed near the Piprda due to NE-SW oriented Girnar Fault. In the SW corner of the Shetrunji R. trunk stream as well as tributaries of lower order flows in a NNE direction and sudden takes turn in SE direction like near Shivad under the influence of NW-SE oriented lineament/fault which is called an Offset Channel (OC). Trunk stream of Shetrunji R. flows in a NNE direction near Dhari village, in a straight course for up to ~ 11.5 km, then takes 90° turn near Ambardi and flows parallel to the E-W oriented lineament/fault for ~ 3.5 km distance. Its biggest offsetting found in Shetrunji R. basin. After that trunk stream, follow its original trend. Apart from this at many places, we have observed offsetting in streams due to presence of E-W, NE-SW and NW-SE oriented lineament/faults. One E-W oriented ridge is also displaced near northern side of the Dhari, which directly indicate that this fault is left-lateral strike-slip fault. We have also observed unpaired terraces near Ambardi, which also indicate that it has oblique slip movement.

Deflection in Streams

Abrupt deflections of streams along a main lineament are synchronous with strike-slip movements (Raj, 2007). Streams naturally tend to gravitate towards the regional flow direction to meet trunk stream but due to any processes, which causes obstacle/topographic barriers in river path, it tries to cut that barrier if it has a sufficient charge it incised the barriers otherwise it follows that barriers (lineaments) which is deflection from its original course direction (Keller and Pinter, 1996). Hiren R. under influence of the Girnar Fault from south of the Chitravad to north up to Piprda shows deflection. Near Talala and upland part towards Shetrunji R., tributaries flowing in a SE direction also deflected due to NE-SW oriented lineament/ Girnar Fault. In Shetrunji R. basin, streams which are in the eastern part with respect to trunk stream flowing in a SE to NW direction and sudden NE-SW deflection marking the influence of the lineaments, which is clearly visible at and around Dhari village. We have marked major deflections at many places along the NE-SW oriented lineament due to fracture and joint patterns, which is clearly visible in satellite data.

Linear Valleys

Linear valleys are a long narrow depression, developed along the fault zones (Keller and Pinter, 1996); however, it can be also generated along alternate layers of different rock type or different beds of tilted same rock type. These often developed because continued movement along fault traces crushes the rock, making it more vulnerable to erosion. Streams commonly follow these zones of weakness and flow some distances along the through (Keller and Pinter, 1996). The development of linear valleys up to scale of few kilometres in bedrock terrain is often related to presence of faults (Twidale, 2004; Raj, 2007), which we have marked as a Long Linear Valley (LLV). Small Linear Valleys (SLV) are formed due to exploitation of fractures by weathering and erosion (Twidale, 2004; Raj, 2007). LLV are present in the tributaries of both the river basins. In Hiren R., near Talala region we have seen LLV and within Shetrunji R. basin, in the NW corner, its tributaries where linear valleys

are oriented in an ENE to WSW direction with a straight course up to few kilometres, which gives direct relation to subsurface structure. SLV are also present in both the river basins along the fractures and joints.

Align Valleys (AV) and Align Drainages (AD)

Linear Valleys are also marked as an Align Valleys (AV) and Align Drainages (AD) if they are aligning in a one particular direction. In Shetrunji R. basin, AV and AD are observed in the 1st to 3rd order streams at the SE corner and in the central part where they align in the NW-SE to NNW-SSE direction. In Hiren R., we have also observed AV and AD along the proximal zone of Girnar Fault.

CONCLUSIONS

Based on lineament and drainage pattern analysis following are the significant findings of the study

1. Presence of landforms such as offset of drainages, deflection of streams, linear drainages, and straight courses in the vicinity of Girnar Fault zone illustrates the influence of Girnar Fault in the fluvial sequences.

2. The NE-SW trending Girnar Fault extends for about 60 km in length, based on geomorphic expression of landforms such as drainage offset, deflected streams, offset in ridge and unpaired terraces illustrates a left-lateral Oblique slip motion.

ACKNOWLEDGEMENT

TS and SPP would like to thank Director General and Director, ISR for infrastructural support and constant encouragement. We thank Government of Gujarat for financial support. The work is part of doctoral thesis of TS. Nisarg Makwana is thanked for field assistance. We also thank anonymous reviewer for their constructive comments, which improved the manuscript to a great extent.

Compliance with Ethical Standards

The authors declare that they have no conflict of interest and adhere to copyright norms.

REFERENCES

Beneduce, P., Festa, V., Francioso, R., Schiattarella, M. and Tropeano, M., 2004. Conflicting drainage patterns in the Matera Horst Area, southern Italy, Phys. Chem. Earth. Parts A/B/C, 29, 717–724.

Biswas, S.K., 1982. Rift basin in the western margin of India and their hydrocarbon prospects, Bull. Am. Assoc. Pet. Geol., 66(10), 1497-1513.

Biswas, S.K., 1987. Regional tectonic framework, structure and evolution of the western marginal basins of India, Tectonophysics, 135, 307–327.

Bhatt, N., 2000. Lithostratigraphy of the neogene quaternary deposits of Dwarka-Okha area, Gujarat, J. Geol Soc. India, 55, 139-148.

Bhatt, N., 2003. The late quaternary bioclastic carbonate deposits of Saurashtra and Kachchh, Gujarat, Western India, A review, Proc. Indian Nat. Sci. Acad., 69(2), 137-150.

Bhattacharya, S.N., Karanth, R.V., Dattatrayam, R.S. and Sohoni, P.S., 2004. Earthquake sequence in and around Bhavnagar, Saurashtra, western India during August– December 2000 and associated tectonic features. Curr. Sci., 86(8), 1165–1170.

Bhonde, U. and Bhatt, N.P., 2009. Joints as fingerprints of stress in the quaternary carbonate deposits along coastal Saurashtra, Western India. J. Geol. Soc. India, 74, 703-710.

BIS, 2002. Indian standard criteria for earthquake resistant design of structures, Part 1- general provisions and buildings. Bureau of Indian Standards, New Delhi.

Ciccacci, S., Fredi, P., Lupia Palmieri, E. and Salvini, F., 1986. An approach to the quantitative analysis of the relations between drainage pattern and fracture trend. Int. Geomorph., II. Wiley and Sons, Chichester, 49-68.

Gandhi, D., Prajapati, P., Prizomwala, S.P., Bhatt, N., and Rastogi. B.K., 2015. Delineating the spatial variability in neotectonic activity along the southwestern Saurashtra using remote sensing, Zeitschrift fur Geomorphologie, 59(1), 21-36.

Gaudemer, Y., Tapponnier, P. and Turcotte, D.L., 1989. River offsets across active strike- slip faults, Ann. Tecton. 3, 55-76.

Hainzl, S., Aggarwal, S., Khan, P.K. and Rastogi, B.K., 2015. Monsoon-induced earthquake activity in Talala, Gujarat, India. Geophys. J. Int. 200, 627–637.

Hodgkinson, J.H., McLoughlin, S. and Cox, M., 2006. The influence of geological fabric and scale on drainage pattern analysis in a catchment of metamorphic terrain: Laceys Creek, southeast Queenland, Australia, Geomorphology, 81, 394–407.

Hubert-Ferrari, A., Armijo, R., King, G., Meyer, B. and Barka, A., 2002. Morphology, displacement, and slip rates along the North Anatolian Fault, Turkey, J. Geophys. Res., 107(9), 1-33.

ISR Annual Report, 2011. http://isr.gujarat.gov.in/pdf/AnnualreportISR20102011.pdf.

Keller, E.A., 1986. Investigation of active tectonics: use of sur□cial Earth processes. In: Wallace, R.E. (Ed.), Active tectonics. Studies in Geophysics, Natl. Acad. Press, Washington DC, 136–147.

Keller, E.A. and Pinter, N., 1996. Active tectonics: Earthquakes, uplift, and landscape. Prentice Hall, New Jersey.

Lin, A., Fu, B., Kano, K., Maruyama, T. and Guo, J., 2002b. Late Quaternary right-lateral displacement along active faults in

the Yanqi Basin, south eastern Tian Shan, northwest China. Tectonophysics, 354, 157–178.

Lupia Palmieri, E., Centamore, E., Ciccacci, S., D'Alessandro, L., Del Monte, M., Fredi, P. and Pugliese, F., 1998. Geomorfologia quantitative e morfodinamica del territorio abruzzese: II il bacino idrografico del Fiume Tordino. Geografia Fisica e Dinamica Quaternaria 21, 113–129.

Naini, B.R. and Kolla, V., 1982. Tectonics and sedimentation along, the continental margin of western India, Pakistan and adjacent Arabian Sea, Am. Assoc. Pet. Geol. Bull., 66(S), 611.

Mahesh, P. and Gupta, S., 2016. The role of crystallized magma and crustal fluids in intraplate seismic activity in Talala region Saurashtra, Western India: An insight from local earthquake tomography, Tectonophysics, 5, 25.

Merh, S.S., 1995. Geology of Gujarat. Geol Soc Ind., 222 pp.

Mishra, D.C., Singh B.G., Rao, S.B.P., Singh, M.R.K., Chandrasekhar, A.P., Hodlur, D.V., Rao, G.K., Tiwari, M.B.S.V., Laxman, V.M., Venkata, R.G., Kumar, D.Ch., Rajesh, V.P., Babu, R.R.S. and Chetty, T.R.K., 2001. Major lineaments and gravity–magnetic trends in Saurashtra, India, Curr Sci., 80(8), 1059–1067.

Raj, R., 2007. Strike slip faulting inferred from offsetting of drainages: lower Narmada basin, western India. J. Earth System Sci., 116, 413–421.

Rastogi, B.K., Kumar, S., Aggrawal, S.K., Mohan, K., Rao, N., Rao, N.P. and Kothyari, G., 2012. The October 20, 2011 Mw 5.1 Talala earthquake in the stable continental region of India, Nat. Hazards.

Rastogi, B.K., Kumar, S., Aggarwal, S.K., Mohan, K., Rao, N., Rao, P.C. and Kothyari, G.C., 2013. The October 20, 2011 Mw 5.1 Talala earthquake in the stable continental region of India. Nat. Hazards, 65(2), 1197–1216.

Ouchi, S., 1985. Response of alluvial rivers to slow active tectonic movement, Geol. Soc. Am. Bull., 96, 504–515.

Sieh, K.E. and Jahns, R.H., 1984. Holocene activity of the San Andreas Fault at Wallace Creek, California, Geol. Soc. Am. Bull. 95, 883– 896.

Sharma, K., Bhatt, N., Shukla, A.D., Cheong D.K. and Singhvi, A.K., 2017. Optical dating of late Quaternary carbonate sequences of Saurashtra, western India, Quat. Res., 87, 133-150.

Singh, A.P., Roy, G.I., Kumar, S. and Kayal, J.R., 2013. Seismic source characteristics in Kachchh and Saurashtra regions of western India: b-value and fractal dimension mapping of aftershock sequences. Nat. Hazards, 77, 33-49.

Singh, C.K., 2014. Active deformation extracted from drainage geomorphology: a case study from southern sonbhadra district, central India, J. Geol. Soc. Ind., 84, 569-578.

Singh, A.P. and Mishra, O.P., 2015. Seismological evidence for monsoon induced micro to moderate earthquake sequence beneath the 2011 Talala, Saurashtra earthquake, Gujarat. India. Tectonophysics, 661, 38-48.

Tricart, J., 1974. Structural Geomorphology: London, Longman Inc., 305.

Twidale, C.R., 2004. River patterns and their meaning. Earth-Sci. Rev., 67, 159–218.

Yadav, R.B.S., Papadimitriou, E.E., Karakostas, V.G., Shanker, D., Rastogi, B.K., Chopra, S., Singh, A.P. and Kumar, S., 2011. The 2007 Talala, Saurashtra, Western India earthquake sequence: tectonic implications and seismicity triggering. J. Asian Earth Sci., 40(10), 303–314.

Received on: 27.2.18; Revised on: 2.4.18; Accepted on: 18.4.18

J. Ind. Geophys. Union (July 2018)
v.22, no.4, pp: 407-417

Drainage Basin Morphometric Analysis of Mountain-Plain (Kosi, Bihar) and Plateau-plain (Kangsabati, WB) Regions of Tropical Environment: A Comparative Analysis

Avijit Mahala

Centre for the study of Regional Development, Jawaharlal Nehru University, New Delhi, India, 110067.
E-mail: mahala.avijit@gmail.com

ABSTRACT

Morphometric analysis is an important indicator to understand the geomorphic, geologic, hydrological and evolutionary characteristics of any region. In this study, morphometric analysis has been carried out to compare the drainage basin characteristics of mountain-plain and plateau-plain region of tropical India. The Kosi basin of the mountain-plain area and Kangsabati basin of the plateau-plain area, are selected for the present study. The geological, geomorphological, hydrological, fluvial characteristics have been traced from different morphometric parameters for these two different morpho-climatic settings. Different drainage morphometric parameters and measurements related to linear, areal, and relief characteristics have been determined through Shuttle Radar Topography Mission (SRTM GDEM, 90m.) and ARC GIS 10.1. The mean Bifurcation ratio indicates that Kosi has greater flood potentiality than Kangsabati Basin. Kosi carries large amount of water due to its near-circular basin shape, compared to Kangsabati basin which has an elongated shape. All the relief characteristics indicate that the Kosi basin is rejuvenated or at the young stage of geomorphic development, than the mature Kangsabati River basin of plateau region. Most of the morphometric characteristics indicate that there are high geologic and geomorphological controls on river basin characteristics.

Key words: Evolutionary characteristics, Tropical India, Fluvial characteristics, Kosi Basin, Kangsabati basin, Morpho-climatic settings, Relief characteristics, SRTM, Geomorphic development.

INTRODUCTION

The morphometric characteristics of any drainage basin play a significant in understanding the underlying structure, geology, geomorphology, as well as the hydrological characters of any basin. Erosion and deposition of connected stream network produces different fluvial landforms (Joji et al., 2013). Morphology, hydrology and evolutionary history of any basin can be best understood through mathematical morphometric characteristics of such basins (Sharma and Sarma, 2013), wherein the size of the basin, shape and dimension can be evaluated through different morphometric indicators. The relationship between various drainage parameters and its underlying geology, geomorphology, hydrology and structure had been well established through the work of Strahler (1952). Different hydrological behaviour (like peak flow and flooding) of any basin, can be understood through different morphometric indicators of linear, areal and relief parameters. Among the different morphometric characteristics, linear drainage parameters (stream order, stream number, bifurcation ratio, strength length, mean stream length), basin parameters (circularity ratio, elongation ratio, drainage density, drainage frequency), relief parameters (dissection index, ruggedness index, hypsometric characteristics) are considered important. Drainage morphometric analysis is also an important tool to understand the fluvial processes (Chorley et al., 1985; Leopold et al., 1969). Stages of geomorphological evolution or the erosional characteristics can also be well understood through their morphometric characteristics (Strahler, 1952). It provides enormous idea to identify the morphological and hydrological problems and helps with related management procedures. The remote sensing and GIS toll is considered important to study such morphometric characteristics. Recently, several workers have used such data in the analysis of drainage morphometric characteristics (Nag and Lahiri, 2012; Ansari et al., 2012; Magesh and Chandrasekar, 2014).

The Kosi basin, which is representative of the mountain-plain region, is an important basin which has been associated with frequent channel shifting (Singh et al., 1993). Many studies have attributed morphometric characteristics for frequent flooding and river course changes (Sinha, 2009; Shrestha et al., 2010). Further, the distribution of flooding is also suggested to be geological and geomorphological controlled (Jain and Sinha, 2008). Similarly, the Kangsabati basin, which is representative of plateau-plain fringe river basin, has distinct types of morphometric characteristics, where erosional features dominate over an extensive part of the basin. Most of the study in recent past indicate that its mature geomorphological evolution condition is related to its morphometric characteristics (Dutta and Roy, 2012). The changes of morphometric characteristics, together with

Table 1. Morphometric parameters of a river basin

	Parameters	Formula
Linear Aspect	Stream No. (Nu)	Nu = No. of streams of a particular order 'u'
	Bifurcation Ratio (Rb)	Rb = (Nu/Nu+1); where, Nu= Number of streams of a particular order 'u', Nu+1= Number of streams of next higher order 'u+1'
	Mean Bifurcation Ratio (Rbm)	Rbm = Mean of bifurcation ratios of all orders.
	Stream Length (Lu)	Lu = Total length of streams (km) of a particular order 'u'
	Mean Stream Length (Lum)	Lum = Lu/Nu; where, Lu = Total length of streams (km) of a particular order 'u', Nu = Total no. of streams of a particular order 'u'.
	Stream Length Ratio (Rl)	Rl = Lum/Lum+1; where, Lu = Mean stream length of a particular order 'u', Lu + 1= Mean stream length of next higher order 'u+1'.
Areal Aspect	Basin Perimeter (P)	P = Outer boundary of a drainage basin (km)
	Basin Area (A)	Total area of a basin (km^2)
	Form Factor (Ff)	$Ff= A/L^2$; where, A= Area of the basin (km^2), L = Basin length (km).
	Circularity Ratio (Rc)	$Rc = 4\pi A / P^2$; where, A = Area of the basin (km^2), P = Outer boundary of a drainage basin (km).
	Elongation Ratio (Re)	$Re = P / \pi L$; P = Outer boundary of a drainage basin (km), L = Basin length(km).
	Compactness constant (Cc)	$Cc = 0.2821\ P/A^{0.5}$, where, A = Bain area (km^2), P = Basin perimeter (km).
	Constant of channel maintenence (CCM)	CCM = 1/Dd; where, Dd = Drainage density
	Stream Frequency (Sf)	Sf = ∑Nu/A; where, Nu = Total no of streams of a given basin, A = Total area of basin (km^2)
	Drainage Density (Dd)	Dd = ∑Lu/Au; where, Lu= length of streams (km), Au=Basin area (km^2).
	Texture ratio (Rt)	Rt = Nu/p, where, Nu = No. of streams, p = Perimeter of the basin (km).
Relief Aspect	Absolute Relief (R)	Hihest height of the basin
	Relative Relief (H)	H = R-r, where,R = Heighest relief, r = Lowest relief.
	Relief Ratio (Rr)	Rr = (H/L max); where, H= Relative relief (m), L= Length of basin (m)
	Dissection Index (Di)	Di = H/R; H = Relative relief (m), R = Absolute relief (m)
	Ruggedness Index (Ri)	Ri = Dd * H/1000; where, Dd= Drainage density, H = Relative relief.

the changes in geomorphology over this basin, is well-established (Pan, 2013; Gayen et al., 2013).

The present study aims to make a comparative study of different morphometric attributes of these two different basins, which has not yet been carried out. The study also aims to understand the geologic, geomorphic, hydrologic influence on basin morphometry of two basins that fall under two different morpho-climatic setting.

STUDY AREA

The Kosi and Kangsabati basins can be considered environmentally and anthropologically distinct, with spectacular environment (Figure 1). Kosi basin lies in an area of neo-tectonic uplift, associated with Himalayan region. The frequent floods and rapid avulsion changes associated with the Kosi basin are well-known (Sinha, 2009). The River is also known as 'Sorrow of Bihar'. Kosi River enters Bhimnagar after crossing Nepal Himalaya and then it joins Ganga near Kursela, after flowing 320 km in northern Bihar. Kosi is also an example of inland delta building agent (Gole and Chitale, 1966). Kosi changed its main course towards 100 km eastward, through the major avulsion process in August 2008 (Sinha et al., 2008). Kosi had abandoned this path before 200 years ago. Some geomorphologist called the flood of August 2008 as human disaster (Shrestha et al., 2010). In comparision, Kangsabati basin lies in an area under eastern Chotanagpur plateau fringe, which is more or less stable geomorphologically. After originating from 'Ajodhya hill' of eastern Chotanagpur plateau, the river associated with this basin flows through the plateau fringe regions of West Bengal, in an eastward direction (Nag and Lahiri, 2012). Different geomorphic characteristics indicate that the basin is in the mature stage of geomorphic development (Pan, 2013; Dutta and Roy, 2012). Compared to Kosi, Kangsabati basin is less flood-prone, due to its elongated areal characteristics (Gayen et al., 2013).

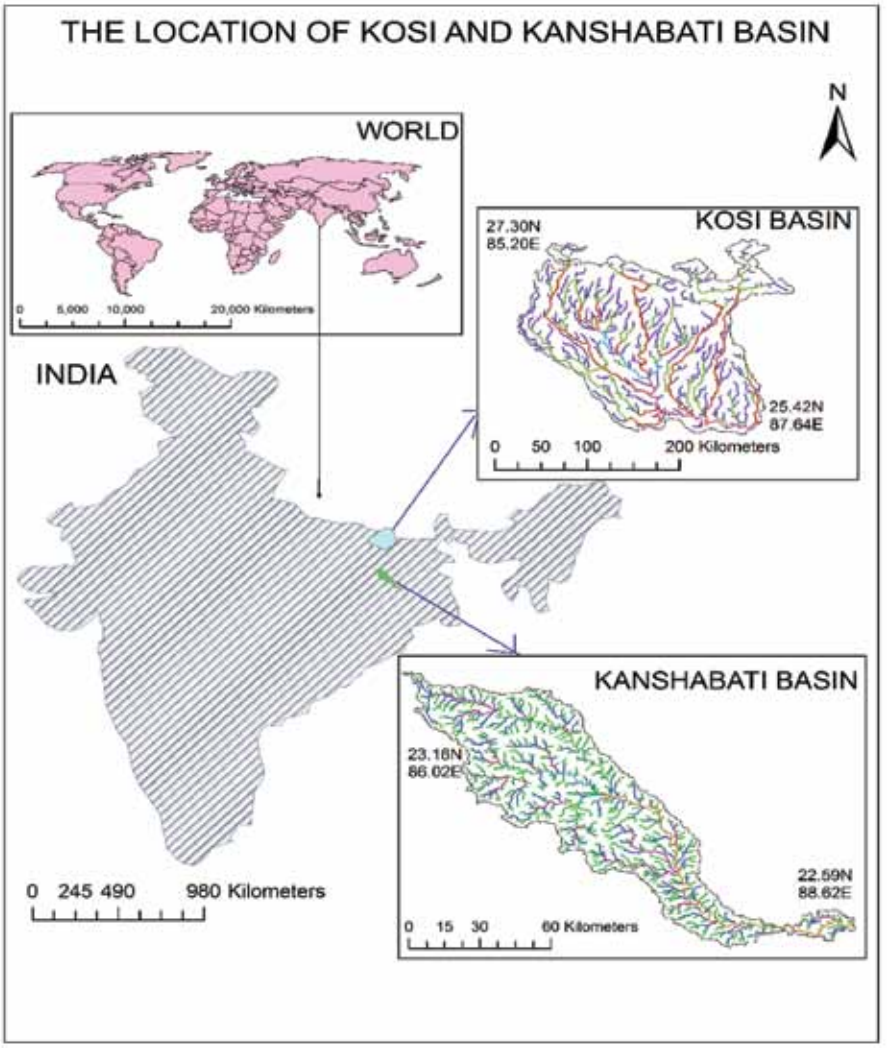

Figure 1. The Location map of Kosi and Kangsabati basins

METHODOLOGY

The measurement of basin morphometry through remote sensing and GIS techniques, followed by their interpretation, are the broad methodology used in the present study. To fulfil the above-stated objective, 'SRTM-GDEM' (30 m.) data has been used for river morphometric analysis, followed by the construction of longitudinal profile. The different basin morphometric parameters have been accessed and calculated through remote sensing and GIS techniques (Table 1) (Figure 2) like, (i) Linear aspect (stream order, bifurcation ratio, mean bifurcation ratio, stream length, mean stream length, stream length ratio, (ii) Areal aspect (stream frequency, drainage density, texture ratio, form factor, circularity ratio, elongation ratio), and (iii) Relief aspect (Relative relief, Relief ratio, Dissection index, Ruggedness index).

RESULTS AND DISCUSSION

Morphometric analysis is a useful tool to understand the hydrological behaviour of sedimentary basins (Castillo et al., 1988; Thomas et al., 2010). It is also useful to understand the underlying geology, structure and geomorphology of the basin (Sharma and Sarma, 2013). Hydro-sedimentary characteristics is also used to quantify the basin characteristics (Raux et al., 2011). Geologically, Kosi basin comes under the Indo-Gangetic plain. Both Himalayan glaciers, as well as precipitation, deeply influence the hydrology of the Kosi River, which is highly notorious due to its high sediment load and migratory trends with antecedent river characteristics. Failure of Kosi embankment and changes in avulsion characteristics is major concerns of recent past. Such phenomena have been interpreted through the local geological adjustment,

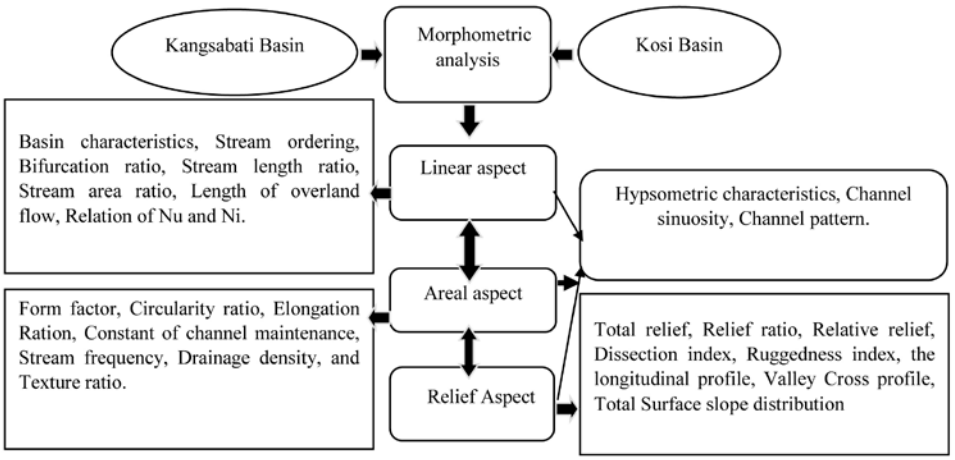

Figure 2. Flow diagram of methodology for drainage morphometric analysis.

Table 2. Linear morphometric aspect of river basins

Morphometric Parameters	**Kangsabati Basin**						**Kosi Basin**						
Stream order (u)	I	II	III	IV	V	VI	I	II	III	IV	V	VI	VII
Stream no. (Nu)	609	279	152	68	25	83	5315	2449	1338	768	551	71	99
Bifurcation ratio (Rb)	-	2.18	1.83	2.23	1.30	0.30	-	2.17	1.83	1.74	1.39	7.76	0.71
Mean bifurcation ratio (Rbm)	1.56						2.6						
Stream length (Lu) in km.	1559	790	350	154	62	194	12396	6595	3463	1756	1327	162	216
Mean stream length (Lum)	2.55	2.83	2.30	2.26	2.48	2.33	2.33	2.69	2.59	2.29	2.41	2.28	2.18
Stream length ratio (Rl)	-	0.90	1.23	1.01	0.91	1.06	-	0.86	1.04	1.13	0.95	1.06	1.04

plate motions and regional geotectonic etc. (Arogyaswamy, 1971; Agarwal and Bhoj, 1992). Recently, Kosi has left its westward extension and flow directly through north-south extension, from Himalayan foothills to Ganga confluence. Whereas, plateau-fringe Kangsabati basin is located in Archaean Gneissic and Schistose terrain. It flows through the semi-arid region of Chotanagpur plateau and receives water from rainfall only. Most of the times, it remains dry (Gayen et al., 2013).

Linear aspects of river basin morphometry

Stream order (Nμ): It is treated as first step of morphometric analysis (Strahler 1952). The smallest tributaries of upper reaches of any basin are named as 1st order streams. The 2nd order of stream forms when two 1st order stream join (Magesh and Chandrasekar, 2014). This stream order depends on basin shape, size and relief characteristics of such basin (Haghipour and Burg, 2014). The total number of streams of Kosi basin are 10591 of which 5315, 2449, 1338, 768, 551, 71, and 99 streams belongs to 1st, 2nd, 3rd, 4th, 5th, 6th, and 7th order respectively (Table 2) (Figure 3). Lower order streams are in higher number due to its mountaineous origin. In general, the number of streams decreases as stream order increase. Kosi enters in north Indian plain after covering Himalayan course. There is sudden decrease in 3rd and 4th order of streams due to this sudden change of slope characteristics. High number of lower order streams (1st, 2nd and 3rd order) increase water receiving amount, which ultimately creates huge water flux on higher order streams (5th, 6th order). On the other hand, Kangsabati basin has total 1216 no. of streams of which 609, 279, 152, 68, 25 and 83 no. of streams belongs to 1st, 2nd, 3rd, 4th, 5th and 6th order respectively (Table 2) (Figure 3). The 1st, 2nd and 3rd order of streams of Kangsabati basin, show less number due to its origin from a matured dissected plateau region. Higher order streams (4th, 5th, 6th order) are less in number due to its plain course. Kangsabati region faces low water pressure or most of times deficient water in its lower reaches due less no. of lower order streams, as well as low water receiving from rainfall.

Bifurcation ratio (Rb): This parameter is defined as the ratio of stream segments of an order to its next higher order. It is considered an important parameter denoting the flood potentiality of any basin. The value normally ranges between 2 to 5 (Joji et al., 2013). High bifurcation value of 1st and 2nd order streams indicate its origin from higher altitude. Less Rb reflects less distorted drainage network and structurally mature condition (Kim and Jung, 2015). The bifurcation ratio for different order of streams in Kosi

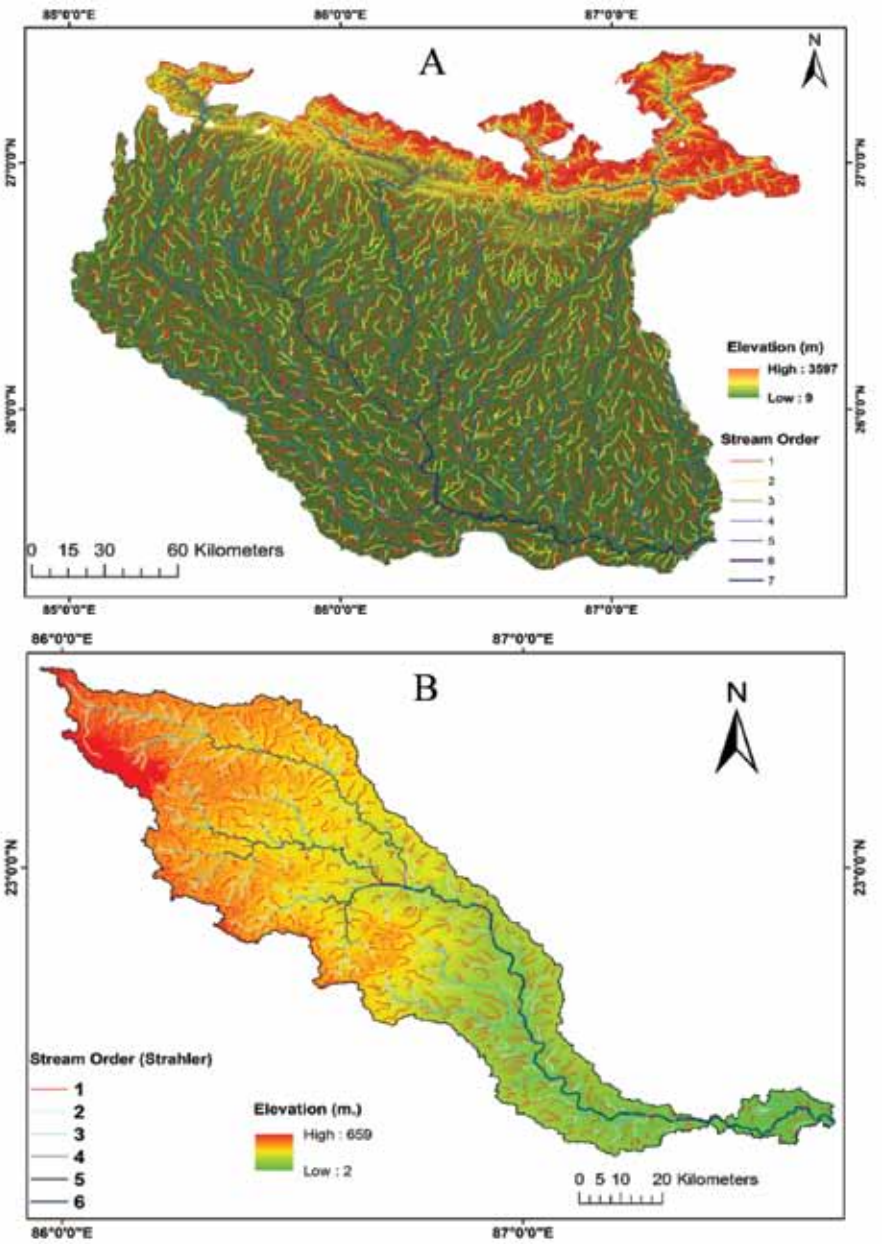

Figure 3. Linear aspect of river basin morphometry. A: Kosi, B: Kangsabati

basin is 2.17 for 1st to 2nd, 1.83 for 2nd to 3rd, 1.74 for 3rd to 4th, 1.39 for 4th to 5th, 7.76 for 5th to 6th, 0.71 for 6th to 7th respectively (Table 2). These values are indicative of inconsistency in structral characteristics. The irregularities are due to geological and lithological discrepancies of the basin. Hence, high bifurcation ratio in higher order streams represent large amount of water collectivity. But, less number of streams available in lower reaches indicates low water carrying capacity. These are supported by its mean bifurcation value which is 2.60. All these ultimately causes heavy flood potentiality in Kosi basin. Whereas, in Kangsabati basin, the bifurcation values are 2.18 for 1st to 2nd, 1.83 for 2nd to 3rd, 2.23 for 3rd to 4th, 1.30 for 4th to 5th and 0.30 for 5th to 6th order stream (Table 2). All these are indicative of its existance in geomorphologically mature area. A constant decrease of Rb throughout the different stream order as well as low mean Rb (1.56) indicates low flood potentiality for the basin.

Stream length (Lu): It is indicative of successive stages of development of stream segments (Castillo et al., 1988). A direct geometric sequence can be approximated from different order stream lengths. The stream length for different stream orders of the present basin is 1st (12396 km), 2nd (6595 km), 3rd (3463 km), 4th (1756 km), 5th (1327 km), 6th (162 km), and 7th order (216 km) (Table 2). The inconsistency of stream length between 6th and

Table 3. Areal morphometric aspect of river basins

Areal aspect	Kosi basin	Kangsabati basin
Basin perimeter (P) (km)	1392	736
Basin area (A) (km^2)	38689	7073
Form factor (Ff)	0.45	0.12
Circularity ratio (Rc)	0.26	0.16
Elongation ratio (Re)	1.52	1.00
Compactness constant (Cc)	2.00	2.46
Constant of channel maintenance (CCM)	1.49	2.27
Stream frequency (Sf)	0.27	0.17
Drainage density (Dd)	0.67	0.43
Texture ratio (Rt)	7.60	1.65

7^{th} order indicates irregularities in basin characteristics. This is also indicative of lithological control on drainage basin. For Kangsabati basin, these are- 1^{st} (1559 km), 2^{nd} (790 km), 3^{rd} (350 km), 4^{th} (154 km), 5^{th} (62 km) and 6^{th} (194Km) (Table 2). The sequence of stream lengths for Kangsabati basin indicates its mature stage of geomorphological evolution.

Mean stream length (Lum): It indicates the characteristic size of drainage network component, which is an important dimensionless component of linear morphometric characteristics. Lum increases with increasing order_of streams in general (Haghipour and Burg, 2014). Table 2 shows the mean stream length of Kosi basin in 1^{st} order (2.33 km), 2^{nd} (2.69 km), 3^{rd} (2.59 km), 4^{th} (2.29 km), 5^{th} (2.41 km), 6^{th} (2.28 km), to 7^{th} order (2.18 km). It indicates youth or rejuvenated stage of geomorphic development. The anomalies are suggesting slope changes and changes in the geological setup, which in turn denotes abrupt changes in flow characteristics. This has also bearing on discrepancies of surface flow discharge and sedimentation. Similarly, the mean stream length for Kangsabati basin are 2.55 km in 1^{st}, 2.83 km in 2^{nd}, 2.30 km in 3^{rd}, 2.26 km in 4^{th} , 2.48 km in 5^{th} and 2.33 km in 6^{th} order respectively (Table 2). The Lum values are more or less similar for plain and plateau areas.

Stream length ratio (Rl): This parameter is an important indicator of surface flow, and discharge characteristics of the basin. It is the ratio between mean stream lengths of one order to the next higher order. Generally, it tends to be similar throughout the different stream orders. The stream length ratio of Kosi basin starts with 0.86 for 1^{st} to 2^{nd} order, 1.04 for 2^{nd} to 3^{rd} order, 1.13 for 3^{rd} to 4^{th} order, 0.95 for 4^{th} to 5^{th} order, 1.06 for 5^{th} to 6^{th} order, and 1.04 for 6^{th} to 7^{th} order (Table 2). The changes in stream length ratio denote that the area is in early stage of geomorphic development and the area have high potentiality of frequent changes in future. Whereas for Kangsabati basin, the Rl is 0.90 for 1^{st} to 2^{nd}, 1.23 for 2^{nd} to 3^{rd}, 1.01 for 3^{rd} to 4^{th}, 0.91 for 4^{th} to 5^{th} and 1.06 for 5^{th} to 6^{th} order of streams respectively. The Rl is more constant in plateau areas (Kangsabati basin) than the plain areas (Kosi basin).

Areal aspects of river basin morphometry

Stream frequency (Sf): It is the number of streams presents in per unit area. It provides drainage basin response to runoff processes. Stream frequency depends on the rainfall, relief, initial resistivity of rocks as well as drainage density of the basin. Lower value of Sf indicates poor drainage network (Thomas et al., 2010). Stream frequency of the Kosi basin is 0.27 (no./km^2), which can be categorized as a moderate stream frequency (Table 3). Such a lower stream frequency is the result of its plain course. Also, lower stream frequency of Kosi basin is the indicative of frequent flood due to its inability to drain the water from large basin. Whereas, the Sf for Kangsabati basin is very low (0.17). The granite-gneiss terrain of this plateau does not permit river to create higher stream frequency. Also semi-arid environment, low relative relief helps for lower Sf in Kangsabati basin.

Drainage density (Dd): This is defined as the ratio of stream length to the basin area. It ranges from 0.27 to 8 km/ km^2 (Joji et al., 2013). The capability of any basin to drains its excess water in monsoon season depends upon the drainage density of the region, which itself depends upon underlain geology, relief, geomorphology, climate and vegetation. In particular, high drainage density increase the water draining capacity of any region or vice-versa. The overall drainage density of Kosi basin is 0.67 (km/km^2), which is very low (Table 3). It shows a direct relationship between drainage frequency and drainage density. High drainage density is found in upper reaches of the basin (Figure 4). It is due to Himalayan location and related high relative relief. Very low drainage density is observed in lower reaches of the plain areas of the basin. Thus, higher

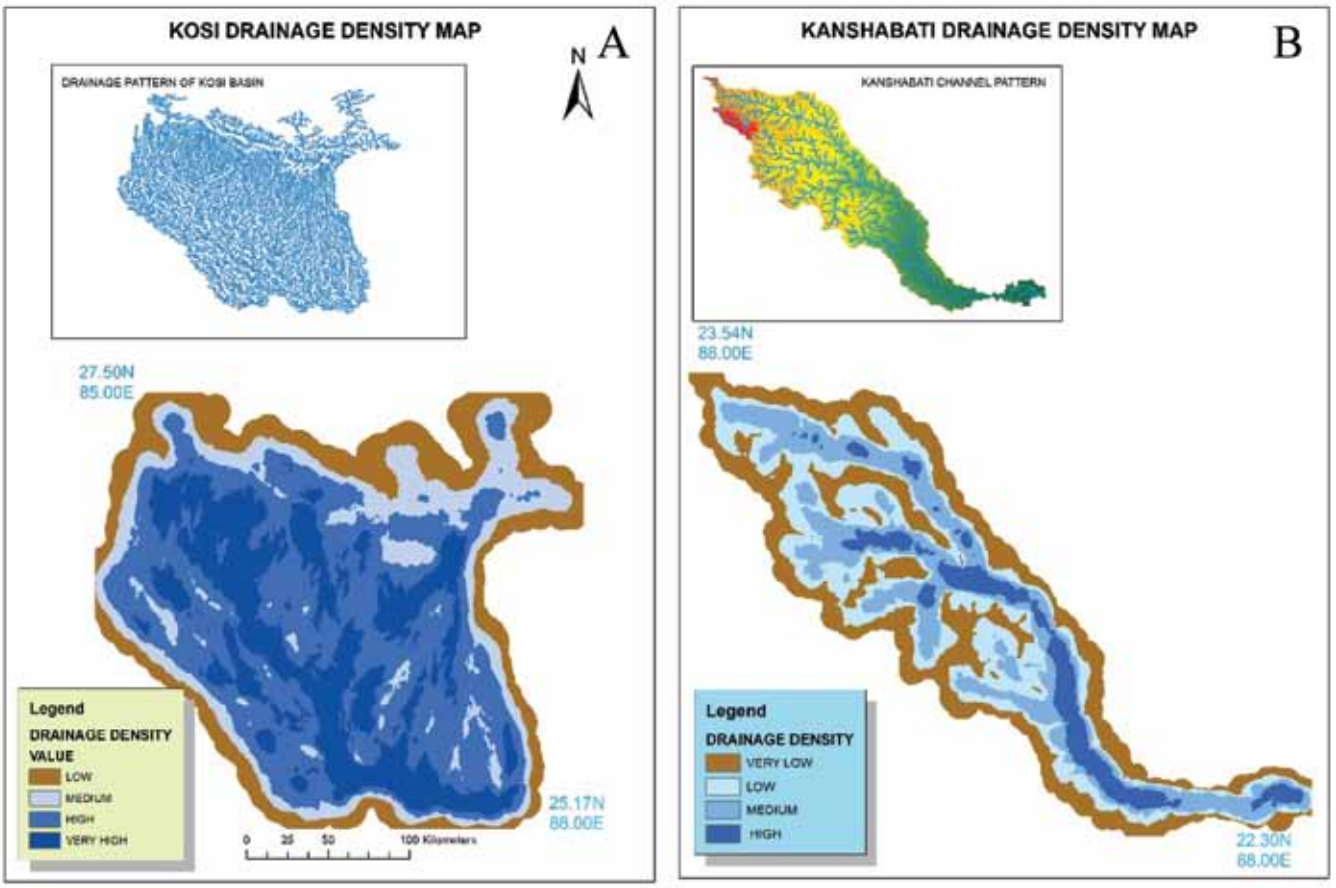

Figure 4. Drainage density characteristics of river basin. A: Kosi, B: Kangsabati.

runoff with greater flow velocity potentiality results into downstream flooding of the basin. Whereas, for Kangsabati basin, the overall Dd is 0.43, which is very low (Figure 4) (Table 3). As discussed earlier, the low relief, low drainage frequency, granite-gneiss geology as well as low vegetation cover and rainfall does not allow the river to increase drainage density. Low drainage density, as well as frequency, is indicative of low draining capacity and frequent flood.

Texture ratio (Rt): It is also an important fluvial parameter, which denotes the relative spacing of drainage network of any basin. It is the product of stream frequency and drainage density (Gayen et al., 2013). Collectively, drainage density and drainage frequency can be called drainage texture. It depends upon number of geological and geomorphological factors. The drainage texture of Kosi basin is 7.60, which indicates coarse drainage texture (Table 3). It is indicative of lower capacity of basin to drain the extra amount of water. Whereas, the Rt of Kangsabati basin is very low as 1.65. It is the result of its elongated basin characteristics, low stream frequency, Archaean geology as well as semi-humid environment.

Form factor (Ff): It is the ratio of the area of basin to the square of basin length, which the flow characteristics of a basin (Castillo et al., 1988). The value '0' indicates elongated characteristics of basin and '1' indicates near circular characteristics of basin, with high peak flow. Flood flows of elongated basin can be easily managed than that of circular basin. The Ff value of Kosi basin is 0.45, which indicates the basin is near circular (Table 3). It also indicates higher peak flow in limited times. Large basin area, with near circular shape and low drainage density, helps Kosi to become an important flood-prone basin in India. Whereas, the Ff value of Kangsabati basin is 0.12. It indicates an elongated shape with less peak flow. Comparatively, small basin area, low rainfall and elongated shape of Kangsabati basin results in low frequency of flood.

Elongation ratio (Re): It is referred as the ratio of diameter of a circle having the same area as of the basin to the maximum basin length (Gayen et al., 2013). It provides idea about the hydrological character of a drainage basin. The value '0' indicates its elongation characteristics, whereas '1' indicates near circularity. The Re value of the Kosi basin is 1.52, which denotes perfect circular characteristics of the basin (Table 3). Kosi have high flood potentiality due to its circular basin shape as well as large

Table 4. Relief morphometric aspects of river basins.

Relief Aspect	Kosi Basin	Kangsabati Basin
Absolute relief (R)	3597	659
Relative relief (H)	3588	657
Relief ratio (Rr)	0.012	0.0028
Dissection index (Di)	0.990	0.996
Ruggedness index (Ri)	2.40	0.282

catchment area. The Re value of Kangsabati basin is 1.00, which indicates its elongated characteristics. Small drainage catchment area and low amount of rainfall helps Kangsabati to become less flood-prone.

***Circularity ratio (Rc)**:* It is defined as the ratio of the area of drainage basin to the area of a circle, having the same perimeter as of basin (Joji et al., 2013). It is a dimensionless quantity. Higher circular basin will be affected by peak discharge in a high rainfall season. The Rc value is mainly concerned with the perimeter and total area of the basin, which ultimately depends upon underlain geology, relief, geomorphology, climatic and edaphic characteristics of the region. The Rc value of the Kosi basin is 0.25, which denotes high peak flood runoff in monsoon season (Table 3). The Rc value of Kangsabati basin is 0.16, which indicates elongated characteristics.

Compactness constant (Cc): It denotes the relationship of circular basin with that of its hydrological characteristics (Haghipour and Burg, 2014). It gives the value equal to unity, if watershed would is nearly circular. The Cc value of the Kosi basin is 2.00, which denotes the flooding potentiality (Table 3). For Kangsabati basin, the Cc value is 2.46.

***Constant of channel maintenance (CCM)**:* It refers to the required minimum area for the maintenance and development of a channel (Dutta and Roy, 2012). It denotes the basin area amount needed for a linear length of the channel. The CCM of the Kosi basin is 1.49 (Table 3). The value shows less channel availability to drain out the excess amount of water. In other words, excess area availability for channel maintenance creates flood situation. The CCM value for Kangsabati basin is 2.27, which indicates slight larger area available to feed a tributary than the Kosi basin. But low rainfall in Kangsabati basin does not create any flood situation.

Relief aspects of river basin morphometry

Basin relief (R, H): Absolute relief (R) and relative relief (H), are important parameters to understand evolutionary characteristics of a basin. For overall basin characteristics, relative relief is important (Gayen et al., 2013). Basin relief depends upon the underlying geology, geomorphology and dissection characteristics of the region. The highest relief of Kosi basin is 3597 m, which is found near Himalayan peak (Table 4). The relative relief is 3588 m., which seems very high for erosional activity. The H value of Kosi shows abrupt changes, when it enters into plain areas of Himalayan foothills whereas, Kangsabati flows through the plateau fringe region. The R and H value for Kangsabati is as lower as 659 and 657 respectively. Dissection hills, undulating plateau are the main landform features in upper reaches of Kangsabati basin. These types of landform increase some amount of relief undulation. But in lower reaches, it is almost flat.

Relief ratio (Rr): *It* denotes the ratio between total relief to the length of principle drainage line (Lindsay and Seibert, 2013). It indicates the overall steepness of the drainage basin and related degradation processes. The Rr of Kosi basin is 0.012, which falls under moderate category (Table 4). Rr is highest in its Himalayan reaches, but as it enters in plain areas, it decrease. The Rr value for Kangsabati basin is as low as 0.0028. Rr is low as it flows the plateau fringe region and enters into the extensive plain in lower reaches. The basin is also prone to waterlogging due to its low Rr value.

Dissection index (Di): It is the ratio between relative reliefs to its absolute relief. It indicates the vertical erosion and dissected characteristics of a basin (Haghipour and Burg, 2014). The stages of landform development of any basin or physiographic region can be accessed through Di. The value of Di ranges between

'0' (absence of vertical dissection) to '1' (Vertical areas). The Di value of Kosi basin is 0.99, which indicate its young or rejuvenated stage of geomorphic evolution (Table 4). It is also indicative of its further development. Whereas, the Di value of Kangsabati basin is around 0.99, which is not because of its young stage of evolution, but due to its greater plain land extension.

Ruggedness index (Ri): This parameter indicates the stages of landform development, as well as instability of the region or basin. The high value of Ri occurs when both drainage density and relative relief are high and slope is also steep (Ansari et al., 2012). This index depends upon underlying geology, geomorphology, slope, steepness, vegetation cover, climate etc. It is measured in consideration of relative relief and drainage density. High values of Ri denotes that the area is more youthful in respect of geomorphic evaluation or vice-versa. The high value of Ri (2.40) for Kosi basin indicates its youthful or

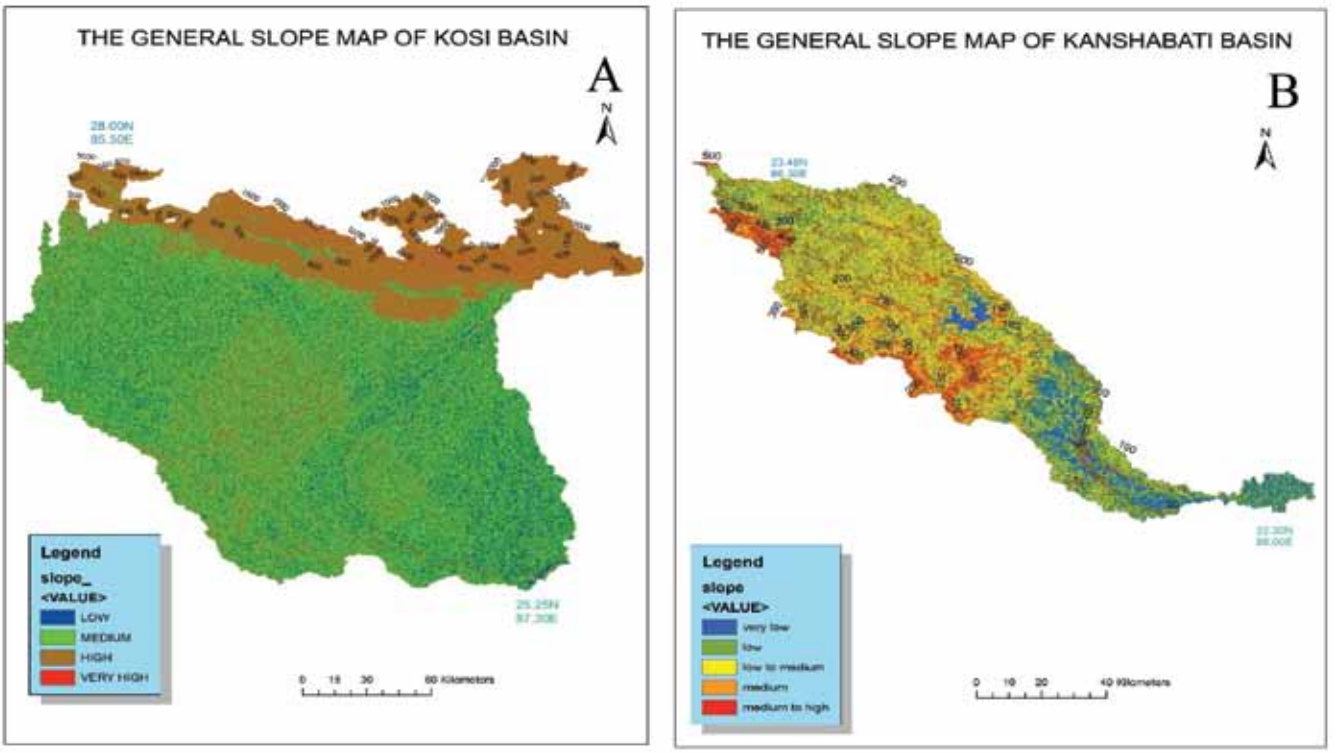

Figure 5. Channel gradient of river basin, A: Kosi, B: Kangsabati.

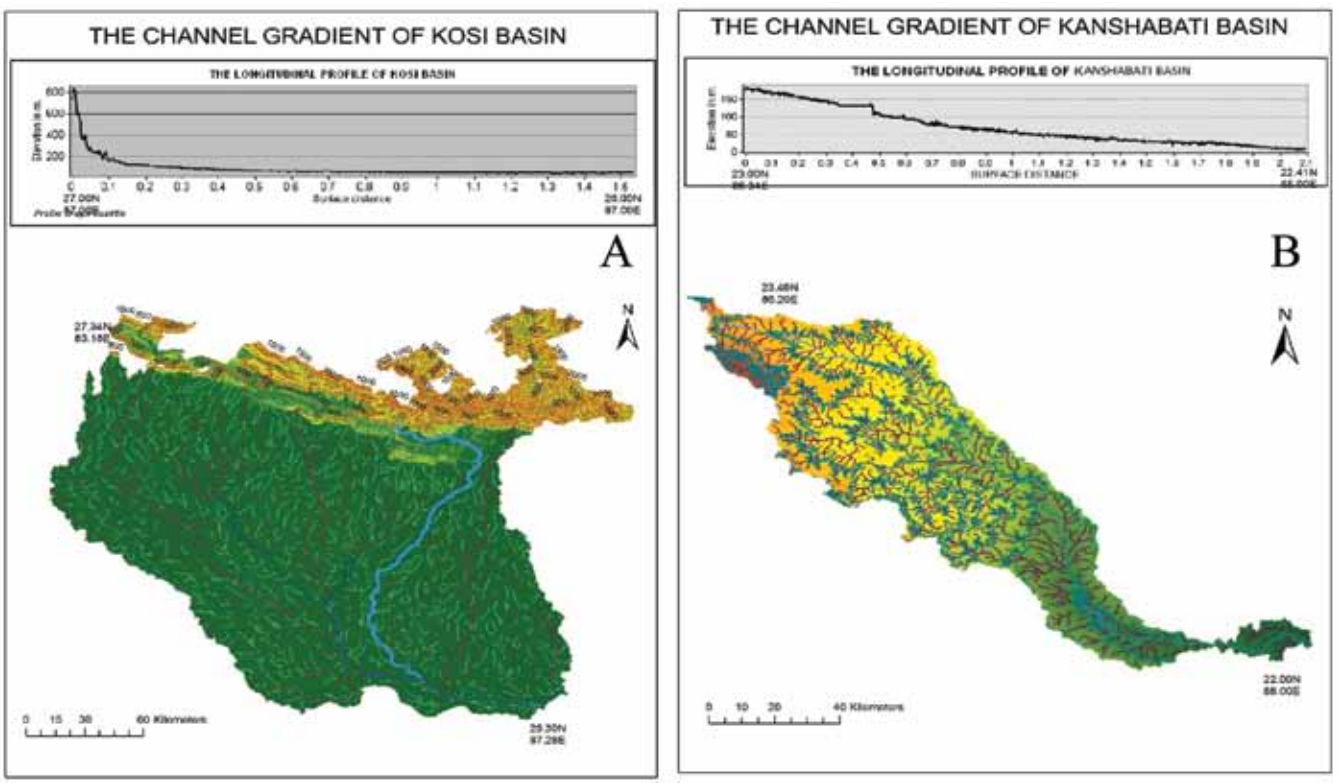

Figure 6. Slope map of river basin, A: Kosi, B: Kangsabati.

rejuvenated stage of basin development (Table 4). The Ri value of Kangsabati is as low as 0.282. After originating from the areas of eastern Chotanagpur plateau, Kangsabati flows through the dissected plateau fringe region in eastward direction. The area is covered by Precambrian gneiss and schists. From millions of years the area converted into a rolling plateau fringe through the erosion of different river and lay in the old stage of geomorphic development.

Channel gradient: This parameter is indicative of the stages of geomorphic evolution, as well as its potentiality for further erosion. The high channel gradient is seen in mountainous course of river and least in plain course of river. It is because of valley deepening is prominent in mountainous course and valley widening is extensive in plain course of river. The Kosi River is almost vertical from source region up to Himalayan foothill areas in its mountain course (Figure 5). Whereas, it is nearly horizontal from Himalayan foothills up to river mouth in its plain course. Such types of gradient characteristics have the potentiality of frequent flooding and consequent embankments failure. Whereas, Kangsabati River, which flows through the plateau fringe, indicates constant slope characteristics in upper reaches of the basin and near flat in lower reaches (Figure 5). As Kangsabati is the representative of mature plateau fringe region, its slope is more or less constant throughout the reaches.

Slope characteristics of any basin represent its overall geomorphic condition. The very high slope (>40°) dominated in the upper reaches of Kosi basin is the true representative primary geomorphic evolution (Figure 6). But slope dramatically decreases as Kosi enters in foothill plain areas. This phenomenon indicates that Kosi high potentiality for further geomorphic development. Whereas for Kangsabati the slope is more or less low (< 10°) throughout the basin indicating low potentiality for further development (Figure 6).

CONCLUSION

The present study is primarily conducted to trace out the morphometric characteristics of two different morpho-climatic settings. From the present study, it can be inferred that different morphometric parameters of any basin are the best representative of geology, geomorphology, relief, slope, climate etc. It is also indicative of the stages of geomorphic evolution of any area. Kosi basin which is representative of the mountain-plain area of tropical environment, has highest number stream order (up to 7th order) related with high amount of water discharge and low-velocity flow, indicating that the basin is highly susceptible to flooding. Rapid decline of bifurcation ratio with increasing order, bears the indication of high susceptible flooding. An anomaly in bifurcation ratio between 6th and 7th order streams, brings strong assumption of current topographic development. The irregular changes of stream length of Kosi river further indicates changes in topography which in turn indicates the younger or rejuvenated stage of Kosi basin development. Whereas, Kangsabati basin which is representative of the plateau-plain region of tropical environment, has low number of stream order and related lower susceptibility to flooding. Less decline of bifurcation ratio, with increasing stream order is indicative of semi-dry region of tropical environment. The mean bifurcation ratio of plateau-plain region of Kangsabati basin is also indicative of low flood susceptible region. The mean stream length and regular changes of stream length ratio are also indicative of mature stages of plateau fringe development.

The calculated value of low drainage density (0.67 km/km^2), low stream frequency (0.27/km^2), and moderate drainage texture (7.60) of Kosi basin indicates the basin has very low relief (plain areas), and low water carrying capacity. All these lead to high overland flow and flood situation. The form factor (0.45), circularity ratio (0.26), elongation ratio (1.52), indicates that the basin is near circular, suggesting it has high flood potentiality and related embankment failure due its large water catchment area. Whereas, very low drainage density (0.43 km/km2), low stream frequency (0.17/km^2) and low texture ratio (1.65) indicates the basin has very mature relief and less water availability about its carrying capacity in Kangsabati basin of plateau fringe region. The form factor (0.12), circularity ratio (0.16), elongation ratio (1.00) indicates the basin is elongated, which is more common in undulating plateau fringe region. The compactness constant (2.46) and constant of channel maintenance (2.27) also supports this view.

The values of relative relief (3588 m.), dissection index (0.990), and ruggedness index (2.40) of mountain-plain flowing Kosi basin indicates the basin is in primary or rejuvenated stages of geomorphic development. The geomorphic and hydrological instability will be more common in future. Whereas in Kangsabati basin, the values of relative relief (657 m.), dissection index (0.996) and ruggedness index (0.282), are indicative of mature stages of geomorphic development.

It can also be concluded that the characteristics of an area regarding its physical (geology, geomorphology, relief, slope), climatological (rainfall, temperature), biological (forest characteristics), can be better accessed through the different morphometric parameters of the basin. These morphometric parameters are the result of aforesaid factors. Remote sensing and GIS can play a significant role in accessing these characteristics. The result can be better utilise for planning and construction purpose.

ACKNOWLEDGEMENTS

The authors are deeply indebted to the University Grants Commission (UGC), Bahadur Shah Zafar Marg, New Delhi-110002, India for the financial support of Junior Research Fellowship (SRF).

Compliance with Ethical Standards

The author declares that he has no conflict of interest and adheres to copyright norms.

REFERENCES

Agarwal, R.P. and Bhoj, R., 1992. Evolution of Kosi river fan, India: structural implications and geomorphic significance, Int. J. Remote Sensing, 13(10), 1891-1901.

Ansari, Z.R., Rao, L.A. and Yusuf, A., 2012. GIS-based Morphometric analysis of Yamuna drainage network in parts of Fatehabad area of Agra district, Uttar Pradesh, J. Geol. Soc. India, 79, 505-514.

Arogyaswamy, R.N.P., 1971. Some geological factors influencing the behaviour of the Kosi. Records Geol. Sur. India, 96, 42-52.

Castillo, V., Diaz segovia, A. and Alonso, S.G., 1988. Quantitative study of fluvial landscapes, case study in Madrid, Spain, Landscape and Urban Planning, 16, 201-217.

Chorley, R.J., Schumm, S.A. and Sugden, D.E., 1985. Geomorphology. London: Methuen and Co. Ltd.

Dutta, S. and Roy, S., 2012. Determination of erosion surfaces and stages of evolution of Sangra drainage basin in Giridih district, Jharkhand, India, Int. J. Geomat. and Geosci., 3(1), 63-73.

Gayen, S., Bhunia, G.S. and Shit, P.K., 2013. Morphometric Analysis of Kangsabati-Darkeswar Interfluves Area in West Bengal, India using ASTER DEM and GIS Techniques, Geol. and Geosci., 2(4), 1-10.

Gole, C.V. and Chitale, S.V., 1966. Inland delta building activity of Kosi River, J. Hydraulics Division, 92, 111-126.

Haghipour, N. and Burg, J.P., 2014. Geomorphological analysis of the drainage system on the growing Makran accretionary wedge, Geomorphology, 209, 111-132.

Jain, V. and Sinha, R., 2003. Geomorphological manifestations of the flood hazard: A remote sensing based approach, J. Geocarto Int., 18(4), 51-60.doi.org/10/1080/10106040308542289.

Joji, V.S., Nair, A.S. and Baiju, K.V., 2013. Drainage basin delineation and quantitative analysis of Panamaram watershed of Kabani river basin, Kerala using remote sensing and GIS, J. Geol. Soc. India, 82, 368-378.

Kim, J.C. and Jung, K., 2015. Fractal Tree Analysis of drainage patterns, Water Res. Manage., 29, 1217 – 1230.

Leopold, L.B., Wolman, M.G. and Miller, J.P., 1969. Fluvial processes in geomorphology. New Delhi: Eurasia Pub. House.

Lindsay, J.B. and Seibert, J., 2013. Measuring the signi□cance of a divide to local drainage patterns. Int. J. Geogra. Infor. Sci., 27(7), 1453–1468.

Magesh, N.S. and Chandrasekar, N., 2014. GIS model-based morphometric evaluation of Tamiraparani sub-basin, Tirunelveli district, Tamil Nadu, India, Arab. J. Geosci, 7, 131 – 141.

Nag, S.K. and Lahiri, A., 2012. Hydrochemical characteristics of groundwater for domestic and irrigation purposes in Dwarakeswar watershed area, India, Am. J. Climate Change, 1, 217-230.

Pan, S., 2013. Application of remote sensing and GIS in studying changing river course in Bankura District, West Bengal, Int. J. Geomatics and Geosci., 149-163.

Raux, J., Copard, Y., Laignel, B., Fournier, M. and Masseï, N., 2011. Classification of worldwide drainage basins through the multivariate analysis of variables controlling their hydro sedimentary response, Global and Planet. Change, 76, 117-127.

Sharma, S. and Sarma, J.N., 2013. Drainage analysis in a part of the Brahmaputra valley in Sivasagar district, Assam, India, to detect the role of nontectonic activity. J. Ind. Soc. Remote Sens., 41(4), 895 - 904.

Shrestha, R.K., Ahlers, R., Bakker, M. and Gupta, J., 2010. Institutional dysfunction and challenges in flood control: A case study of the Kosi flood 2008, Eco. Pol. Weekly, 2, 45-53.

Singh, H., Prakash, B. and Gohain, K., 1993. Facies analysis of the Kosi megafan deposits, Sedimentary Geol., 85(1-4), 87-113.

Sinha, R., 2009. Dynamics of a river system – the case of the Kosi river in north Bihar. Earth Sci. India, 2, 33–45.

Sinha, R., Bapalu, G.V., Singh, L.K. and Rath, B., 2008. Flood risk analysis in the Kosi river basin, north Bihar using multi-parametric approach of analytical hierarchy process (AHP), J. Indian Soc. Remote Sens., 36, 335-349.

Strahler, A.N., 1952. Hypsometric analysis (area-altitude) of erosional topography. Bull. Geol. Soc. Am., 63, 117-142.

Thomas, J., Joseph, S. and Thrivikramaji, K.P., 2010. Morphometric aspects of a small tropical mountain river system, the southern Western Ghats, India. Int. J. Digital Earth, 3(2), 135-156.

Received on: 3.4.18; Revised on: 3.5.18; Accepted on: 15.5.18

J. Ind. Geophys. Union (July 2018)
v.22, no.4, pp: 418-424

The observational case study of total columnar ozone associated with meteorological synoptic conditions over the Indian peninsular station

M.N. Patil*, G.S. Meena, G. R. Chinthalu, T. Dharmaraj and Devendraa Siingh

Indian Institute of Tropical Meteorology, Pune - 411008, India
*Corresponding Author: patil@tropmet.res.in

ABSTRACT

The Total Columnar Ozone (TCO_3) was measured over the rural site of Mahabubnagar of south India, as a part of Cloud Aerosol Interaction and Precipitation Enhancement Experiment – Integrated Ground Observations Campaign (CAIPEEX-IGOC), during October-November 2011. Along with TCO_3, the collocated high resolution profiles of air temperature, water vapor and wind speed up to mid-stratosphere (~ 30 km) was also obtained by GPS Sonde. The TCO_3 variations show higher amount of TCO_3 in the morning hrs than that of evening hrs. Also a sudden reduction of TCO_3 of the order of 100 - 110 DU in 12 h time scale was observed.

Key words: Total column ozone, cyclonic storm, Atmospheric chemistry, Atmospheric electricity, CAIPEEX.

INTRODUCTION

Ozone is very rare gas in the atmosphere, but plays a vital role with the human life. The ozone layer in the stratosphere around the globe absorbs most of the biologically damaging ultraviolet sunlight and filters them from reaching the ground and thereby protects the whole biosphere from its harmful effect (Kondratyev and Varotsos, 1996; Katsambas et al., 1997). On the other hand, tropospheric ozone is a strong contributor to the global warming. At the earth surface, ozone plays a destructive role as its high levels are toxic to living systems and have harmful effect on the crop production. The changes in total ozone influence the biologically active UV radiation (Calbo et al., 2005), and since the detection of the Antarctic ozone hole, the development on monitoring the Earth's ozone has been a key focus in atmospheric research (Farman et al., 1985). Ozone occurs naturally at ground-level in low concentrations.

There is a large latitudinal variation in ozone concentrations worldwide, generally depicting high values in polar region and low in the tropics. On a seasonal timescale, the total ozone content in the atmosphere is controlled by both transport of ozone within the stratosphere and photochemical processes. Daily tropospheric ozone data derived from Aura OMI (Ozone Measuring Instrument) and MLS (Microwave Limb Sounder) measurements found lowest global values of tropospheric ozone (20 DU or less) over the broad tropical Pacific and in the southern polar region in summer and autumn months (Ziemke et al., 2006). The OMI/MLS tropospheric ozone climatology exhibits large temporal and spatial variability which includes ozone accumulation zones in the tropical south Atlantic year-round and in the subtropical Mediterranean/Asia region in summer months (Ziemke et al., 2011). High levels of tropospheric ozone in the Northern Hemisphere also persist in mid-latitudes over the eastern part of the North American continent extending across the Atlantic Ocean and the eastern part of the Asian continent extending across the Pacific Ocean; and the largest stratospheric ozone lies in the Northern Hemisphere and extends from the eastern Asian continent eastward across the Pacific Ocean and North America (Ziemke et al., 2011). The systematic seasonal variation pattern of TCO_3 could be due to the general circulation pattern in the stratosphere (Raj et al., 2004). Over the Antarctic region, a study shows the possibility of precipitating charged particles role to decrease short-lived ozone through production of OH radical (Sonbawne et al., 2009). Atmospheric composition has changed significantly over the past few decades from increasing urbanization and as a response to environmental policy changes (Wenig et al., 2003; Vingarzan 2004; Parrish et al., 2009). In the present scenario, with increasing populations, more automobiles and industries contributed for the increasing ozone in the lower atmosphere. The ozone which is a byproduct of certain human activities does become a problem at ground level.

Over the Tibetan Plateau region, lower value of total ozone of ~190 DU reported by Bian et al., (2006). Such rapid and localized reduction and recovery in TCO_3 (1000-3000 km spatial and 1-5 days time scale) is referred as an 'ozone mini hole' event (Newman et al., 1988). Such events have frequently been observed throughout in the mid-latitudes of both the hemisphere with greater frequency over North Atlantic European sector (James 1998a; James 1998b). The dynamic processes contributing to ozone mini hole in high latitudes of Europe have been well documented on the meridional transport of sub-tropical ozone poor air

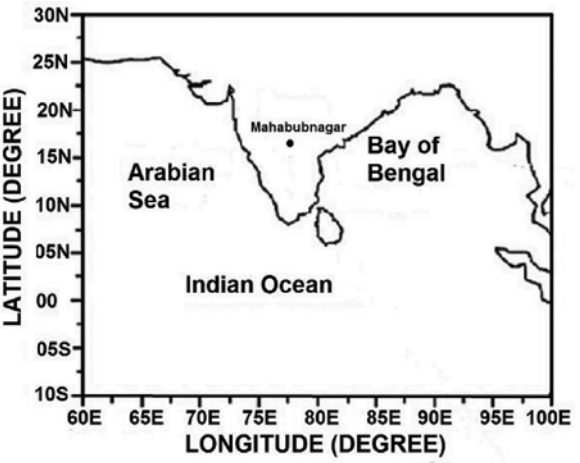

Figure 1. Map showing the location of experimental site (Mahabubnagar).

near the tropopause air and divergence of ozone rich air out of the air column in the lower troposphere (Koch et al., 2005; Keil et al., 2007). In the Asian continent, over Tibetan Plateau, such reduction of TCO_3 was observed, which attributed to the ozone reduction in upper troposphere and lower stratosphere region (below 25 km). This region generally caused by up-liftment of the local tropopause and northward transport of tropical air which contain low ozone concentrations associated with an anomalous anticyclone in the upper troposphere (Liu et al., 2010). In this paper, we explore high-resolution measurements of TCO_3 using ground-based portable spectrometer and air temperature, water vapour and wind speed observations with GPS radiosonde. An attempt has been made to investigate the local distribution of TCO_3 associated with the cyclonic storm formed in the Arabian Sea.

DATA AND METHODOLOGY

The Portable spectrometer (UV-VIS-NIR Range) and GPS radiosonde systems were installed over a station Mahabubnagar (16.44° N, 77.59° E, 498 m a.s.l.) in south India in the October-November 2011 as a part Cloud Aerosol Interaction and Precipitation Enhancement Experiment – Integrated Ground Observations Campaign (CAIPEEX-IGOC). The measurement site is in the outskirt of the city having rural characteristics. The location of experimental station is shown in Figure 1.

Ground-based observations of zenith-sky scattered sunlight were performed (Meena et al., 2016). The spectrometer used in the present study, is a high-spectral resolution spectrometer Model HR2000, manufactured by Ocean Optics, Dunedin, Florida, USA. It is the first model of a new line of modular optical bench spectrometers. It is a modular spectrometer having high-optical resolution of 0.035 nm and focal length of 101.6 mm at 5f/4, works on symmetrical crossed Czerney-Turner optical design. The high-reflectivity AgPlus mirrors facilitates high-resolution measurements in low-light level situations. Moreover, it is extremely low power (~ 05 W) device. The detector is a linear CCD array with 2048 pixels (each 14 μm × 200 μm). The instrument has been mounted on the top roof stairs of a 20 m tall building. The scattered sunlight is received by a telescope with 46 mm diameter and 300 mm focal length, and lead to spectrometer through a quartz fiber. Observations of TCO_3 from spectrometer were taken for half an hour just after the sunrise and before sunset period for the zenith angle between 85° – 90°. The spectrometer data are analyzed using Differential Optical Absorption Spectroscopy (DOAS) technique. Absorber (trace gas) concentration n is derived from Lambert–Beer's law as

$$I = I_o \exp(-\sigma n l) \quad \text{.....(1)}$$

Where, I is the measured spectrum intensity (i.e., zenith sky scattered light intensity) at the ground, I_o is the reference spectrum intensity outside the atmosphere, however, it is difficult to measure the spectra outside the atmosphere. Therefore, noon time spectrum is taken as a reference spectrum, l is the optical path length (cm), σ is the absorption cross section (cm^2 $molecule^{-1}$) of the absorbing molecule and n is the absorber concentration (molecules cm^{-3}). To obtain the vertical profiles of winds, temperature and dew point (water vapor), the Vaisala make GPS upper-air sounding system was used. The synoptic weather analysis by India Meteorological Department shows that a low level cyclonic circulation was existed over the southeast and adjoining east-central Bay of Bengal from October 12, 2011 onwards (India Meteorological Department, 2012). There was an active east-west shear zone passing through this circulation. As a result, the low level relative vorticity and convergence was increased. The upper tropospheric ridge at 200 hPa level was to far north of the area of circulation (around 19° N on October

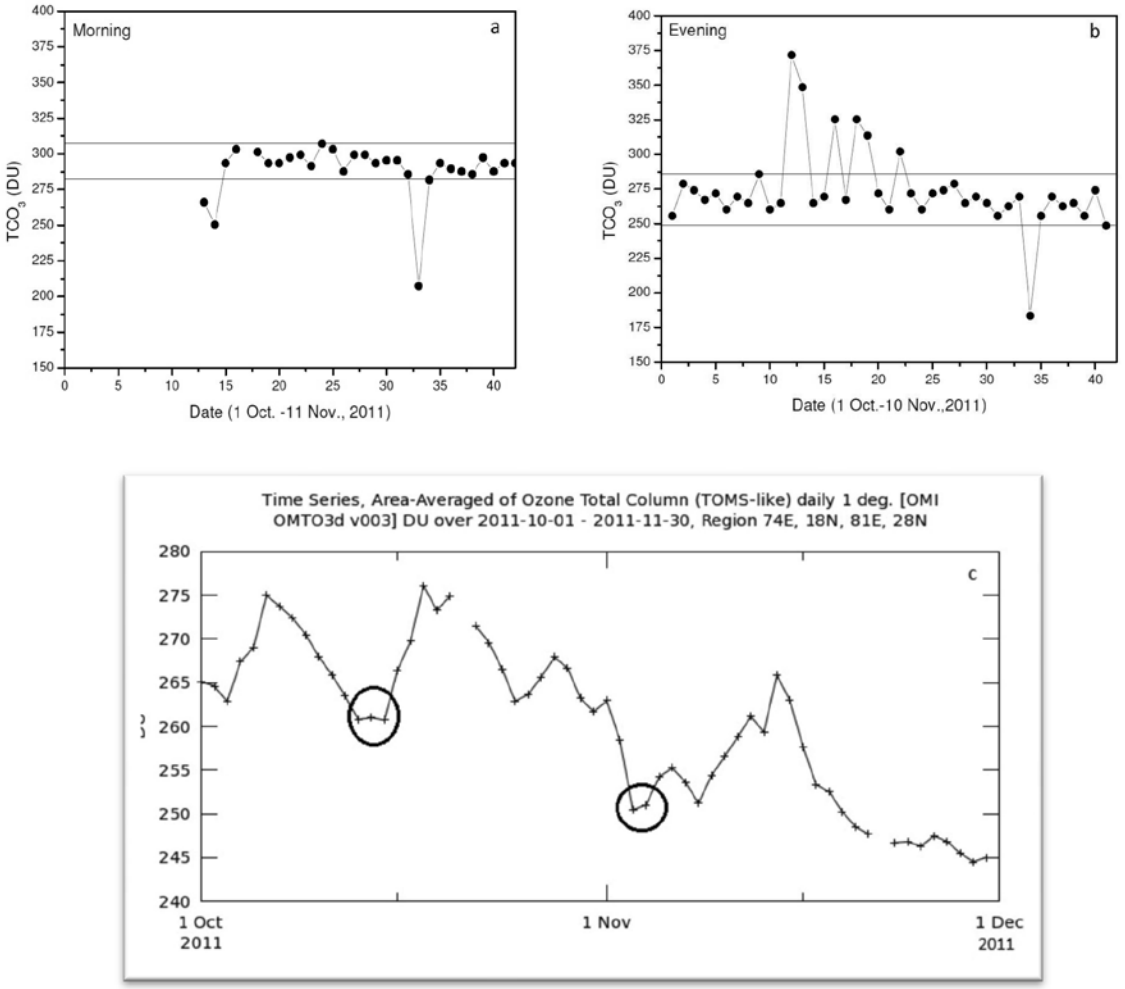

Figure 2. Daily variation of TCO_3 during the (a) sunrise (b) sunset period and (c) day to day observations of TCO_3 over Indian subcontinent from 1 October to 30 November 2011 by OMI.

15, 2011) and provided the required divergence over the region. The cyclone, Banyan over the South China Sea existed as a depression near 17.5° N and 116° E on October 14, 2011 and became less marked on October 15, 2011. Under the influence the cyclonic circulation, a low pressure area formed over the Bay of Bengal region with associated cyclonic circulation extending up to mid tropospheric level on October 17, 2011. It became well marked over east central and adjoining north and west central Bay of Bengal on October 18, 2011. The well marked low pressure area was concentrated into a depression over north Bay of Bengal and centered at 00 UTC of October 19, 2011 over north Bay of Bengal near latitude 20° N and longitude 90.5° E.

RESULTS AND DISCUSSION

During the observational period, the TCO_3 concentration was ranging from 183.5 to 371.5 DU (Figure 2 a, b). The monthly mean of TCO_3 for October 2011 was 284.82 DU. In the earlier study (Kalita et al., 2011), based on satellite observations, the monthly mean of TCO_3 over the nearby area of observational site was in the range of 255-260 DU for the months of October 2007. The difference of ~30 DU in the satellite observed TCO_3 and measured by the ground based remote sensing instrument in the present study could be due to the different instrumentations and methodology adopted in both the studies.

During the sunset of October 12, 2011, the TCO_3 was increased to 371.7 DU from its previous concentration of 264.9 DU, sudden rise of TCO_3 is 106.8 DU in 12 h. Similarly, during sunrise of November 2, 2011, the TCO_3 was 285.7 DU which suddenly reduced to 183.5 DU in the sunset showing sudden fall of 102.2 DU in just 12 h. The largest 24 h change (sunset to sunset) in TCO_3 concentration was found to be 107.7 DU, whereas it was 75.0 DU during sunrise to sunrise. As seen in Figure 2b, six days with greater TCO_3 concentrations, recorded during the sunset time from October 12-22, 2011. These days were

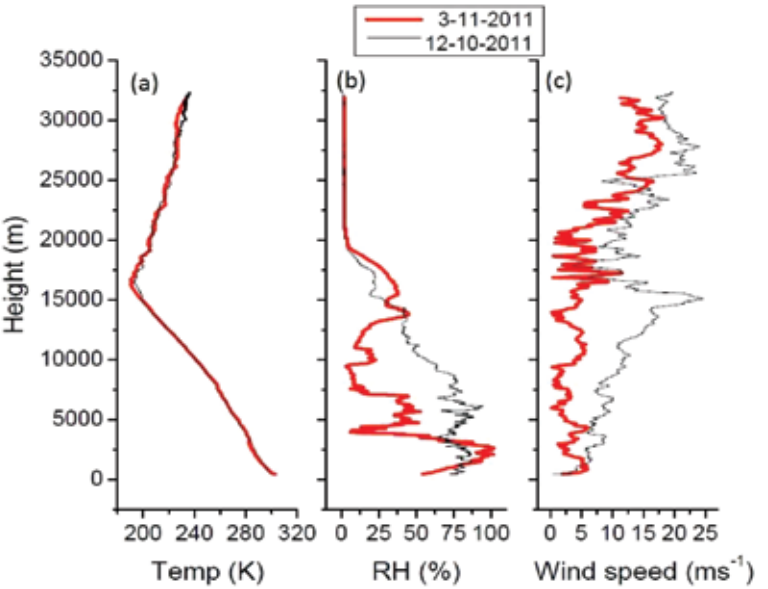

Figure 3. Air temperature (a), relative humidity (b) and wind speed (c) profiles observed on October 12, 2011 and November 3, 2011.

associated with the cyclonic synoptic weather conditions over the Indian subcontinent. The development of low pressure system in the Bay of Bengal could have played the role in exchanging air mass. The greater amount of ozone (~ 90%) is mainly found in the lower portion of the stratosphere (20 - 30 km), though its thickness varies seasonally and geographically. Hence, it is important to look change in relevant parameters with respect to TCO_3 in this region. To show this, one day with high TCO_3 concentration (October 12, 2011) and one day with low TCO_3 concentration (November 2, 2011) was selected. The TCO_3 concentration was low (183.5 DU) on November 3, 2011, evening and it was high (371.7 DU) on October 12, 2011 evening. Daily time series of total column ozone (Toms-like) (OMTO3d v003) with 1 degree spatial resolution (source OMI) derived from Giovanni data for the period of 1 October – 30 November 2011 are shown in Figure 2c. This time series also show the reduction of TCO_3 around 12 October 2011 and 3 November 2011. We do not found any significant change in the observed air temperature in lower stratospheric region on the above two days (Figure 3a). It is seen that, on the day of high TCO_3, there was an increase in the water vapor in the mid to upper troposphere (4-14 km) region (Figure 3b).

Also, the wind speed was very high from surface to lower stratosphere (Figure 3c). The opposite scenario, i.e., low water vapor in the mid -to- upper troposphere and low wind speed in troposphere and stratosphere, was observed on a day of low TCO_3.

To verify the synoptic feature, the cloud pictures for those two days are shown in Figure 4 (a-b) associated with lightening events (Figure 5). There was less cloudiness (Figure 4a) and less number of lightening events (Figure 5a) on the day of low TCO_3 concentration. On the contrary, there was greater cloudiness (Figure 4b) and high lightening events (Figure 5b) on the day of high TCO_3 concentration.

Thus, the synoptic weather conditions may have played a significant role in enhancing the TCO_3 concentrations drastically. As shown in Figure 2, during October 31, to November 4, 2011, the TCO_3 concentration was fluctuated from 183.6 to 293.5 DU. It is seen that a sudden reduction (78.3 DU) in TCO_3 concentration was observed from the morning of November 1 and November 2, 2011. It was further increased by 74.4 DU on morning of November 3, 2011. In the evening of November 3, 2011 the TCO_3 was again decreased by 98.2 DU and the concentration was 183.6 DU. Again in the morning of November 4, 2011 it increased by 109.9 DU and the concentration was 293.5 DU. This sudden reduction in the TCO_3 concentrations is likely to resemble with the localized ozone mini hole (Figure 2a,b). We cannot attribute this reduction to the cyclone formed in the Arabian Sea, but it was associated with the transition of cyclonic storm 'Keila' in the Arabian Sea. A cyclonic storm 'Keila' developed over the southeast Arabian Sea with genesis of depression on October 29, 2011. It moved initially west-northwestwards and then northwestwards and crossed Oman coast close to north of Salalah as shown in Figure 6.

It then emerged into Arabian Sea and dissipated gradually. The track of the cyclone 'Keila' was rare in nature as it made a loop after the landfall over Oman near Salalah. One speculation is that, this cyclone could have pooled the ozone rich air from the observational site and later, the air mass over the observational site is replaced with

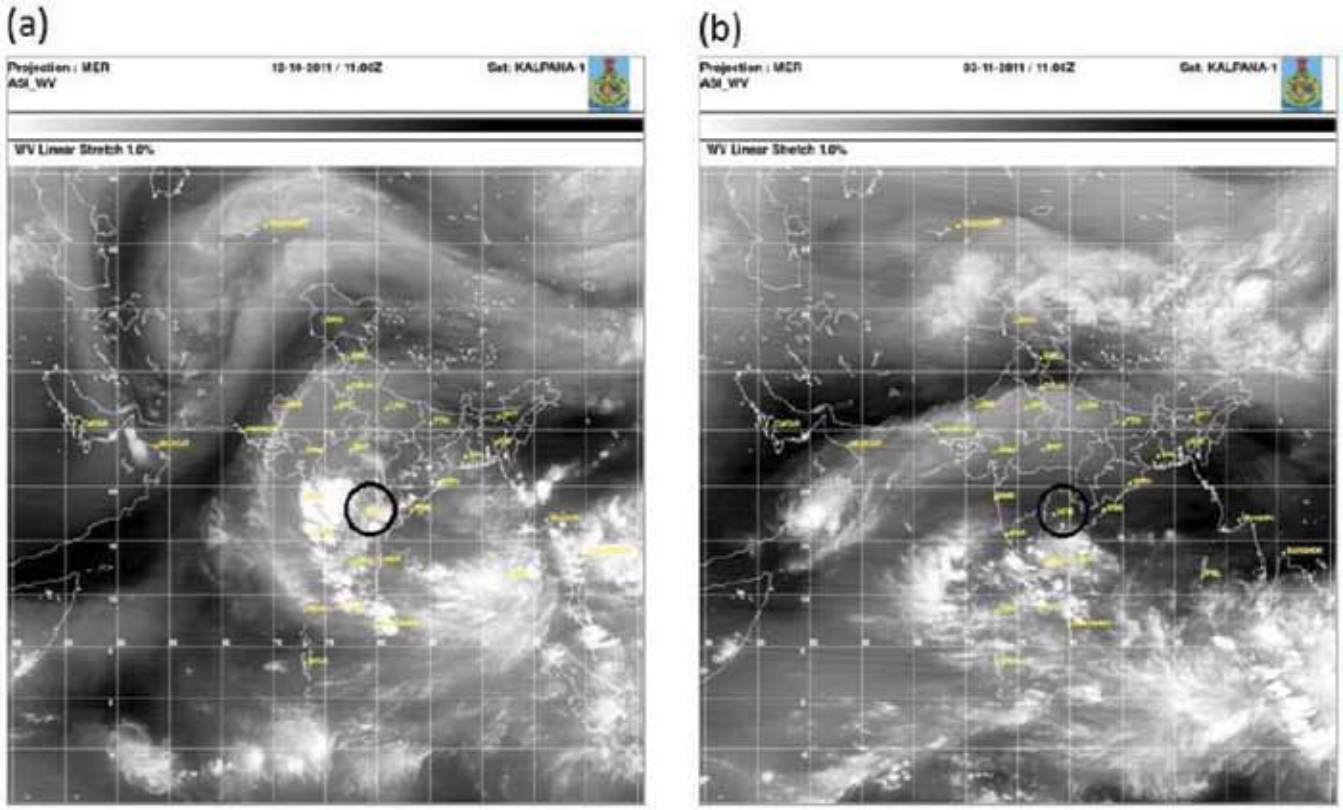

Figure 4. Clouds (water vapour) by Kalpana-1 satellite on (a) October 12, 2011, evening (b) November 3, 2011, evening. The area circled over India depicts the region near observational station.

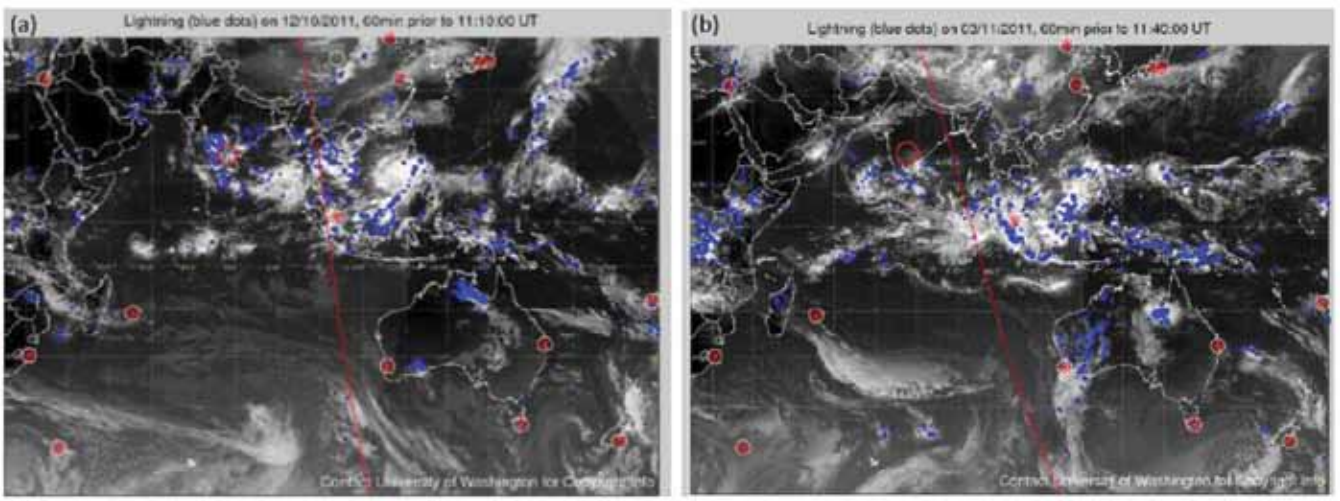

Figure 5. The lightening that occurs on (a) October 12, 2011, evening (b) November 3, 2011, evening. The area circled over India depicts the region near observational station.

poor ozone concentration air mass. Similar to the results reported in this study, in Aura-OMI satellite observations and high resolution ground-based measurements, sharp spikes and dips in TCO_3, of the order of 20 DU within less than 2 h, associated mostly with highly dynamic weather systems such as pressure changes, passage of a cold front with high stratospheric ozone content, or intrusion of low ozone air from lower latitudes (Tzortziou et al., 2012). The chemistry climate model study shows chemistry-induced effects of increasing water vapor lead to an overall decrease of the TCO_3 by about 1% in the tropics (Wenshou et al., 2009).

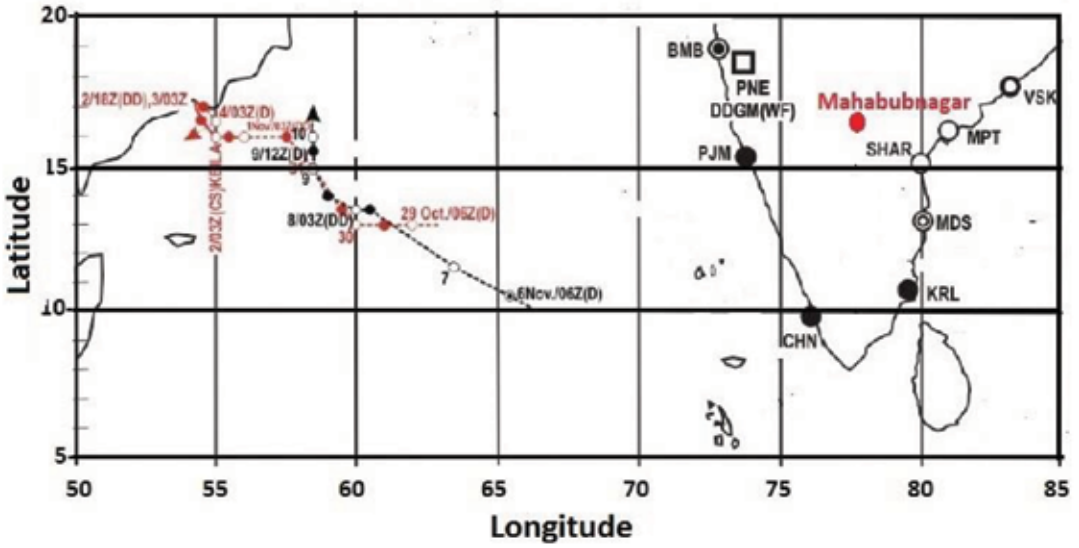

Figure 6. Track of the cyclonic storm Keila in Arabian Sea during 29 Oct-4 Nov, 2011.

SUMMARY AND CONCLUSIONS

The analyses presented in this article include the concentrations of Total Column Ozone obtained in a monitoring campaign that took place at a south Indian site of Mahabubnagar during 42 days in the post-monsoon season. The results indicate that, on most of the days, the TCO_3 was ranging from 250-300 DU. It is found that the water vapor and wind speed in the upper troposphere and lower stratosphere plays a role in controlling the TCO_3 concentrations. The existence of high water vapor and strong winds were associated with high TCO_3. Similarly, more lightning strike events were also associated with high TCO_3. Localized sudden decrease of ~ 110 DU of TCO_3 with time scale of 12 h was observed, first time over the Indian subcontinent, in association with the cyclonic storm Keila formed in the Arabian Sea.

ACKNOWLEDGMENTS

The authors express their gratitude to the Director, Indian Institute of Tropical Meteorology, Pune for inspiration. The CAIPEEX-IGOC program was fully funded by the Ministry of Earth Sciences, Govt. of India, New Delhi. The team members of the CAIPEEX-IGOC are acknowledged for their help in collection of valuable observations used in the analysis. Time series of area averaged values of TCO_3 used in this manuscript were produced with the Giovanni online data system, developed and maintained by the NASA GES DISC.

Compliance with Ethical Standards

The authors declare that they have no conflict of interest and adhere to copyright norms.

REFERENCES

Bian, J., Wang, G., Chen, H., Qi D., Lü D. and Zhou, X., 2006. Ozone mini-hole occurring over the Tibetan Plateau in December 2003. Chinese Sci. Bull., 51(7), 885-888.

Calbo, J., Pages, D. and Gonzalez, J.A., 2005. Empirical studies of cloud effects on UV radiation: A review. Rev. Geophys., 43, doi: 10.1029/2004rg000155.

Farman, J.C., Gardiner, B.G. and Shanklin, J.D., 1985. Large losses of total ozone in Antarctica reveal seasonal ClOx/NOx interaction. Nature., 315, 207–210.

India Meteorological Department, 2011. Report on cyclonic disturbances over north Indian Ocean during 2011, RSMC-Tropical Cyclone Report No 02/2012.

James, P.M., 1998a. An interhemispheric comparison of ozone mini-hole climatologies Geophys Res. Lett., 25(3), 301-304.

James, P.M., 1998b. A climatology of ozone mini-holes over the northern hemisphere; International. J. of Climatol., 18(12),1287-1303.

Kalita, G., Pathak, B., Bhuyan, P.K. and Bhuyan, K., 2011. Impact of zonal wind on latitudinal variation of total columnar ozone over the Indian Peninsula. International Journal of Rem. Sens., 32(24), 9509-9520.

Katsambas, A., Varotsos, C.A., Veziryianni, G. and Antoniou, C., 1997. Surface solar ultraviolet radiation: a theoretical approach of the SUVR reaching the ground in Athens, Greece. Environ. Sci. and Poll. Res., 4, 69-73.

Keil, M., Jackson, D.R., and Hort, M.C., 2007. The January 2006 low ozone event over the UK. Atmos. Chem. and Phys., 7(3), 961-972.

Koch, G., Wernli, H., Schwierz, C., Staehelin, J. and Peter, T., 2005. A composite study on the structure and formation of ozone miniholes and minihighs over central Europe. Geophys. Res. Lett., 32(12), 1-5.

Kondratyev, K.Y. and Varotsos, C.A., 1996. Global total ozone dynamics – impact on surface solar ultraviolet radiation variability and ecosystems. Environ. Sci. and Poll Res., 3, 205-209.

Liu, C., Liu, Y., Cai, Z., Gao, S., Bian, J., Liu, X. and Chance, K., 2010. Dynamic formation of extreme ozone minimum events over the Tibetan Plateau during northern winters 1987-2001. J. Geophys. Res. 115, D18311, doi:10.1029/2009JD013130.

Meena, G.S., Devara, P.C.S. and Patil, M.N., 2016. Diurnal asymmetry in slant column density of NO2, O3, H2O and O4 during CAIPEEX−IGOC over Mahabubnagar, a rural site in Southern Peninsular India. Natural Hazards, 82, 389-400.

Newman, P.A., Lait, L.R. and Schoeberl, M.R., 1988. The morphology and meteorology of Southern Hemisphere spring total ozone mini□holes. Geophys. Res. Lett., 15(8), 923-926.

Parrish, D.D., Millet, D.M. and Goldstein, A.H., 2009. Increasing ozone concentrations in marine boundary layer air inflow at the west coasts of North America and Europe. Atmos. Chem. and Phys., 9, 1303-1323.

Raj, P.E., Devara, P.C.S., Pandithurai, G., Maheshkumar, R.S., Dani, K.K., Saha, S.K. and Sonbawne, S.M., 2004. Variability in sun photometer derived ozone over a tropical urban station J. Geophys. Res., 109, D08309.

Sonbawne, S.M., Raj, P.E., Devara, P.C.S. and Dani, K.K., 2009. Variability in sun photometer derived summertime total column ozone over the Indian station Maitri in the Antarctic region. International J. Rem. Sens., 30(15-16), 4331-4341.

Tzortziou, M., Herman, J.R., Cede, A. and Abuhassan, N., 2012. High precision, absolute total column ozone measurements from the Pandora spectrometer system: comparisons with data from a Brewer double monochromator and Aura OMI Journal Geophysics Res., 117, D16303 doi: 10.1029/2012JD017814.

Vingarzan, R., 2004. A review of surface ozone background levels and trends. Atmos. Environ., 38, 3431–3442.

Wenig, M., Spichtinger, N., Stohl, A., Held, G., Beirle, S., Wagner, T. and Jahne BPlatt, U., 2003. Intercontinental transport of nitrogen oxide pollution plume. Atmos. Chem. and Phys., 3, 387-393.

Wenshou, T., Chipperfield, M.P. and Daren, L., 2009. Impact of Increasing Stratospheric Water Vapor on Ozone Depletion and Temperature Change, Adv. in Atmos. Sci., 26(3), 423-437.

Ziemke, J.R., Chandra, S., Duncan, B.N., Froidvaux, L., Bhartia P.K., Levelt, P.F. and Waters, J.W., 2006. Tropospheric ozone determined from Aura OMI and MLS: Evaluation of measurements and comparison with the Global Modeling Initiative's Chemical Transport Model. Journal Geophysics Res., 111, D19303, doi: 10.1029/2006JD007089.

Ziemke, J.R., Chandra, S., Labow, G.J., Bhartia, P.K., Froidevaux, L. and Witte, J.C., 2011. A global climatology of tropospheric and stratospheric ozone derived from Aura OMI and MLS measurements. Atmos. Chem. and Phys., 11(17), 9237-9251.

Received on: 30.1.18; Revised on: 5.3.18; Accepted on: 9.4.18

J. Ind. Geophys. Union (July 2018)
v.22, no.4, pp: 425-435

Estimation of Dar-Zarrouk parameters for groundwater exploration in parts of Chopda Taluka, Jalgaon district, Maharashtra (India)

S.N. Patil, N.R. Kachate*, and S.T. Ingle

School of Environmental and Earth Sciences, North Maharashtra University, Jalgaon, Maharashtra.
*Corresponding Author: kachatenandkishor@gmail.com

ABSTRACT

Vertical Electrical Soundings using Schlumberger technique with a maximum current electrode spacing (AB/2) of 150 m were carried out at 34 locations to delineate the ground water potential zones in Chopda taluka of Jalgaon district (Maharashtra), covered by Deccan trap inliers in the center surrounded by alluvium. The results indicate that the study area encompasses a multilayer admixture of pebbles, sand, silt and clay, with resistivity values in the range of 18-25 Ω-m. The area comprised of three types of aquifers which is (i) loose clayey or silt with intercalation of sand (< 10 Ω-m), (ii) clayey-sand layer (10-25 Ω-m), and (iii) compacted clay or pebbles/cobbles and sand (25-50 Ω-m). VES 29 and 15 inliers, are seemingly composed of fractured and weathered basaltic formation. Hard rock is revealed at 12-25 m and exposed at some locations in Chahardi area. Four resistivity profiles revealed a clear picture of the continuity of aquifer and movement of water, while the sounding data provided 2-5 geoelectric layers of different thickness. Dar-Zarrouk parameters i.e., (i) Longitudinal conductance (S) (ii) Longitudinal resistivity (ρl) (iii) Transverse resistance (T) (iv) Transverse resistivity (ρt) and (v) Electrical anisotropy (λ), derived from resistivity data helped in categorizing the study area with respect to protective capacity rating of different aquifers. The S map suggest that about 17 % of the area falls under 'very good' to 'excellent' and protective capacity, while about 50 % falls under 'good' protective capacity rating. A large variation is observed in λ map, ranging from 0.38 to 2.73 over the studied region. This indicates the anisotropic nature of the aquifers in such hard rock terrain. Several lineaments are cris-crossing the study area and the intersection points are considered favorable zone for groundwater exploration.

Key words: Vertical Electrical Sounding, Alluvium, Dar Zarrouk parameters, Longitudinal conductance

INTRODUCTION

Water level depletion is increasing day by day because of fast growing industrialization and increasing agricultural practices. The study area is characterized by different aquifer behaviors due to the complex hydrogeological conditions comprising of trap rock in the middle part.

The electrical resistivity technique has been widely used by many researchers (Gupta et al., 2010, 2015; Patil et al., 2015; Khalil et al., 2015; Srinivasamoorthy et al., 2014; Narayanpethkar et al., 2009; Golekar et al., 2014) for groundwater exploration studies in different parts of India. Deccan traps, consist of multiple layers of solidified lava flows and behave as a multilayered aquifer system and VES is a suitable technique to map the depth distribution of litho units. (Rai et al., 2013). The D-Z parameters of different layers derived from geoelectric parameters have been used for groundwater exploration studies of the aquifers in different parts of the world, such as in Nigeria (Udoinyang et al., 2012; Egbai et al., 2015), Brazil (Antonio Celso de Oliveira Braga et al., 2006) and in India (Mondal et al., 2013; Gupta et al., 2015; Shailaja et al., 2016). Earlier studies (Patil et al., 2015) in Chopda taluka have been carried out using 10 sounding data, while in present study, the sounding was extended further in parts of south and north-east area also. D-Z parameters are calculated to understand the groundwater regime and the aquifer protective capacity of different layers based on the variation of longitudinal conductance (S), longitudinal resistivity (ρl), Transverse resistance (T), Transverse resistivity (ρt), Anisotropy (λ).

STUDY AREA

The study area (figure 1) is in the northern part of Chopda Taluka of Jalgaon district, Maharashtra bounded by latitudes 21°8′N to 21°22′N and longitudes 75°12′ E to 75°22′E. Ratnavati, the main river of Chopda taluka is a tributary of Tapi river. The study area is characterized by semi-arid climatic conditions with annual rainfall of 647.1 mm during 2017. In study area well inventory survey was carried to know the lithology and condition of groundwater. During survey observed static water level of the study area ranges from 14.1m to 20.2m in the month of May-2017. The mean minimum temperature varies from 12^0C to 38^0C throughout the year and high relative humidity occurs during the rainy season, viz. June to October. The important crops cultivated are Banana, Sugarcane, Cotton and Wheat.

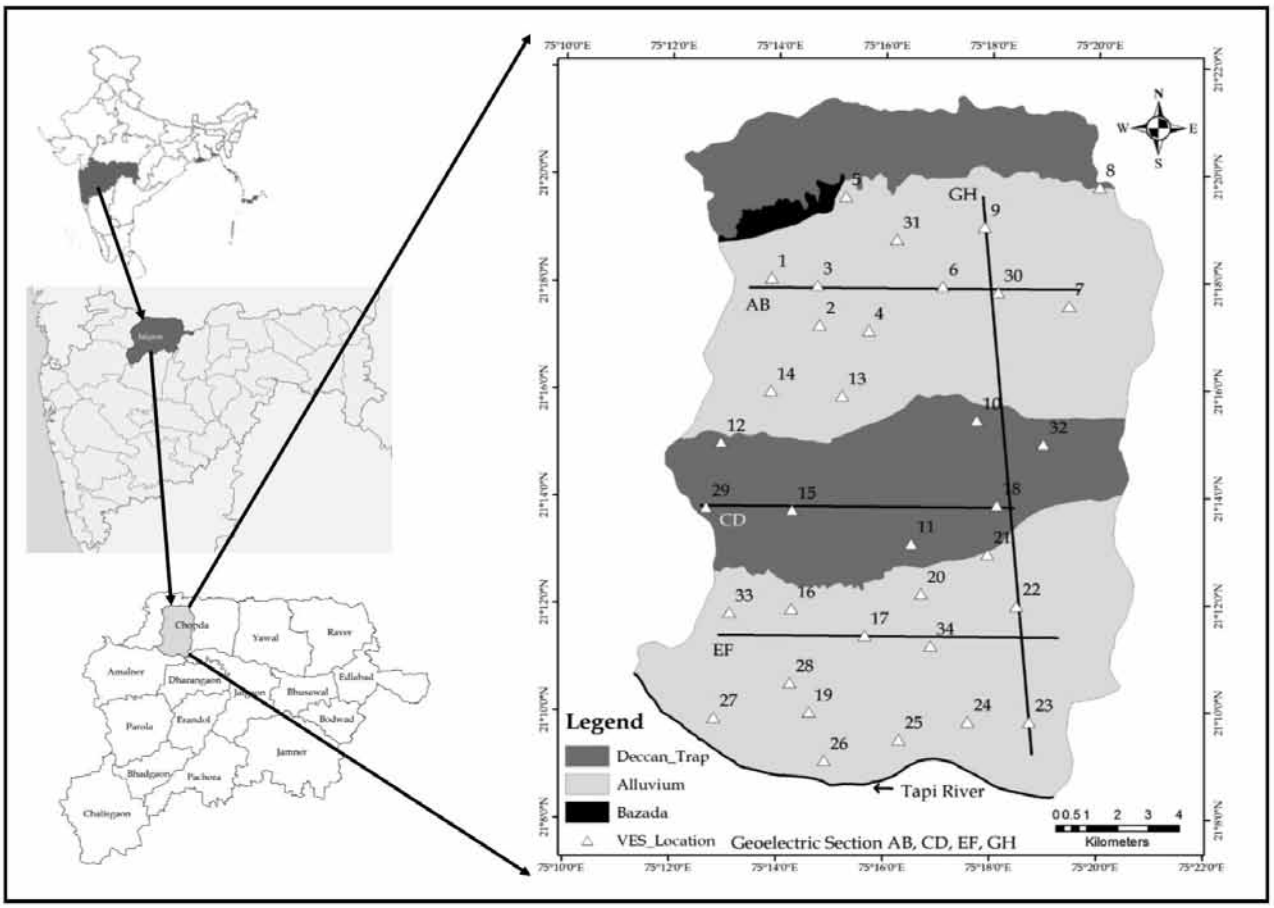

Figure 1. Location and Geological Map of study area.

Table 1. Resistivity values of different rock type in the study area (Source: CGWB website: http:// cgwb.gov.in/CR/ achi_geo_stu.html).

Geological Formation	Resistivity (Ω m)
Alluvium, Black cotton, Bole bed	5-10
Weathered /fractured/vesicular basalt Saturated with Water	20-40
Moderately Weathered/Fractured /Vesicular Basalt with Water	40-70
Massive Basalt	> 70

GEOLOGY OF THE STUDY AREA

The northern part of the study area (figure 1) comprises of Satpuda ranges covered by the Deccan Volcanic Basalts (Upper Cretaceous to lower Eocene age), while the southern part is occupied by thick alluvium (Quaternary age) as seen at gullies and river bank. The different formations in the study area are (CGWB, 2013)

Deccan Traps: The central part of study area covered by Deccan traps formed due to the enormous lava flows which extend over huge areas of western, central and southern India at the end of Mesozoic era. Deccan traps (basaltic flows) consist mainly two units, Aa flow which consists of dark fine to medium grained sparsely porphyritic and Pahoehoe flow – medium grained, sparsely porphyritic. (Deshpande, 1998; GSI, 1984)

Alluvium: Alluvium mainly consists of layers of clay, sand, gravels, and boulders of variable thickness. The sand and gravel occur in one or more beds. The alluvium occupies the southern part of the area under study. The alluvium is clayey and yellowish to light brownish in colour as observed in exposures around Tapi bank (GSI, 1984) it is associated with calcrete nodules.

The topography in combination with type of soil, high run-off, medium to high infiltration, over exploitation of groundwater (particularly for banana crops) resulted in lowering of groundwater resources in the area further accentuated by the unpredictable fluctuations of seasonal rainfall.

Table 2. Dar-Zarrouk parameters in Study area of Chopda Taluka

VES	Name	Total depth		Longitudinal Conductance	Transverse Resistance	Longitudinal Resistivity	Transverse Resistivity	Anisotropy
		H(m)	Error (%)	S	T	ρ_l	ρ_t	λ
1	Chaugaon	38.97	0.795	6.73	292.54	5.79	7.51	1.14
2	Chunchale	35.248	0.794	4.91	400.46	7.18	11.36	1.26
3	Krishnapur	44.2	0.897	9.26	389.54	4.78	8.81	1.36
4	Mamalde	28.36	0.814	26.19	117.57	1.08	4.15	1.96
5	Angurne	62.26	0.797	17.85	419.18	3.49	6.73	1.39
6	Varad 1	35.2	0.804	2.21	635.04	15.95	18.04	1.06
7	Adgaon	102.5	0.748	10.91	1071.21	9.40	10.45	1.05
8	Virwade	37.03	0.681	12.72	311.36	2.91	8.41	1.70
9	Nagalwadi_1	1.673	0.52	0.11	107.96	15.50	64.53	2.04
10	Chopda Urban_1	92.355	0.471	0.95	5658.95	97.03	61.27	0.79
11	Vele	21.7	0.712	2.05	374.71	10.60	17.27	1.28
12	Kazipura	30.829	0.489	0.62	216.05	49.45	7.01	0.38
13	Akkulkhede	37.461	0.549	5.34	297.82	7.02	7.95	1.06
14	Hingone	21.935	0.693	6.68	231.65	3.28	10.56	1.79
15	Chahardi_1	92.97	0.811	2.82	3467.86	32.98	37.30	1.06
16	Chahardi_2	102.1	0.672	17.18	613.87	5.94	6.01	1.01
17	Chahardi_5	34.72	0.674	0.70	2618.41	49.40	75.42	1.24
18	Chopda Gartad Rd	16.49	1.75	8.07	155.67	2.04	9.44	2.15
19	Nimgavan_1	1.21	2.1	0.00	637.67	527.00	527.00	1.00
20	Hol	15.71	0.473	1.58	157.87	9.93	10.05	1.01
21	Gartad	12.16	0.808	2.44	96.10	4.98	7.90	1.26
22	Dhanwadi	5.997	1.65	0.05	5485.25	122.59	914.66	2.73
23	Sanpule	15.2	0.895	3.77	61.26	4.03	4.03	1.00
24	Kurwel	5.685	0.939	2.05	17.10	2.77	3.01	1.04
25	Tavse Bk_1	46.2	0.665	7.01	304.46	6.59	6.59	1.00
26	Khachne	4.198	0.74	1.06	44.90	3.95	10.70	1.65
27	Tandalwadi	33.28	0.524	4.45	250.96	7.47	7.54	1.00
28	Nimgavan_2	7.12	0.6	0.75	87.00	9.51	12.22	1.13
29	Chahardi_3	88.79	0.911	2.71	3234.42	32.82	36.43	1.05
30	Nagalwadi_2	1.448	0.716	0.11	103.90	13.11	71.75	2.34
31	Varad_2	35.2	0.501	1.80	758.08	19.53	21.54	1.05
32	Chopda Urban_2	102.348	0.451	0.92	6082.56	111.79	59.43	0.73
33	Chahardi_4	102.1	0.915	15.39	694.73	6.64	6.80	1.01
34	Tavse Bk_2	11.83	0.861	1.22	116.66	9.73	9.86	1.01

METHODOLOGY

34 vertical electrical soundings (VES) carried out at different locations (figure 1) were interpreted with the help of the interactive semi-automated technique using IPI2WIN software 3.0.1.a7.01.03 (Bobachev, 2003). A few representative sounding curves along with layer parameters are shown in figure 7.

Based on the three to four layered models, obtained over the 34 locations of the area, four geoelectric sections were drawn (3 in E-W direction and one in N-S) spread over the study area. The resistivity data was compared with the tube well data existing in the study area to aid in recommending sites for drilling. The resistivity ranges (Table 1) were used in the present study area as suggested by Central Ground Water Board (CGWB).

DAR-ZARROUK PARAMETERS (METHODS OF ESTIMATION)

Dar-Zarrouk parameters (D-Z) termed by (Maillet, 1947) play an important role in geoelectrical resistivity soundings. They have been used in computing a distribution of surface potential and the section consists of *n* geoelectric layers with thicknesses h_1, h_2, h_3, …., h_n and resistivity ρ_1, ρ_2, ρ_3, …..ρ_n for a block of unit square area and thickness

$$H = \sum_{i=1}^{n} hi$$

The D-Z parameters, i.e., S, T, ρ_l, ρ_t & λ are defined as following.

A geoelectric unit is characterized by two basic parameters the layer resistivity (ρi) and the layer thickness

Table 3. Longitudinal Conductance/Protective capacity rating (Oladapo and Akintorinwa, 2007).

Longitudinal Conductance (Ω^{-1})	Protective Capacity Rating
>10	Excellent
5 – 10	Very good
0.7 – 4.9	Good
0.2 – 0.69	Moderate
0.1 – 0.19	Weak
<0.1	Poor

(h*i*) for *i* th layer (*i* =1 for the surface layer). Two further electrical parameters can be derived for each layer from the respective resistivity and thickness; these are called the Longitudinal Conductance, Transverse Resistance.

$$S = \sum_{i=1}^{n} \frac{hi}{\rho i}$$ .....(1) longitudinal conductance

The longitudinal resistivity of the current flowing parallel to the layers is given by,

$$\rho l = \frac{H}{S}$$ .....(2) longitudinal resistivity

$$T = \sum_{i=1}^{n} hi * \rho i$$ .....(3) Transverse resistance

This is the "transverse resistance".

The transverse resistivity to the current flowing perpendicular to the layers is given by,

$$\rho t = \frac{T}{H}$$ Where $H = \sum hi$

H is the depth to the bottom most geoelectric layer.

$$\rho t = \frac{T}{H}$$ .....(4) Transverse resistivity

The coefficient of pseudo-anisotropy (λ) is given by:

$$\lambda = \sqrt{\frac{\rho t}{\rho l}}$$ .....(5) Anisotropy

RESULT AND DISCUSSION

Result of DZ Parameter

The results of DZ parameter estimated from the inverted resistivity sounding data and geo electric layer sequence in the study area as are shown in Table 2.

Longitudinal unit conductance (S)

In present study, the longitudinal conductance values were classified according to (Oladapo and Akintorinwa, 2007) into poor, weak, moderate, good, very good and excellent protective capacity zones showed in Table no.3. It can be concluded (Table 2) that VES Station 4,5,7,8,16 and 33 ranging from 10.91 – 26.19 siemens and the thickness (H) of the sounding stations vary between 28 and 102.5 m. The stations with high S values may be due to increase in H values and *vice versa* (Murali and Patangay, 2006). Those VES stations with increase in S values may corresponds to an average increase in the clay content that would result decrease in the transmissivity of the aquifer (Oteri, 1981). The litholog data available at VES 4, suggests layers comprised of a black cotton soil with sand and kankar followed by admixture of pebbles and sand with clay.

The longitudinal conductance value at VES 4 is 26.19 and it falls under excellent protective capacity rating. VES station 1,3,13,14,18 and 25 falls under the very good protective capacity rating which is ranging from 5.34 – 9.26 siemens and the thickness (H) of the sounding stations varies between 16.49 – 44.2 m. VES 18, encompassed overburden of black cotton soil (2 m) with resistivity 47 Ω-m and which may be followed by loose soil (13 m) with resistivity 1.71 Ω-m and further moving with a hard and compact rock. The longitudinal conductance map (figure 2) revealed that 17.65 % area falls under the 'excellent' and 'very good' protective capacity categories of the area and about 50 % of the area falls under 'good' protective capacity and remaining 2.94 %, 5.88 %, 5.88 % area under the moderate, weak and poor protective capacity rating respectively. This study suggests that a major part of the study area can be categorized as relatively good to very good protective capacity ratings.

Longitudinal Resistivity (ρl)

A spatial distribution map of longitudinal resistivity (figure 3) of the study area shows the values ranging between 1.08 – 526.72 Ω-m while 82 % of the study area is covered by values between 1.08 - 34.06 Ω-m. VES station 19, reveals a very high Longitudinal resistivity of 526.72 Ω-m while those at VES station 10, 32, 22 and surrounding part of VES 19 show values ranging between 34.06 - 89.72 Ω-m. In present study, less longitudinal resistivity observed than transverse resistivity which shows different layers present below the earth surface (Flathe, 1955). The different layers of pebbles-sand, pebbles-sand-silt, pebbles-sand-silt-clay bed was seen at litholog at VES Dhanwadi and Mamalde. The overall area can be categorized as low longitudinal resistivity meaning that different layers of pebbles, sand, silt and clay were present in study area.

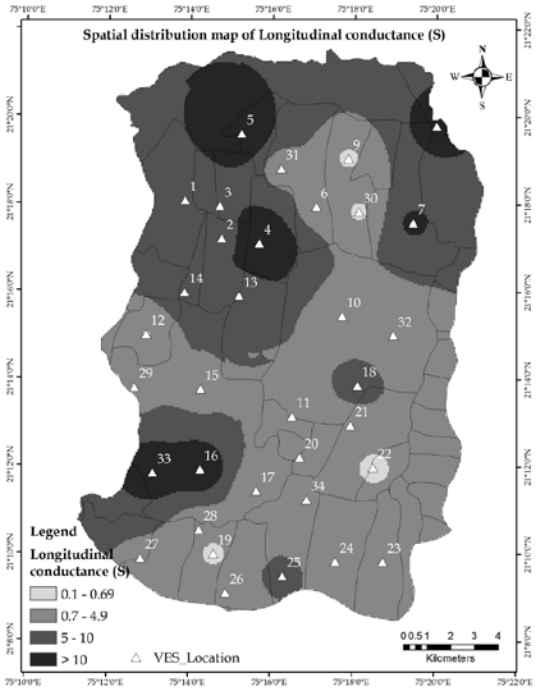

Figure 2. Spatial Distribution of Longitudinal Conductance.

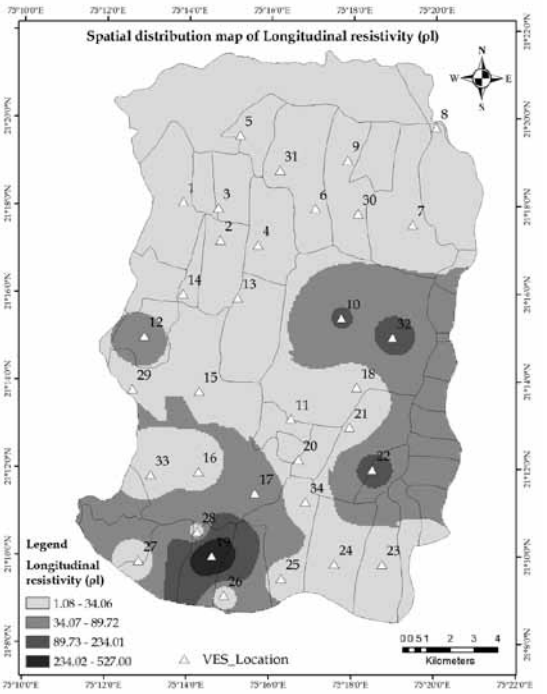

Figure 3. Spatial Distribution of Longitudinal Resistivity.

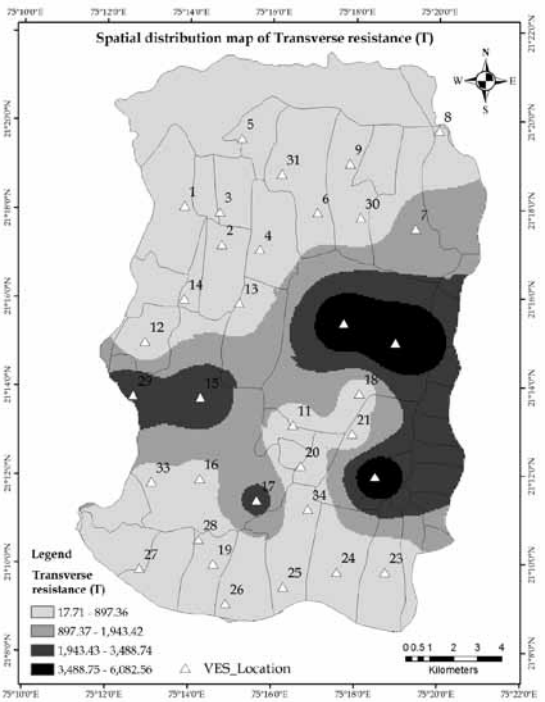

Figure 4. Spatial Distribution of Transverse Resistance.

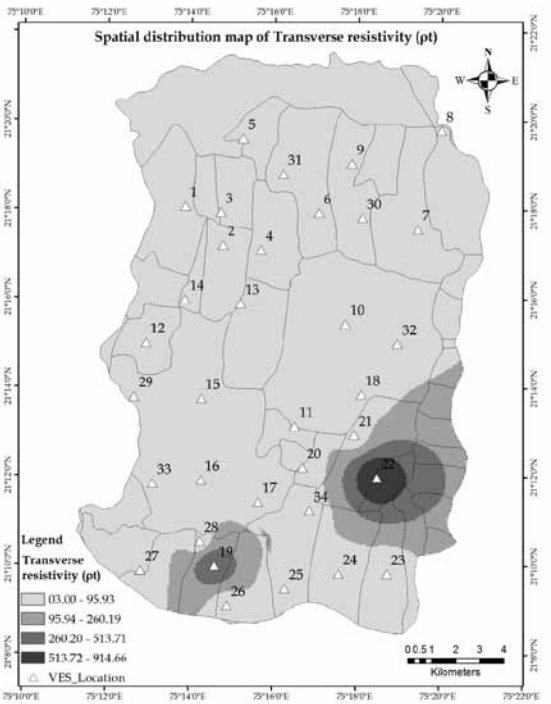

Figure 5. Spatial Distribution of Transverse Resistivity

Transverse Resistance (T)

Figure 4, illustrates that, 79.42 % of the area shows transverse resistance values below 897.36 Ω-m^2 with a minimum of 17.10 Ω-m^2 at VES 24. The North, North-Western, some central and Southern part are mostly covered by T value (<897.36 Ω-m^2). Three VES station, 29, 15 and 17 show values ranging between a 1943.42-3488.74 Ω-m^2 which is 8.82 % of the area. High T Value indicates high transmissivity of aquifers suggesting porous medium for water movement. The highest T value at VES 32 and 10, is a 6082.56 Ω-m^2 which is a good aquifer and it ranges in a map between 3488.74-6082.56 Ω-m^2. VES stations 7,10,15,17,22,29,32 with above T values (1000 Ω-m^2) have

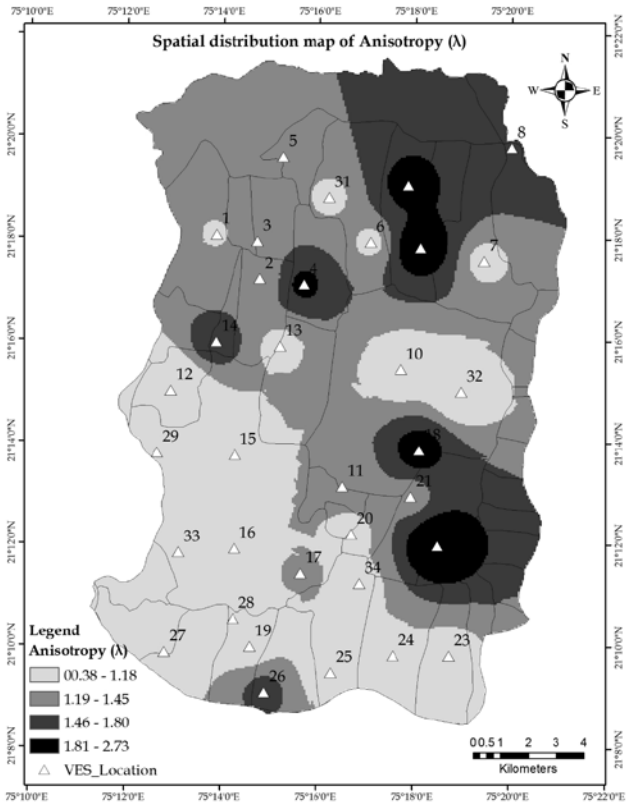

Figure 6. Spatial Distribution of Anisotropy.

a moderately high transmissivity which may be due to high clay content with pebbles-sand and silt bed in alluvial basaltic formations, as a result, fractured or exposure of basaltic rock on surface at some places in Chahardi area. The northern, north-western and south-west part of the study area reflects a high longitudinal conductance values (figure 2) which indicates high clay content resulted in less transmissivity of the area.

Transverse resistivity (ρt)

Figure 5, depicts the spatial distribution map of transverse resistivity (ρt) showing 94 % area with low resistivity ranging from 3.09 Ω-m - 95.93 Ω-m while the eastern part of study area shows very high values between 914.66 Ω-m at VES station 22 and 527 Ω-m at VES 19 respectively. At VES station 22 highest value observed which is due to may be clay with siliceous material is present at 6 m. There is not much effect of any layer in the transverse resistivity.

Anisotropy (λ)

The anisotropy map (figure 6) shows 61.76 % of the area ranges between 0.38 to 1.18 with the low anisotropy at South-western and some central part of VES 10, 32, 7, 6, 31, 1, and 13 The average of Electrical anisotropy for the entire study area is 1.29. VES station 5,3,2,11,21 and 17 ranges in between 1.18-1.45 which is cover a 17.64 % the area. The higher values (2.04, 2.34, 1.96, 2.15, 2.73) observed at VES station 9, 30, 4, 18 and 22 corresponds to hardness and compaction of rocks as suggested by (Keller and Frischknecht, 1966). A large variation is observed in λ map, ranging from 0.38 to 2.73 in the study area which indicates the anisotropic nature of the aquifers in such hard rock terrain. In present study area, high anisotropy (1.80-2.73) value inferred that presence of lineaments or fractures. The lineaments are crossing over each other and these points are good for exploration of groundwater.

RESULT OF VES DATA

The 2D geoelectrical section over four selected profiles in the study region (figure 1) provided the aquifer geometry in the study area. The pseudo cross section was generated by using IPI2WIN Software. With the help of resistivity data obtained in the present study it is compared with the exposed lithology in the dugwell (VES 4 and 22) and it facilitates to classify the area into different alluvial formation. Where the resistivity value is less than 10 Ω m, they are loose clayey/silty layer with intercalation of sand. The part having resistivity ranges between 10-25 Ω m are exhibiting clayey sand layer; area with compacted clay or with pebbles/cobbles and sand having a resistivity ranges 25-50 Ω m.

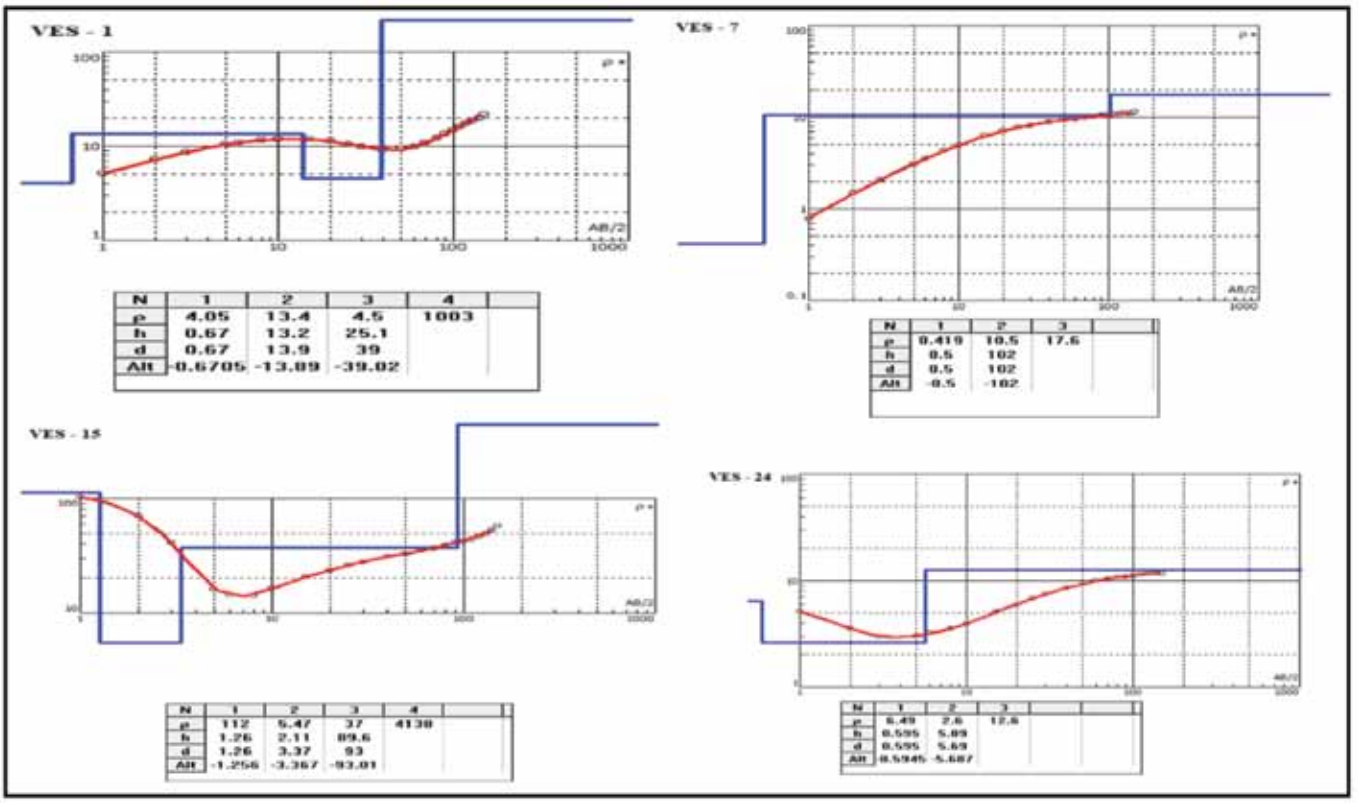

Figure 7. Resistivity curves and tables showing thickness.

Profile – AB

E-W trending profile AB comprises of VES station 1,14,3,2,5,13,4,31,6 and 30 located in alluvium formations. From the section (figure 8), a zone having a resistivity below 10 Ω-m is seen at shallow (10 m) as well as deeper level up to depth of investigation at VES 13 and 4 corresponds to loose clayey/silty layer with intercalation of sand layer. A litholog at VES 4, a layer with mixing of sand, black cotton soil admixture with kankar further below a loose sand with different sizes of pebbles, and compacted sand with gravel present up to 28 m. Below 28 m layers of sand and pebbles were observed up to 49 m fine to coarse sand with calcareous kankar. The lithological cross-section of bore hole at VES 4 (figure 12 B) suggests that, the aquifer zone lies at depths of about 49 m. The longitudinal conductance at VES 4 is 26.19 and falls under the category of excellent protective capacity rating. The resistive (< 10 Ω-m) feature was observed at VES 1,14,3,2, and 5 at deeper level (20 – 120 m) which may show a loose clayey/silty layer with intercalation of sand or clayey-sand layer. VES 31 and 6 are characterized by resistivity (> 26 Ω-m) feature which could be due to compacted clay with pebble up to 10 m. Further east of the profile, low resistivity feature (< 10 Ω-m) was identified with a thickness of about 30 to 35 m at deeper level of VES 30. By observing profile most of the area comprises of the < 25 Ω-m up to a shallow aquifer 25-30 m, which shows a clay/silty or sand layer. VES 7, it can be concluded (figure.7) that top layer (about 1 m) consisted of a loose soil with resistivity 0.41 Ω-m further it moves, 102 m thickness with 10.5 Ω-m resistivity may comprised of a clayey sand layer. VES site 14, 13 and 4 may form a good potential zones are over this profile.

Profile - CD

The profile CD (figure 9) passes through the VES stations 12,29,15,11 and 18 located in the basaltic formations. This cross section reveals that top (2-3 m) layer of profile comprised resistive layer (> 50 Ω-m) indicating hard weathered material which is a spread at VES 29 and 15, further below a (10-30 Ω-m) resistivity may comprised of a fractured or less weathered basaltic formation which is a good potential zone for exploration of water and at basement a hard compact rock may present at the depth of 50m with resistivity > 50 Ω-m. At VES 11 and 18, a low resistive (7-20 Ω-m) feature was observed at the depth of 6 m and 15 m respectively which may give an enough groundwater.

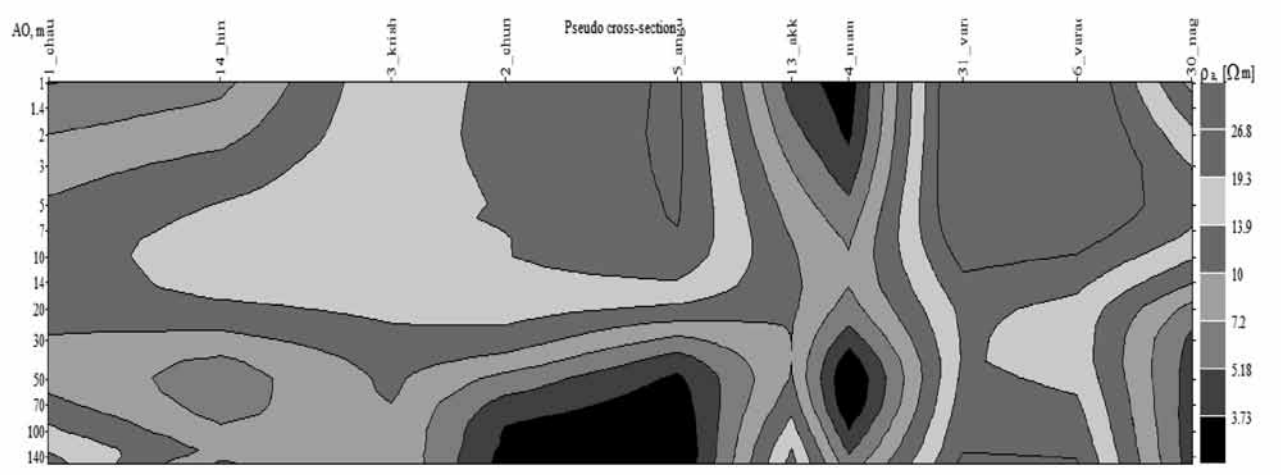

Figure 8. Profile AB Resistivity pseudo cross section.

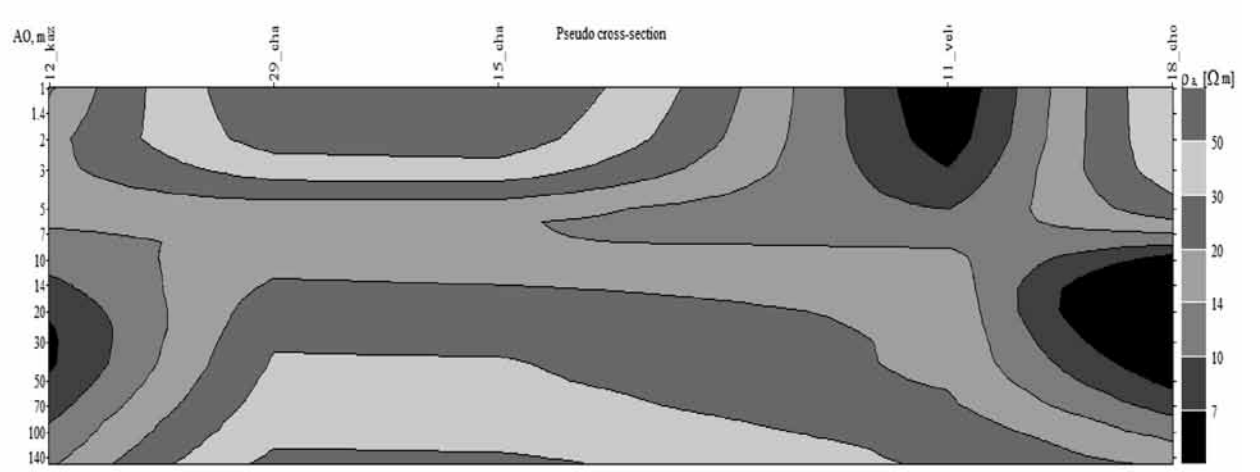

Figure 9. Profile CD Resistivity pseudo cross section.

Profile - EF

E-W trending Profile EF (figure 10) passes through VES stations 33,27,16,28,19,26,17,25,20 and 34. The entire shallow as well as deep sections of VES 33,27 and 16 show a resistivity (< 10 Ω-m) layer which could be a clayey with intercalation of sand layer. VES 28,19 and 26, with a resistivity 28-31 Ω-m may comprised of admixture of clay, sand and pebbles up to 5-6 m, further below a resistive (< 10 Ω-m) feature was observed which might be a clayey with intercalation of sand layer up to depth of investigation. VES 17, shows a resistivity (28-31 Ω-m) throughout depth of investigation which may covered admixture of clay, sand and pebbles. VES 25, 20 and 34 which may have comprised of a clayey with intercalation of sand layer with resistivity < 10 Ω-m up to depth of investigation. VES 24, (figure 7) encompasses of a < 10 Ω-m which may be a clayey with intercalation of sand layer throughout the depth of investigation.

The entire profile suggested that, most of the area covered by clayey sand layer at deeper (from 30 m) section and presence of admixture clay, sand and pebbles which might be porous and permeable in nature to percolate water while clayey-sand layer is less permeable. VES 19, 27,28,26,25 and 34 are the good source for extraction of water from this profile.

Profile - GH

N-S trending profile GH (figure 11) comprises of VES station 8,9,30,10,32,18,21,22 and 23. The deep layer (from 15 m) of the VES 8, 9 and 30 is of resistivity < 10 Ω-m feature, it may have consisted of clayey or silty layer with intercalation of sand. At VES 30 a shallow zone (up to 15 m) with resistivity (26 Ω-m) having compacted clay with pebbles. VES 10 and 32 comprised of a high resistive feature 37 Ω-m which may be fractured basalt at deeper section (below 50-55m), VES 18 shows a resistivity ranges

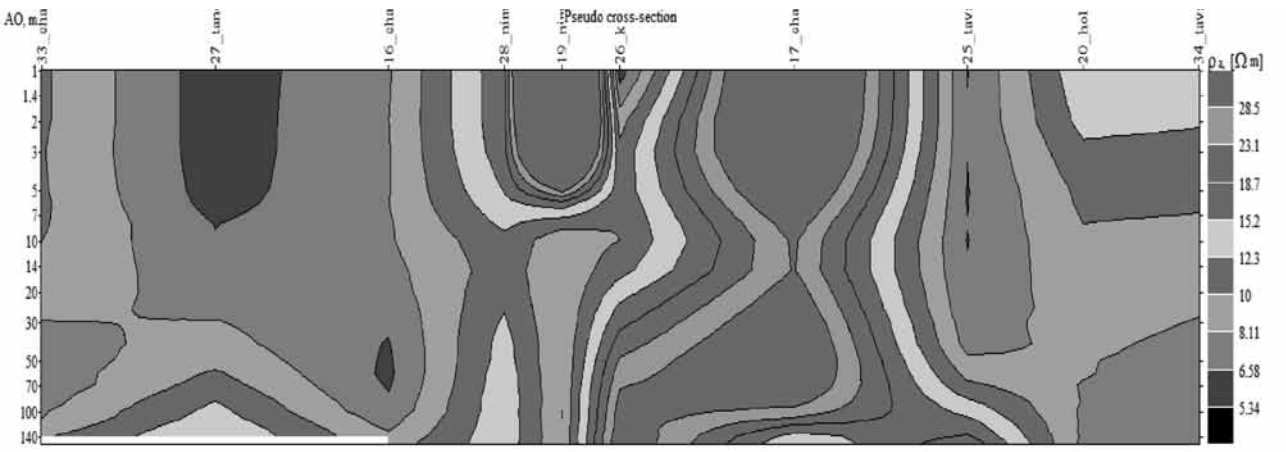

Figure 10. Profile EF Resistivity pseudo cross section.

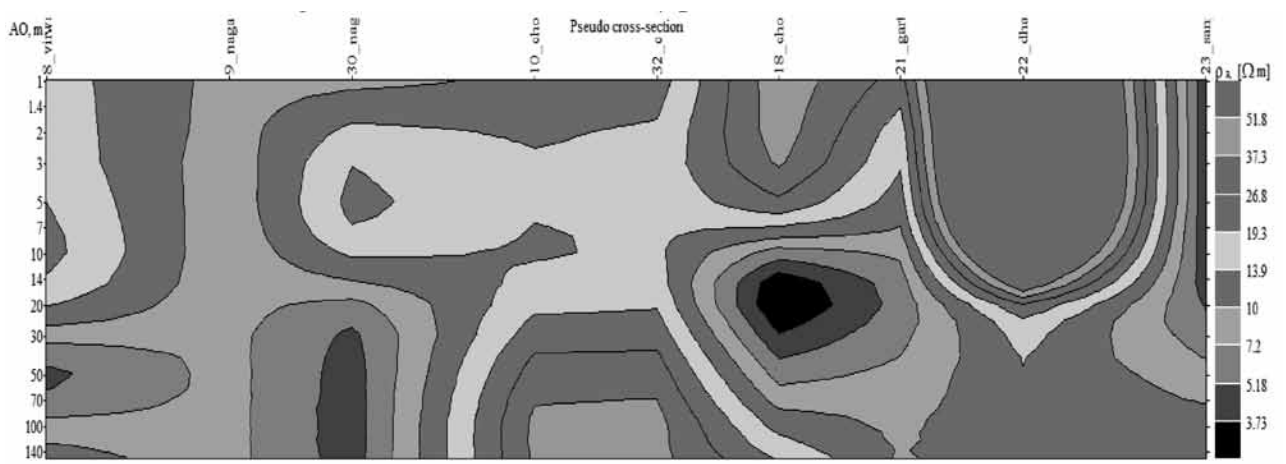

Figure 11. Profile GH Resistivity pseudo cross section.

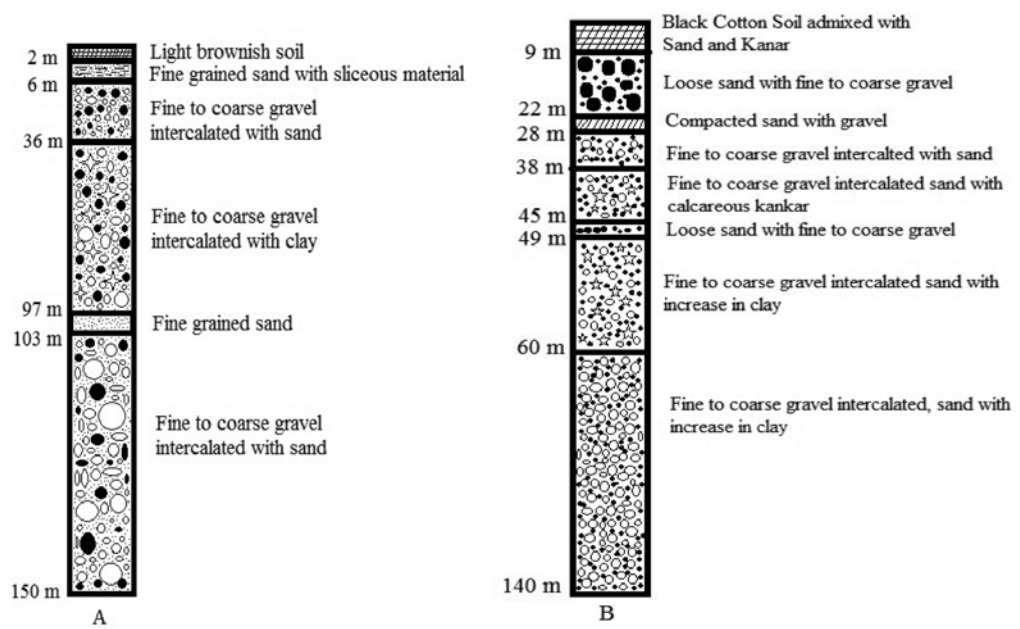

Figure 12. Borehole litholog from the study area showing the major lithological distribution (A-Dhanwadi, B-Mamadle)

26-51 Ω-m which may be a highly fractured basalt at 5-7 m. VES 21 may have alternate layers of clayey-sand layer or intercalation of pebbles in clay/sand layer with > 10 Ω-m resistivity. The borehole lithological cross section at VES 22 is shown in figure 12 A. The litholog suggest that aquifer zone lies at depth 36 m. At VES 22 having a resistivity (> 51 Ω-m) up to 7 m which might be due to contains of clayey-sand layer with siliceous material further it continues with intercalation of pebbles in clay/sand layer. VES 23 comprised of a resistive (< 10 Ω-m) feature, indicating a loose clayey/Silty layer with intercalation of sand. This N-S Profile encompasses with lithological unit i.e loose Clayey/Silt with intercalation of sand, clayey sand layer, compacted clay with pebbles and fractured/weathered basalt.

CONCLUSION

The geophysical survey was carried out in Chopda tehsil of Jalgaon district to identify probable aquifer zones with the help of schlumberger electrical sounding, DZ parameter and borehole lithology. In present study, geologically it is comprising of basaltic and alluvium formation. From resistivity survey, it can be concluded that, the central portion of the study area signifies presence of a basaltic, fractured and weathered part of the area and northern and southern part comprised of alluvium which is of a clay, sand and pebbles. The result of sounding, Dar-Zarrouk parameters and lithology will suggest a probable site 14, 13, 4, 30, 29, 15, 12, 19, 27, 28, 26, 25, 34, 9 and 23 for the exploration of groundwater. The north-western-central part of the area has high ground water potential which is presence of a Bazada zone.

In Earlier research (Patil et al 2015), concluded that VES 15 signifies the presence of fractured or weathered rock at 3-15 m which is a good potential zone for exploration of water. VES 11 (S = 0.71) and 13 (S = 0.54) have comprised a layer of loose clayey/silty layer with intercalation of sand which indicates a low S value in present study. The earlier work of sounding has supported by DZ parameters in present study area.

The vertical electrical sounding data helps to identifies three types of aquifers present in the study area. The first type of aquifers has a resistivity less than 10 Ω-m which comprised of a loose clayey or silt with intercalation of sand, this type of aquifer has a high clay content which is generally characterized by a low resistivity values and have a low permeability, whereas second type has a resistivity 10-25 Ω-m which is a consisted of clayey-sand layer. The third aquifer ranging from 25-50 Ω-m which is of a compacted clay or with pebbles/cobbles and sand.

The estimation of D-Z parameter will use full to understand distribution of groundwater and sub-surface litholog and to identify a potential aquifer zone. The longitudinal conductance map suggests 17 % of the area falls under the category of very good and excellent protective capacity rating which suggest a high transmissivity in north-western-central part of the area which forms the potential aquifers. Longitudinal resistivity shows a different layer present in terms of the loose clayey/silt with mixing of clay, clayey-sand, compacted clay with pebbles/cobbles. A large variation of anisotropy will help in to identify that some lineaments or fractures present in the area. The spatial distribution map of D-Z Parameter S, ρl, T, ρt and λ shows a variation in basaltic and alluvium formation with respect to aquifers which is helpful for analyzing the different geological formation or structure of the study area.

The combine result of litholog, sounding data, D-Z parameters signify the various effective result to find out most suitable site for groundwater exploration. This study is beneficial to the farming community for exploration and management of ground water.

ACKNOWLEDGMENT

Authors are thankful to UGC-BSR (RFSMS) Government of India for the valuable research grant sanctioned to School of Environmental and Earth Sciences, North Maharashtra University, Jalgaon. The co-operation of North Maharashtra University, Jalgaon officials is also acknowledged.

Compliance with Ethical Standards

The authors declare that they have no conflict of interest and adhere to copyright norms.

REFERENCES

Antonio Celso de Oliveira Braga, Walter Malagutti Filho. and Dourado, J.C., 2006. Resistivity (DC) method applied to aquifer protection studies, Revista Brasileira de Geofísica, 24(4), 573-581.

Bobachev, A., 2003. Resistivity Sounding Interpretation IPI2WIN, Version 3.0.1, a 7.01.03. Moscow State University.

Central Ground Water Board (CGWB), 2013. Ground Water information Jalgaon district, Maharashtra, Central region, Nagpur.

Deshpande, G.G., 1998. Geology of Maharashtra, Geological society of India, Bangalore, pp: 129-160.

Egbai, J.C., and Emekeme I.R.E., 2015.Aquifer transmissivity Dar Zarrouk parameters and groundwater flow direction in Abudu, Edo State, Nigeria, Int. J. Sci. Env. Tech., 4(3), 628-640.

Geological Survey of India (GSI), 1984. Systematic Geological mapping in parts of Chopda Tehsil of Jalgaon district, Maharashtra, (TS 46 O/8).

Golekar, R.B., Baride, M.V. and Patil S.N., 2014. 1D resistivity sounding geophysical survey by using Schlumberger electrode configuration method for groundwater explorations in catchment area of Anjani and Jhiri river, Northern Maharashtra (India), J. Spatial Hydrology, 12(1), 22-35.

Gupta, G., Erram, V.C., Maiti, S., Kachate, N.R. and Patil, S.N., 2010. Geoelectrical studies for delineating seawater intrusion in parts of Konkan coast, Western Maharashtra, Int. J. Env. Earth Sci., 1(1), 62-79.

Gupta, G., Patil, S.N., Padmane, S.T., Erram, V.C. and Mahajan, S.H., 2015. Geoelectric investigation to delineate groundwater potential and recharge zones in Suki river basin, north Maharashtra, J. Earth System Sci., 124(7), 1487-1501.

Ibrahim, Khalil., Golam, Rasul., Ratan, Kumar. Majumder., Mohammad, Zafrul Kabir., Farah Deeba., Farhana, Islam., Shanjib, Karmaker., Jalal Uddin Rumi., K.M. and Rahnuma Siddique., 2015. Geo-electrical soundings and analysis to investigate groundwater aquifers at Khulna City, coastal area of Bangladesh, Arabian J. Geosci., 8(8), 5325-5334.

Keller, G.V. and Frischknecht, F.C., 1966. Electrical methods in geophysical prospecting, Pergamon, Oxford, 526.

Srinivasamoorthy, K., Chidambaram., S., Vasanthavigar, M., Anaandan, P. and Sarma, V.S., 2014. Geophysical Investigation for groundwater in a hard rock terrain Salem district, Tamil Nadu, India, Bull. Eng. Env., 73(2), 357-368.

Maillet, R., 1947. The fundamental equations of electrical prospecting, Geophysics, 12(4), 529-556.

Mondal, N.C., Singh, V.P. and Ahmed S., 2013. Delineating shallow saline groundwater zones from Southern India using geophysical indicators, Environmental Monitoring Assessment, 185(6), 1573-2959.

Murali, S. and Patangay, N.S., 2006. Principles of application of groundwater geophysics, Association of Geophysicists, Hyderabad, India, 371.

Narayanpethkar, A.B., Sabale, S.M. and Ghodake, V.R., 2009. Studies on subsurface resistivity structures for groundwater harvesting in Dhubdhubi Basin, Solapur district, Maharashtra, India, J. Indian Geophys. Union, 13(4), 209-216.

Oladapo, M.I. and Akintorinwa, O.J., 2007. Hydrogeophysical study of Ogbese South western, Nigeria, Global J. Pure. Appl. Sci., 13(1), 55-61.

Oteri, A.U., 1981. Geoelectric investigation of saline contamination of chalk aquifer by mine drainage water at Tilmanstone, England, Geoexploration, 19(3), 179-192.

Patil, S.N., Kachate, N.R., Marathe, N.P., Ingle, S.T. and Golekar, R.B., 2015. Electrical resistivity studies for groundwater exploration in some parts chopda block of Jalgaon district, Maharashtra India, Int. Res. J. Earth Sci., 3(8), 8-13.

Rai, S.N., Thiagarajan, S., Kumari, R.Y., Rao, A.V. and Manglik, A., 2013. Delineation of aquifers in basaltic hard rock terrain using vertical electrical soundings data, J. Earth System sci., 122(1), 29-41.

Shailaja, G., Laxminarayana, M., Patil, J.D., Erram, V.C., Suryawanshi, R.A. and Gupta, G., 2016. Efficacy of anisotropic properties in groundwater exploration from geoelectric sounding over trap covered terrain, J. Indian Geophys Union, 20(5), 453-461.

Efiong, U.I. and Igboekwe, M.U., 2012. Aquifer Transmissivity, Dar Zarrouk Parameters and the direction of flow of suspended particulate matter in boreholes in MOUAU and the Kwa Ibo River Umudike-Nigeria, Greener J. Physical Sci., 2(3), 70-84.

Received on: 28.11.17; Revised on: 2.4.18; Accepted on: 4.5.18

J. Ind. Geophys. Union (July 2018)
v.22, no.4, pp: 436-443

Assessment of urban pollution from heavy metals concentration in road dust in Greater Hyderabad Municipal Corporation (GHMC), Telangana State, India

R.Sudarshan[1], B.Madhusudan Rao[1*], B.Nagaraju[1], S.K.Patil[2], K.Lohith kumar[3]

[1]Centre of Exploration Geophysics, Osmania University, Hyderabad, Telangana State, India.
[2]K.S.Krishnan Geomagnetic Laboratory (KSKGRL) Allahabad, India.
[3] CSIR-National Geophysical Research Institute (NGRI), Hyderabad, India.
[*]Corresponding Author: profmadhurao@gmail.com

ABSTRACT

Greater Hyderabad Municipal Corporation (GHMC) is witnessing fast urbanization characterized by rapid urban sprawl, population growth, infrastructural construction, industrialization and motorization, which is leading to environmental degradation, placing human health at risk. Presently, heavy metals in road dusts are used as proxies to illustrate environmental changes of GHMC area. In this study 307 dust samples were collected along the roads of GHMC in one season of the year 2014.Further, measurements like Magnetic susceptibility(χ), Anhysteretic remanent magnetization (ARM) and Isothermal Remanent Magnetization (IRM), on these samples have revealed high concentration of magnetic minerals like magnetite and hematite in the urban road dust. The results indicate increasing trends, though not steady, in traffic and industry contributed pollution. Regular measurement and monitoring of these pollution markers in different seasons and for longer periods can help understand area-wise ill-effects of the present trend of urbanization and therefore guide the city planners and rulers.

Key words: Environmental Magnetism, Urbanization, Traffic, Road dust, GHMC.

INTRODUCTION

The problem of urban soil contamination is drawing the attention of city administrators and gaining more importance in solving air pollution. The problem of urban soil contamination with heavy metals is due to rapid industrialization and urbanization. The modernization of industry and the presence of intensive human activities in urban areas have exacerbated the problem of heavy metal contamination in urban soils (Sun et al., 2010). In soil, the total ferrimagnetic component may include primary minerals such as titanomagnetites with geological origins, secondary minerals such as magnetite and maghemite derived through chemical and bacterial processes or produced during burning, and contaminitating polluting dusts containing magnetic spherules (Thompson and Oldfield 1986). In urban areas, pollutants are mainly due to vehicle emission, industrial wastes, the sedimentation of dust and suspended substances in the atmosphere, the combustion of coals and the dry and wet precipitation of other pollutants (Sun et al., 2010). The concentration of these pollutants containing heavy metals vary significantly in urban soils and cause detrimental hazards to human health as it can be easily ingested into human bodies from suspended dust or by direct contact (Madrid et al., 2002; Wang and Yong, 2005). The composition and quantity of chemical matrix of road dust are indicators of Environmental pollution, which results in development of different elements and the high concentration of these elements becoming toxic. Metals such as Pb or Cr, may be tolerated by the ecosystem in low concentration, but become harmful in higher concentrations (Allowayand Ayres 1997; Nriagu 1988).

Hyderabad, the capital city of Telangana State and a major political, industrial and economic center in India, has an area of 650km^2 and has population over 8.7 million. Greater Hyderabad Municipal Corporation (GHMC) is a planned extension of older Hyderabad Municipal Corporation, by adding surrounding municipal corporations.This extension has added some advantages and some disadvantages due to various reasons.One can call GHMC as a newly structured urban conglomeration of importance. It comprises an industrial system strengthened by the presence of organised supporting departments complete with all the facilities.It is planned to give priority to automobile, petrochemical , mechanical processing, electronic, pharmaceutical, aviation, metallurgy, building materials industries, to name a few. Thus it has become absolutely necessary to study the pollution caused by the road dust that has increased phenomenally since the recent past. The main objectives of this study are (1) to determine the concentration and distribution of heavy metals in road

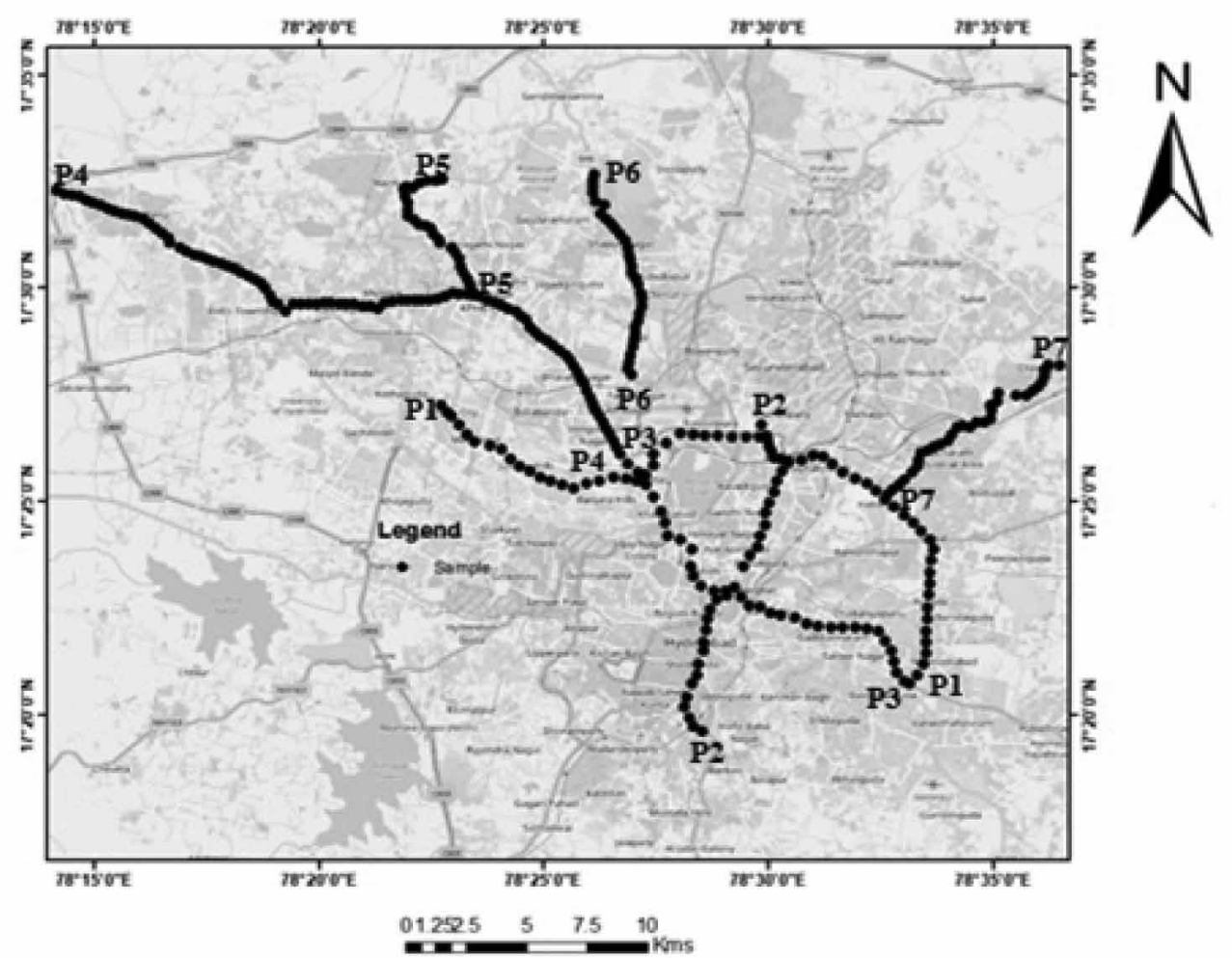

Figure 1. Location Map of the Study Area.

dust of GHMC; (2) to identify the varieties and sources of heavy metals in samples; and (3) to assess the heavy metal grain size in dust samples.

STUDY AREA

The Hyderabad being capital city of Telangana State has several roads, scattered all over the city to meet the transportation needs of the population. Out of these, there are seven major roads which pass through important junctions connected to industrial, academic, scientific labs etc. These roads due to heavy traffic generates considerable air pollution in the city affecting human health. In view of this phenomenal growth of air pollution the entire GHMC area is identified as the study area. The study was carried out along the major roads in the GHMC. Hyderabad produces around 4,500 tonnes of solid waste daily, which is transported from the waste collection points to the dumpsite in Jawaharnagar. Disposal is managed by the Integrated Solid Waste Management project, which was started by the GHMC in 2010. Rapid urbanisation and increased economic activity has also led to increased industrial waste, air, noise and water pollution, which is monitored and regulated by the Telangana Pollution Control Board (TPCB). The contribution of different sources to air pollution in 2006 was: 20–50% from vehicles, 40–70% from a combination of vehicle discharge and road dust, 10–30% from industrial discharges and 3–10% from the burning of household rubbish. This is further exacerbated by inadequately treated effluent discharged from industrial treatment plants polluting the water sources of the city.The GHMC is a city with many and newly emerging industries coupled with high infrastructural development and road construction activities. It has major road and rail links for transporting agricultural produce, textiles and leather goods and wood products. The city has shown tremendous growth in terms of population, infrastructure and traffic density during the last five to six years. Figure 1 presents the map of Telangana State showing the sampling locations in GHMC.

Table 1. Environmental Magnetic Parameters in GHMC

Profile No.		χ_{lf} (10^{-8} m^3 kg^{-1})	$\chi_{fd\%}$,	SIRM (10^{-5} $Am^2 \cdot kg^{-1}$)	χ_{ARM} (10^{-8} $m^3 \cdot kg^{-1}$)	χ_{ARM}/SIRM ($10^3 m.A^{-1}$)	SIRM/ χ_{lf} ($10^3 m.A^{-1}$)	χ_{ARM}/χ_{lf},	S_{-300mT}	SOFT ($10^{-5} Am^2 \cdot kg^{-1}$)
	Max.	1087.48	10.67	6996.73	3552.33	0.95	8.76	5.63	103.81	1872.78
P1	Min.	224.48	0.04	620.31	12.68	0.003	0.70	0.01	88.73	4.71
	Average	564.16	1.56	3412.56	686.78	0.20	6.20	1.14	95.04	310.57
	Max.	868.26	8.70	7060.31	2987.82	0.54	10.27	3.44	105.41	1682.36
P2	Min.	253.70	0.15	984.07	60.21	0.03	3.01	0.16	82.95	35.19
	Average	467.26	1.92	3049.09	550.24	0.16	6.45	1.08	98.13	322.03
	Max.	870.32	7.75	4605.85	1719.03	0.75	7.31	4.69	105.42	483.39
P3	Min.	288.03	0.11	1185.25	11.18	0.004	3.24	0.02	93.93	47.30
	Average	500.68	2.00	2641.31	335.24	0.13	5.34	0.73	98.67	270.99
	Max.	1022.67	9.33	7851.33	2731.74	0.87	13.06	5.79	142.25	1229.65
P4	Min.	127.96	0.03	900.79	31.38	0.01	2.36	0.08	88.78	2.60
	Average	432.51	1.95	3214.20	512.53	0.16	7.42	1.21	97.63	235.47
	Max.	535.89	11.43	3840.72	1582.50	0.68	8.67	4.35	100.58	390.87
P5	Min.	83.83	0.44	588.89	75.32	0.05	3.07	0.21	94.15	5.13
	Average	305.43	5.14	1837.70	412.83	0.21	6.12	1.41	96.43	151.69
	Max.	1283.11	3.73	10296.45	4698.98	0.62	10.81	5.77	101.78	1059.40
P6	Min.	287.91	0.01	562.24	68.68	0.02	0.63	0.12	86.24	16.06
	Average	691.87	1.58	5010.65	1371.68	0.26	7.49	2.06	97.02	322.51
	Max.	1417.41	10.43	9575.80	2735.30	0.71	8.67	2.44	102.73	6643.98
P7	Min.	338.16	0.05	1057.73	114.58	0.02	0.74	0.12	75.78	53.46
	Average	886.69	2.08	5504.49	615.13	0.12	6.35	0.68	96.93	1016.02

P1- LB nagar to Shilparamam, P2-Jublee Bus Station to Falaknuma, P3- LB nagar to Ameerpet, P4- Ameerpet to Patancheru, P5- Miyapur X road to Bachupally, P6- Balanagar to Suraram X road, P7- Habsiguda to Cherlapally.

Laboratory Analysis

The 307 road dust samples have been collected dividing the entire GHMC area into 7 profiles (P1-P7) during December 2013 and February 2014 (Winter Season) from major traffic hotspots as indicated in figure 1 with personal protection. The samples have been collected on the road using a clean broom with dust pan and a plastic packer. On each pickup sample at regular interval of 0.25km distance has weighed between 100g to 150g. The samples have been collected in a new plastic zip cover and properly labeled for later packing. These samples have been wrapped in thin polythene films and packed firmly in pre-weighed standard non-magnetic (styrene) cubic sample holders of 10 cc volume. Magnetic mineral composition in road dust samples have been determined using a magnetic susceptibility (χ) implement.The mineral composition of 1gr samples has been determined using a dual frequency (470 and 4700 Hz) Bartington Instrument`s MS2 sensor and frequency dependent magnetic susceptibility (χ fd%) implement. The anhysteretic remanent magnetization (ARM) is studied by a DC bias field,superimposed over peak alternating (decaying) field of 100 mT using the Molspin Alternating Field Demagnetizer. The isothermal remanent magnetization (IRM) acquisition and its backfield demagnetization curves have been measured with the pulse magnetizer, where the applied field has been progressively increased up to 1 Tesla at room temperature.

RESULTS

The magnetic measurement results of the dust samples are summarized in Table 1. The evaluated magnetic parameter low field susceptibility (χ_{lf}), Satturation isothermal remanent magnetization (SIRM), SOFT [{(SIRM-IRM_{-20mT})/2}/mass] and χ_{ARM} (ARM susceptibility) are along

the 7 profiles P_1-P_7. The details are presented in Table 1 as maximum, minimum and average level values to explain their variation on each profile.The profile along a road reflects the concentration of magnetic materials in the sample, while $\chi_{fd\%}$, χ_{ARM}/χ, χ_{ARM}/SIRM, SIRM/χ, S_{-300mT} (backward remanence) are related to the grain size and the type of the magnetic materials in the sample (Li et al., 2010). The Table 1 shows value of Magnetic susceptibility (χ_{lf}).It varies from 83.83×10^{-8} to 1417.41×10^{-8} $m^3\cdot kg^{-1}$ (average 533.84×10^{-8} $m^3\cdot kg^{-1}$) and the SOFT from 2.60×10^{-5} to 3544.06×10^{-5} $Am^2\cdot kg^{-1}$ (average 324.11×10^{-5} $Am^2\cdot kg^{-1}$), indicating the different types and concentrations of magnetic material in the study area. The range of ARM/SIRM is $(0.003\sim 0.95)\times10^{-5}$ $m\cdot A^{-1}$ (average 0.18×10^{-5} $m\cdot A^{-1}$) and the range of χ_{ARM}/χ is 0.01∼5.79 (average 1.18). These parameters show the diversity and similarity of road dust in GHMC.

Distribution of Magnetic Mineral Content

The statistics of magnetic parameter details (Table 1) shows that the magnetic susceptibility (χ) varies in the Hyderabad city of GHMC area. The maximum values of χ along the P1-P7 (1087.48, 868.26, 870.32, 1022.07, 535.89, 1283.11, 1417.41×10^{-8} $m^3\cdot kg^{-1}$), and the minimum values along the P_1-P_7 (224.54, 253.70, 288.03, 127.96, 83.83, 287.91, 388.16×10^{-8} $m^3\cdot kg^{-1}$) shows the variation details. The SIRM and χ_{ARM} show the point distribution. The maximum and minimum values of SIRM along the P1-P7 (6996.73, 7060.31, 4605.85, 7851.33, 3840.72, 10296.45, 9575.80×10^{-5} $Am^2\cdot kg^{-1}$), (620.31, 984.07, 1185.25, 900.79, 588.89, 562.24, 1057.73×10^{-5} $Am^2\cdot kg^{-1}$) and χ_{ARM} is (3552.33, 2987.82, 1719.03, 2731.74, 1582.50, 4698.98, 2735.31×10^{-8} $m^3\cdot kg^{-1}$), (12.68, 60.21, 11.18, 31.38, 75.32, 68.68, 114.58×10^{-8} $m^3\cdot kg^{-1}$) respectively.The variation in these parameters like χ, SIRM and χ_{ARM} are contoured and presented in Figure 2 (a,b,c), respectively. The result clearly shows that variation is different along each profile.

Types of Magnetic Mineral

To explain the magnetic nature of road dust the back-field demagnetization (B/mT) curves have been drawn between the IRM/SIRM.The collected road dust samples of seven profiles at different fields have been utilised for this study (Figure 3). The result shows that all the samples have a remanence coercivity less than 50 mT, indicating that the dominant magnetic mineral is magnetically soft and magnetite-like component. However, there are differences in the curves obtained from the dust samples. The curves of samples P_1 21, P_2 23, P_3 13, P_4 83, P_5 3, P_6 14 and P_7 31 show a rapid rise below 100mT, reaching 80% SIRM at a magnetic field of 100 mT, and reaching nearly saturation of remanence at 300 mT.The S_{-300mT} has also gone beyond 20%, indicating that the magnetically soft but hard mineral is the dominant magnetic mineral. Further it is noticed that in the entire area of GHMC the road dust particles with more magnetically soft and hard components are present. However, hard particles are more in percentage than the soft in the area ,which is due to contribution from heavy traffic and presence of high level of industrial confluence.

Similarly, the linear correlation between SIRM and χ, SOFT and SIRM (Figure 4) also indicates significant presence of the magnetic properties of the road dust samples. The result exhibited in the figure 3 indicates that the dust samples are dominated by ferromagnetic minerals.

Grain Size of Magnetic Mineral

In the present study the evaluated parameters of the road dust reflect the characteristics of magnetic material with different grain size. To explain this the King plot graph is plotted (from Table 1)for the samples collected in GHMC area (King et al., 1982). The results show that the samples are of 1-5μm in size.This in turn suggests that most of the magnetic domain is a combination of pseudo-single domain (PSD) and multidomain (MD) (Figure 5). χ_{ARM}/SIRM (Figure 5a) shows the relative content of SD and PSD, the higher the ratio value the more the concentration of SD and PSD (Li et al., 2010). Analysis of the χ_{fd}% and χ_{ARM}/SIRM could semi-quantitatively interpret the magnetic mineral grain size. Further, to study the domain of the samples, the Dearing-plot (Figure 5b) is plotted between ARM/SIRM and χ_{fd}%.It indicates that the domain size of the road dust in GHMC area is mainly a composition of PSD and MD. Besides the low χ_{fd}%, could also indicate the low concentrations of super paramagnetic (SP) particles in the samples (below 75%) (Dearing et al., 1997).

DISCUSSION AND CONCLUSIONS

The evaluated magnetic parameters from road dust samples of GHMC area are χ, SIRM and $\chi_{ARM.}$ They indicate the high concentration of magnetic minerals in the samples. Compared to the dust particles caused by natural factors, the samples of street dust consist mainly of coarse MD and PSD grains, due to high level of concentration of industries coupled with anthropogenic pollution caused by heavy traffic, building materials and road friction. The χ, SIRM and χARM values of samples of road dust are higher. However, the values of χARM/SIRM and χARM/χ are lower in the area (Table 1). This variation could be due to the magnetic enhancement in dust samples created by heavy traffic and high concentration of industrial belt. The study shows that degree of pollution changes in an area with traffic and other factors, which contribute and generate the dust.

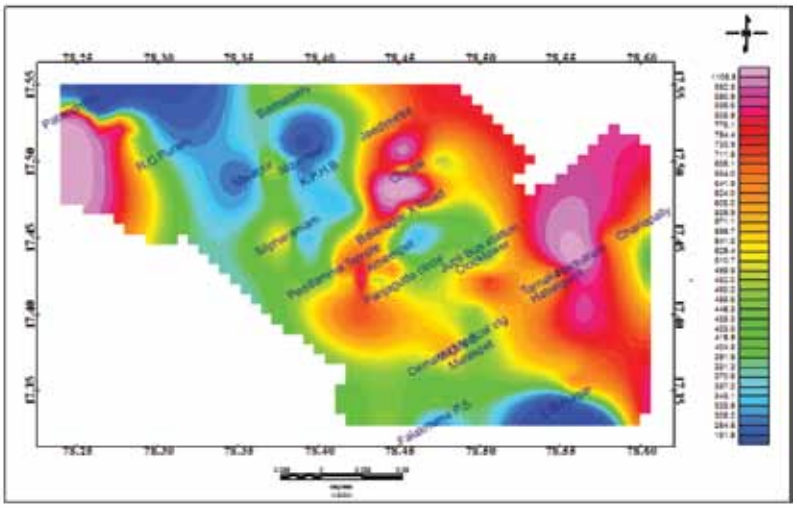

Figure 2(a). Contour map of χ (10^{-8} $m^3 \cdot kg^{-1}$).

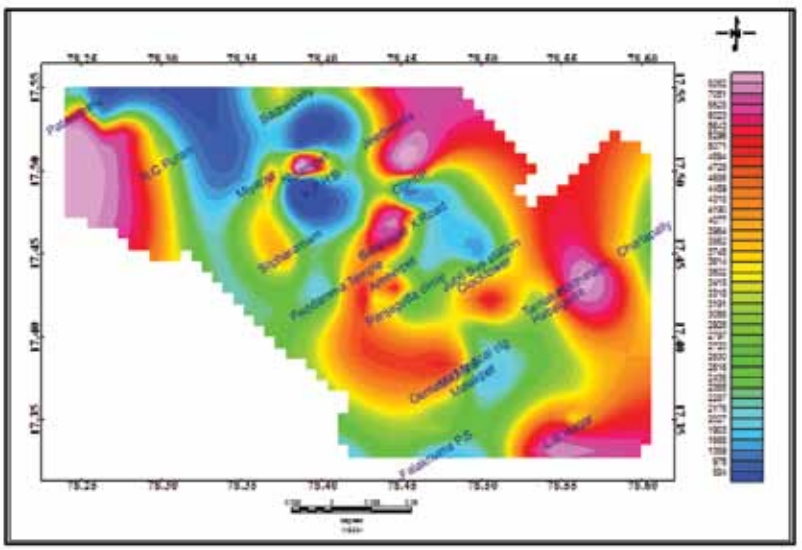

Figure 2(b). Contour map of SIRM (10^{-5} $Am^2 \cdot kg^{-1}$).

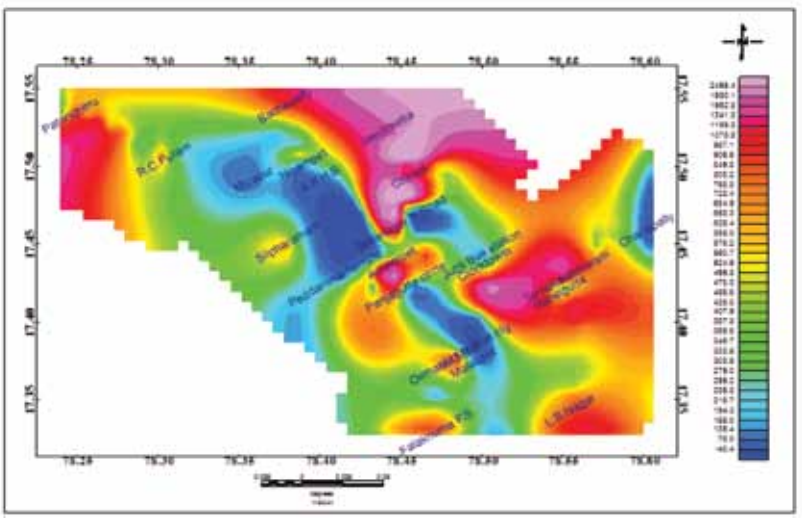

Figure 2(c). Contour map of χARM (10^{-8} $m^3 \cdot kg^{-1}$).

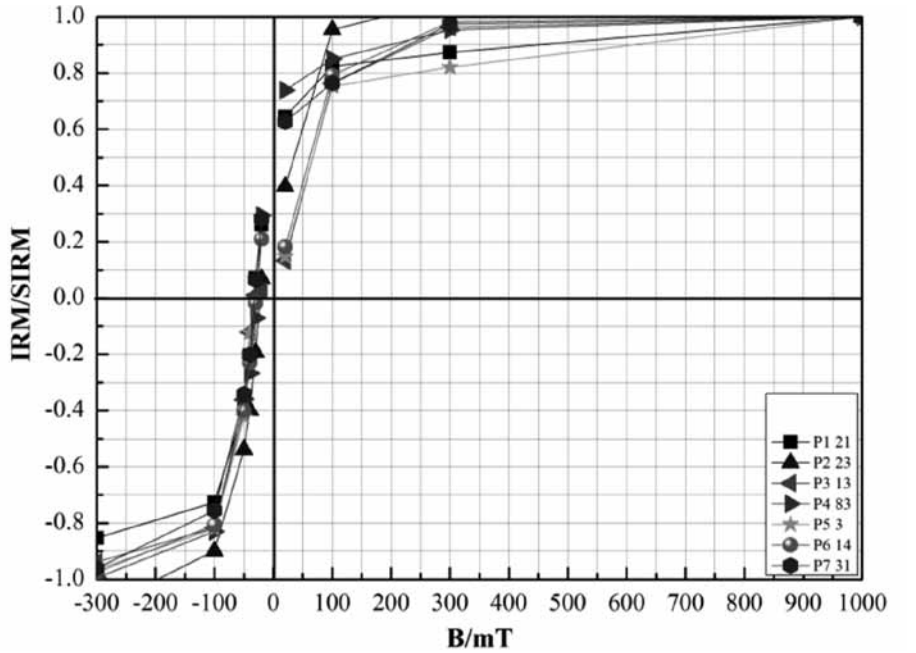

Figure. 3. IRM acquisition curves of typical road-dust samples.

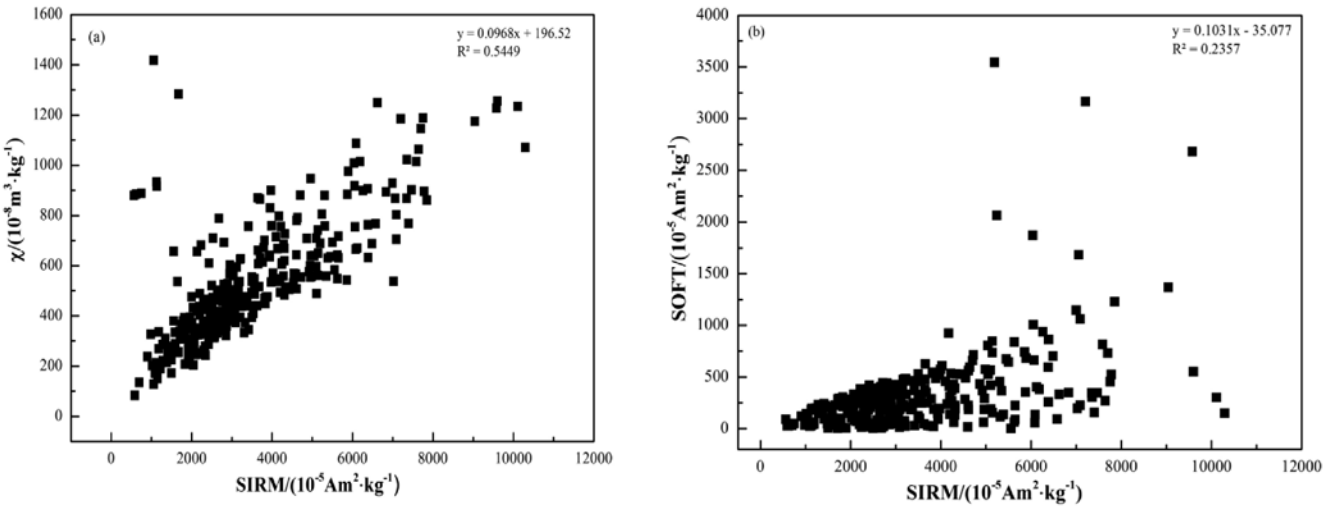

Figure 4. Bi-plots of different magnetic parameters in road-dust samples showing correlation between χ and SIRM; (b) correlation between SOFT and SIRM.

From the Table 1, the χ value of road dust sample in GHMC area exhibits an amount ferromagnetic mineral content with high magnetic nature. The results of Figure 2, show that the values of χ, SIRM and χ_{ARM} are different. This indicates the degree of pollution in the area. The χ presents a regional distribution related to the strength of heavy traffic and industries. The SIRM and χARM present the distribution related to both the level and type of heavy traffic and industrial area. Thus the pollution distribution can be known by the analysis of χ, SIRM and χ ARM.

The study reveals: 1) Ferromagnetic minerals dominate the magnetic properties of the samples. 2) The value of the magnetically soft and hard mineral component in samples of profiles P_1 21, P_2 23, P_4 83, P_5 3, P_6 14 and P_7 31 are from heavy traffic and high concentration of industries in the GHMC. This may result the degree of pollution levels related to traffic density. Thus, the specific technique of magnetic methods used in the present study is significantly effective in studying pollution created by the dust along heavily used roads.

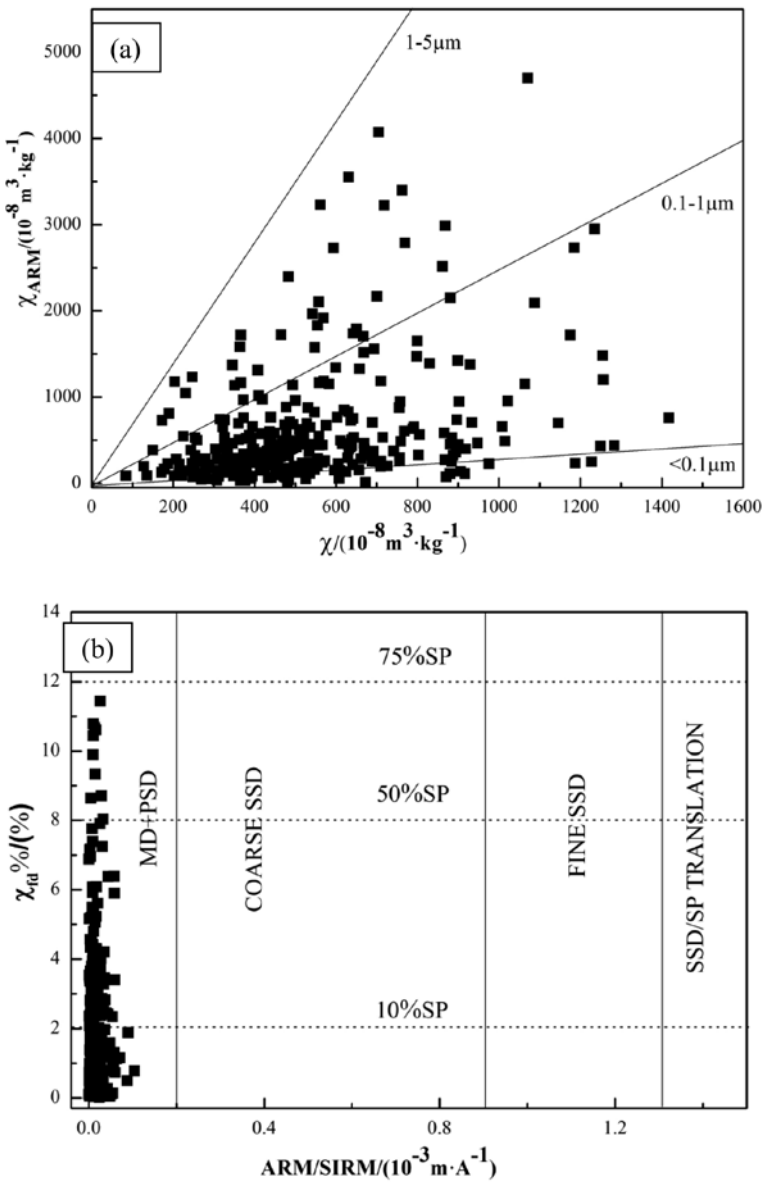

Figure 5: (a) King plot exhibitingcorelation between χ_{ARM} and susceptibility, and (b) Dearing plot exhibiting corelation between χ_{fd} and ARM/SIRM.

The magnetic mineral content in road dust samples of GHMC area, is related to traffic density and presence of industrial corridor. The magnetic measurement thus, could be used as a potential tool for identifying the zones of pollution and classifying the causative sources. Adoption of this technique could be used by the GHMC in monitoring the civic development and urbanization.

ACKNOWLEDGMENTS

We are grateful to CSIR-UGC for providing funds to do the research, and we acknowledge to Dr.K.S.Krishnan Geomagnetic Research Laboratory (KSKGRL), Allahabad for utilizing laboratory facilities. We are thankful to Prof.B.V.S.Murthy for his encouragement and guidance.We are indebted to Dr.P.R.Reddy for systematic reviewing and apt editing.

Compliance with Ethical Standards

The authors declare that they have no conflict of interest and adhere to copyright norms.

REFERENCES

Alloway, B. and Ayres, D.C., 1997. Chemical principles of environmental pollution. CRC press.

Dearing, J.A., Bird, P.M. and Dann, R.J.L., 1997. Secondary ferromagnetic minerals in Welsh soils: a comparison of

mineral magnetic detection methods and implications for mineral formation. Geophys. J. Int., 130, 727-736.

King, J., Banerjee, S.K. and Marvin, J., 1982. A comparison of different magnetic methods for determining the relative grain-size of magnetite in natural materials-some results from lake-sediments. Earth Planet. Sci. Lett., 59(2), 404-419.

Li, P., Qiang, X.K., Xu, X.W., Li, X.B. and Sun, Y.F., 2010. Magnetic properties of street dust: A case in Xi'an city, Shaanxi province, China. Chinese J. Geophys, 53(1), 113-120.

Madrid, L., Diaz-Barrientos, E. and Madrid, F., 2002. Distribution of heavy metal contents of urban soils in parks of Seville. Chemosphere, 49(10), 1301-1308.

Nriagu, J.O., 1988. Production and uses of chromium. Chromium in the natural and human environments, 20, 81-104.

Sun, Y., Zhou, Q., Xie, X. and Liu, R., 2010. Spatial, sources and risk assessment of heavy metal contamination of urban soils in typical regions of Shenyang, China. Journal of hazardous materials, 174(1), 455-462.

Thompson, R. and Oldfield, F., 1986. Environmental magnetism. London: Allen and Unwin.

Wang, X.S. and Yong, Q.I.N., 2005. Correlation between magnetic susceptibility and heavy metals in urban topsoil: a case study from the city of Xuzhou, China. Environ. Geol., 49(1), 10-18.

Received on: 1.12.17; Revised: 22.2.18; Accepted on: 30.4.18

J. Ind. Geophys. Union (July 2018)
v.22, no.4, pp: 444-449

Preliminary ground based measurements of Aerosol Optical thickness over Udaipur (Rajasthan), India

Roshni Dave*[1] and Malini Aggarwal[2]

[1]Department of Physics, Silver Oak College of Engineering &Technology, Ahmedabad, India, 382481
[2]Indian Institute of Geomagnetism, Navi Mumbai, India, 410206
*Corresponding Author: roshnidave.gn@socet.edu.in

ABSTRACT

We have carried out studies to understand the variability of Aerosol Optical Thickness (AOT) and precipitable water-vapour content (PWC) over Udaipur (24.58°N, 73.71°E), using hand-held microprocessor based MICROTOPS sun photometer-540 (1020 nm and 936 nm) from February, 2002 to March, 2004, excluding the rainy days (total of 156 days of clear-sky observations). We found that monthly AOT varied between 0.16 and 0.54 during the whole period and was higher in summer (mean value ~0.32) than the winter months (mean value ~0.19) with highest value in pre-monsoon month of June (0.54). The day-to-day variability of AOT is also higher in summer than winter months and is lowest during the post-monsoon months. We also found PWC to be maximum in monsoon month (July, ~3 cm) and minimum in December-February (~0.5 cm) winter months. A positive moderate correlation (0.45) between monthly AOT and PWC over the station during the study period is reported. This suggests that the production and loss of aerosol particles, which are hygroscopic in nature, are also associated with precipitable water-vapour content along with the other meterological factors.

Key words: Aerosol, Climate, precipitable water-vapour, atmosphere.

INTRODUCTION

Aerosols (tiny suspended particles in the atmosphere) are in the forefront of climate studies since last three decades, owing to the role they play in the Earth-Atmosphere system by absorbing or scattering the incoming solar radiation thus warming or cooling the atmosphere and hence playing an important role in the earth's radiation budget (Bellouin et al., 2005; Carlo et al., 2017). Atmospheric aerosols are contributed by natural as well as anthropogenic sources. Their natural source includes volcanoes, dust, forest, vegetation and sea-spray. Natural sources, such as volcanic activity, produce synoptic scale effects; while other sources, such as wind-blown dust, sea-spray, convective and general circulations produce regional-scale effects in modulating the background aerosols. Anthropogenic aerosols are short-lived and mostly produce negative radiative forcing. The major sources of anthropogenic aerosols are fossil fuel and biomass burning and these sources are also associated with degradation of the air quality and acid deposition. On a global scale, the natural sources of aerosols are more important than the anthropogenic aerosols but regionally, anthropogenic aerosols are considered more important (Kaufman et al., 1994 and Ramanathan et al., 2001). Moreover, aerosols influence the solar radiation both directly and indirectly through their various sizes and thus have different optical and physical properties. When aerosol particles are small, they act as cloud condensation nuclei and help in the formation of clouds and when sufficiently large in size, they scatter and absorb sun light (Rosenfeld, 2006). Although the dynamics change the aerosol size spectrum during their residence time, the particle population highly relies on the strength of their source and sinks mechanisms. As a result, concentrations of ambient aerosol differ to a great extent between urban and remote areas, and between industrialized and rural regions (Rao et al., 2001). The aerosols in the size 0.1-1 μm are considered most effective in attenuating the sunlight.

One of the important parameters related to the aerosol is the Aerosol Optical Depth (AOD) which is defined as a measure of extinction of solar radiation passing through the atmosphere due to absorption or scattering by the aerosols. There are several recent studies for the measurements of AOD over the whole globe (Engström and Ekman, 2010; Altaratz et al., 2013) and also over the Indian sub-continent (for e.g., Ranjan et al., 2007; Srivastava et al., 2008; Ramachandran et al., 2012). The seasonal and annual mean trends in AOD for a decade (2002-2012) have been derived using MODIS (Moderate Resolution Imaging Spectrometer) Level 2 data over different locations in India where AODs values were found to increase across India (Ramachandran et al., 2012). The AOD trends exhibited spatial, seasonal and annual mean variations. They found that both AODs and rainfall increases in that decade over most of the study locations like Delhi, Shimla, Dehradun, Jaipur, Hyderabad and Bengaluru.

The seasonal and inter-annual variability in AOD and aerosol size distribution were investigated using sun photometer, sun/sky radiometer, MODIS and MSIR (M Radiometer) satellites over stations: Ahmedabad,

Gurushikhar, Karachi, Kanpur and Gandhi College in Balliyan District of Uttar Pradesh in South Asia during 2006-2008 by Ramachandran (2013). They found that the AOD value was almost double over Karachi and Ahmedabad of the value observed at Gurushikhar, a high altitude remote site. Their study of ground-based and MODIS (Terra and Aqua) retrieved AODs showed that AODs do not change significantly in an hour. The comparative studies of column ozone content using MICROTOPS, TOMS and DOBSON unit over a low-latitude station, Udaipur is obtained by Pandey and Vyas (2004) and found a similar trend by three measurement techniques for column ozone during January 2001 respectively The correlative measurements of Ozone by MICROTOPS and TOMS was observed to be good (r=0.92) and MICROTOPS values were in 10% range of TOMS. Inspite of these observations, more studies on temporal and spatial distribution of AOD and their associated properties are needed to be accomplished regularly to understand the role of aerosols in the weather modification and climate change and related predictions. Hence, the aim of the present study is to investigate the variability of the AOD and precipitable water-vapour content (PWC) over Udaipur which is situated in desert area along with the lakes. This study shows the observations during 2002-2004 using MICROTOPS sunphotometer over Udaipur and hence may enhance the understanding of air-quality and the regional characteristics of the aerosols over a temperate city like Udaipur, which is considered as a pollution-free city. This may also serve as an investigation of background aerosols in a clean city which can be compared with the polluted cities. The AOD which acts as a proxy for the aerosol concentration also explains the variations in the cloud fraction atleast to some extent (Andreae, 2009).

Data Set

Udaipur city (24.58°N, 73.71°E) known as 'city of lakes' (~598 m above sea level), located among the lush green hills of Aravali range, lies in the western part of India under the tropical climate. The region experiences three main seasons viz. summer (mid-March to June), monsoon (July to September) and winter (October to March) respectively. Being located in the desert lands of Rajasthan, the climate and weather of Udaipur is usually hot during summer (25-40°C) and cool and dry during winter (10-28°C). Monsoons arrive in the month of July heralded by dust and thunderstorms. The city annually receives around 63.7 cm of mean rainfall. This scanty amount of rainfall makes Udaipur more humid. The humidity reaches to the extent of 90% during the months of Monsoon.

The Microtops II Sun photometer available in Mohanlal Sukhadia University, Udaipur is capable of measuring the atmospheric aerosol thickness (AOT≈AOD) which is a basic measure of aerosol in the atmosphere and is also an evaluation of decrease of solar radiation while passing through a column of atmosphere. Using Microtops II Sun photometer, we determined the AOT at a single wavelength, 1020 nm only. It is also used to measure the water vapor content at 936 nm wavelength. The complete details of the sun photometer and measuring technique have been described by Morys et al., (2001). The AOT measurements using this sun photometer are of limited use as the size distribution of aerosols cannot be attempted. We obtained the daily measurements of AOT at 1020 nm and precipitable water content (PWC) at 936 nm over Udaipur region. The AOD values are inversely proportional with the wavelength (Kohil et al., 2017). The wavelength 936 nm is water absorption band whereas 1020 nm is not.

Aerosols in Udaipur are unique of its kind in terms of its sources. There are marble, zinc and cement mining units in the city which are considered as potent source of loading of aerosols and hence cause environment pollution (Pandey and Vyas, 2004). We made the observations of AOT and PWC for about two years from February, 2002 to March, 2004, excluding the monsoon periods. Due to variable weather conditions and monsoon periods, observations were not regular and continuous and hence the data for such months are not available. The Figure 1 represents the total number of observations made in each month respectively. We found a total of 156 days of clear-sky observations during the study period. As the aerosols have a relatively weaker optical signal that often suffers from a low signal-to-noise ratio, it becomes even harder in the vicinity of clouds, as the separation between clouds and aerosols is not always clear (Koren et al., 2007) and hence the probability of cloud contamination (contribution of small and thin clouds to the aerosols signal) becomes higher (Zhang et al., 2005). In addition, clouds can illuminate the aerosols in their vicinity (Marshak et al., 2006) and such an illumination may falsely be interpreted as enhanced AOD, hence we have selected only the clear sky. The figure shows that more number of observations were made during April and October, 2003 than other months due to a restriction of clear-sky weather.

Since the sun-photometer can take the observations only when sun is available and therefore due to variability of weather conditions, the data sets are not taken continuously. Hence, the gap in the observational data is obvious. Number of observations in different months has been further affected by the cloud conditions and hence, the observations were avoided on such days.

For the validation of MICROTOPS sunphotometer measurements, we compared the AODs and PWC as measured by MICROTOPS and MODIS (Moderate Resolution Imaging Spectrometer)-Aqua measurements. This data validation covers the period since the MODIS instrument data is available (July 2002) to the March 2004 respectively. MODIS measures the Earth leaving radiances in 36 high resolution bands from 0.4 to 14.0 microns with

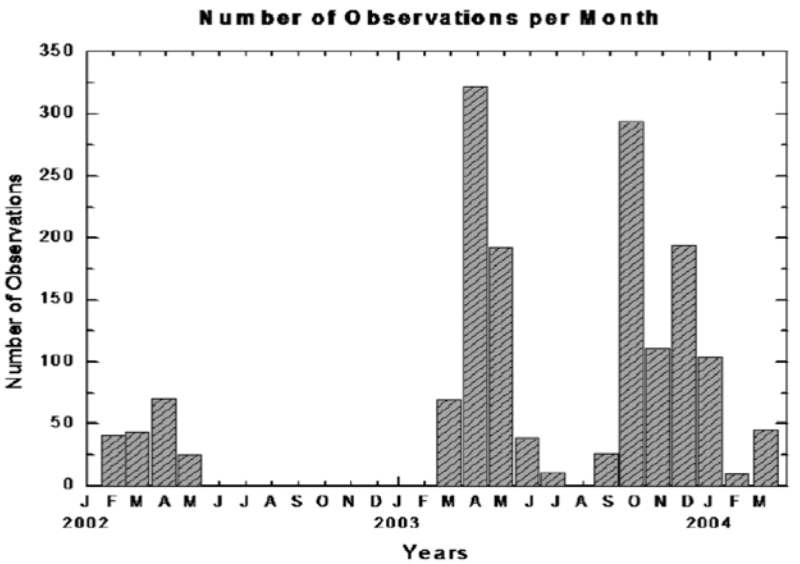

Figure 1. Representation of the number of observations in each month during February, 2002 to March, 2004.

a spatial resolution of 250 m, 500 m and 1 km depending on the wavelength. Its large swath of 2330 km allows the nearly global coverage within 1 or 2 days. We obtained the dataset belonging to the Collection 6 MODIS level 3 monthly mean AODs at 550 nm (variable name "Deep_ Blue_Aerosol_Optical_Depth_550_Land") and Atmospheric water vapour (variable name "Atmospheric_Water_Vapor_ Mean") within a 1 × 1 degree grid cell respectively, which are produced from higher order level 2 data (Patrick et al., 2015).The averaged monthly AOD and Atmospheric water vapour (AWV, equivalent to Precipitable water vapour content, PWC in atmosphere) is obtained over 73.5°-74.5°E and 24.5°-25.5° N respectively.

RESULTS AND DISCUSSION

Aerosol optical thickness at 1020 nm

The daily values of aerosol optical thickness (AOT) at 1020 nm in each month were measured for the period from February 2002 to March 2004. The monthly mean values of AOT at 1020 nm and AOD at 550 nm with their standard deviation values for each month is represented in Figure 2. The monthly AOT values varied between 0.16 and 0.54 for the whole period. The length of the bar for each point indicates its variability in particular month which is higher in summer months This represents that the mean value of AOT at 1020 nm increases from winter (mean ~0.19) to summer months (mean ~0.32), peaks just prior to monsoon (~0.54) and falls suddenly after the monsoon respectively. The highest AOT was recorded in June month. Here, the loading of aerosols during the pre-monsoon months and washing out during the monsoon months are clearly indicated. A similar trend using different wavelength filter has also been reported earlier by Narasimhamurthy et al., (1998); Niranjan et al., (1998) and Ranjan et al., (2007) over other Indian stations: Mysore, Visakhapatnam and Rajkot respectively. The MODIS-AODs at 550 nm also exhibits similar seasonal trend but the values are lower in winter months but matches well in summer and monsoon months. The day-to-day variability of MODIS-AODs as observed by standard deviations is also higher in summer months than winter months, which is in agreement to the MICROTOPS observations. The correlation is found to be moderate (0.50) between the AODs at 1020 nm by MICROTOPS-II and the AOD at 550 nm by MODIS. Misra et al., (2008) also compared the MODIS derived AODs with the ground based Microtops sunphotometer over Indian station, Ahmedabad (72.5°E, 23.03°N) and found the best correlation in pre-monsoon (April-May) and the least during dry season (December-March) respectively. Jethva et al., (2005) found a systematic overestimation by MODIS during summer and an underestimation during winter respectively.

Precipitable water-vapour content (PWC) at 936 nm

The monthly variation of precipitable water vapour content (PWC) at 936 nm and the atmospheric water vapour (AWV) measurements at infra-red with their standard deviations showing the daily variabilities for each month is shown in Figure 3. The distribution of water vapour content in the atmosphere is considered a good indicator of the dynamics of the circulation systems in the atmosphere (Raj et al., 2004). The hygroscopic growth of aerosols gets controlled by the relative humidity (RH) of the atmosphere which changes the physical and optical properties of the aerosols.

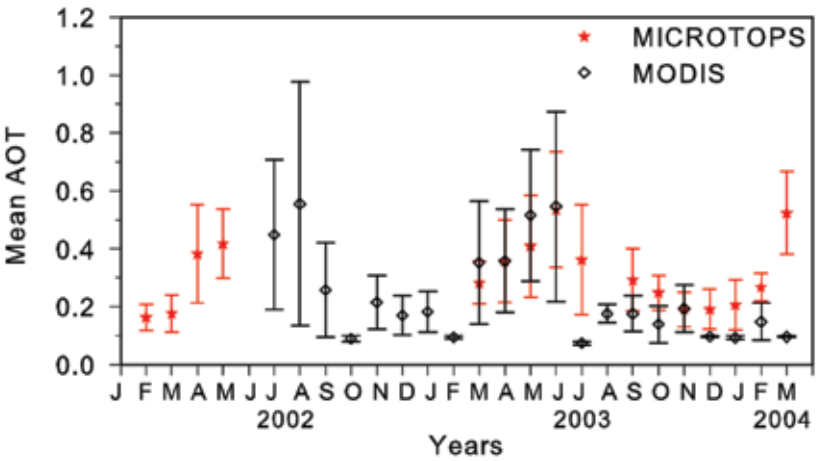

Figure 2. Monthly mean aerosol optical thickness at 1020 nm by MICROTOPS-II and at 550 nm by MODIS with their standard deviations during the study period.

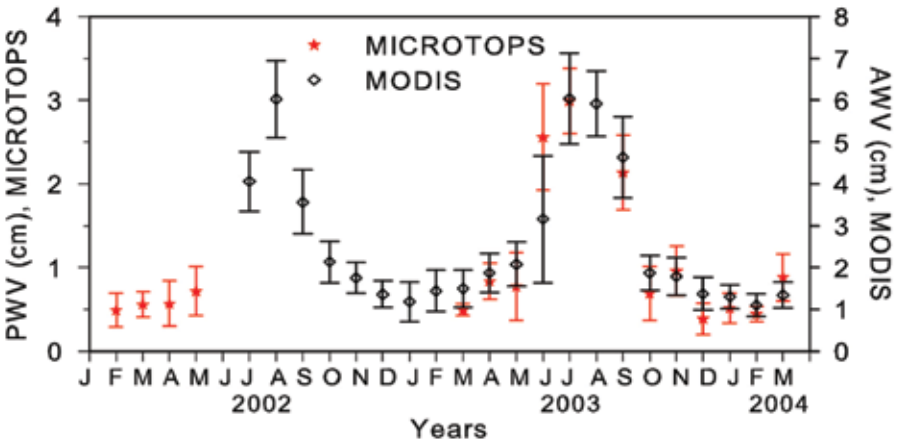

Figure 3. Monthly mean precipitable water content at 936 nm by MICROTOPS and atmospheric waver vapour content at Infra-red by MODIS with their standard deviations during the study period.

The monthly PWC varied between 0.3 and 3 cm during the whole period. The variability in PWC is found to be higher during the months of June, July and September and monthly mean value is highest (~3 cm) in the month of July and minimum in December-February i.e. winter months (~0.5 cm). This is expected as these are the normal monsoon months (July-September) for Udaipur. The lower values of PWC are observed for the months of October to May. Similar variability is observed by the MODIS-AWV, but the values are higher than that of MICROTOPS and highest values are observed in monsoon (~6 cm). The AWV varies between 1 and 6 cm during the whole period with highest variability in monsoon months. The correlation between the PWC as obtained by MICROTOPS-II and the AWV at infra-red by MODIS is found to be very strong (0.92).

Relation between AOT and PWC

As both observed AOT and water-vapour content by MICROTOPS exhibits similar trend and may be related, we plotted them together in figure 4 to find if any relation exists. We considered the PWC as a variable as in high humidity regions, aerosols may take up water vapor which increases the AOT. A high relative humidity is also important for cloud formation and thus AOT and cloud fraction could be correlated as a result of variations in the relative humidity (Engstrom and Ekman, 2010).

The value of the correlation coefficient between monthly AOT and PWC for the whole study period was found to be 0.45 implying that the annual variation of PWC followed that of AOT but moderately. The moderate correlation occurs due to the monsoon period and the November 2003 month when both AOT and PWC does not show a clear relation. The AOT was highest in the June month of year 2003 (~0.54), whereas water vapour was higher (~3 cm) in the July month of the same year. This indicates that higher AOT in the summer months (pre-monsoon period) gets washed away by the rains in the monsoon period (July-September) due to this reason, and

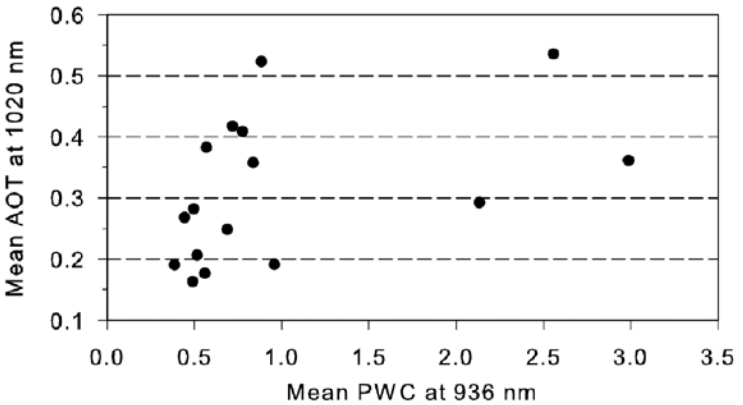

Figure 4. Plot showing the variability of monthly precipitable water vapour content and aerosol optical thickness.

hence the AOT value decreases to ~0.35 in the July month. In other winter and summer months, both AOT and PWC exhibits a stronger correlation (~0.78), as both are either lower/higher in winter/summer months respectively. The moderate positive correlation observed between AOT and PWC also suggested that the growth of aerosols, which are hygroscopic in nature is seldom associated with higher PWC and are also associated occasionally with other meterological factors like temperature, pressure, humidity and/or wind speed and direction. By examining the covariation of AOD and cloud fraction with different meteorological variables, Engstrom and Ekman (2010) found that the 10-meter wind speed correlates significantly with both AOD and cloud fraction. Similar short term trends of AOT and PWC have also been reported by Pandey and Vyas (2004) at Udaipur using tropospheric ozone content over same station. The similar trends were also observed in our observations for AOT and PWC in the months of April and May, 2002 where the column water increased, following AOT just before monsoon in June, 2002. Both AOT and water column content attained lower levels during winter months of November, December and January. Our results are in the qualitative agreement with the results reported by other investigators at other Indian stations (Narasimhamurthy et al., 1998, Moorthy et al., 1993, 1998).

CONCLUSIONS

The aerosol size distribution depends on their production mechanism. Some particles are small in size as they are formed by gas-to-particle conversion. Some particles are large in size as they are formed by mechanical actions such as wind lifting of dust, wave-breaking, etc. In general, the anthropogenic aerosols are smaller in size and the naturally produced particles are of bigger size. Generally the AOT at higher wavelength (1020 nm) is because of aerosols of coarse size. Hence, AOD measurements made in our study are aerosols of bigger size which are naturally produced.

These preliminary observations of aerosol optical thickness (AOT) and Precipitable water-vapour content (PWC) has helped us in knowing the air-quality and understanding the existence and behaviour of the aerosols and water-vapour content present over Udaipur (24.58°N, 73.71°E) during February, 2002 to March, 2004 respectively. The monthly AOT values at 1020 nm varied between 0.16 and 0.54, whereas PWC at 936 nm varied between 0.3 and 3 cm respectively as obtained by the ground-based MICROTOPS II sunphotometer. The AOT measurements exhibited seasonal variability of aerosol where AOT increased gradually from winter (~0.19) to summer (~0.32) months and was highest in pre-monsoon (~0.54) which reduces drastically for the post-monsoon months. The variability in PWC is found to be higher in June, July and September with highest value in July (~3 cm) and minimum in December-February winter months (~0.5 cm). The MODIS-AODs at 550 nm and Atmospheric water vapour content (AWC) also exhibited trends similar to MICROTOPS measurements but AWC measurements were higher by MODIS. The correlation is found moderate (0.50) for AOD measurements and very strong (0.90) for PWC between the MICROTOPS-II and MODIS measurements. The correlation coefficient between observed monthly AOT and PWC was found to be positive and moderate (0.45) implying that the annual variation of PWC followed that of AOT but moderately and also dependant on other meterological factors like rainfall, temperature, humidity, wind speed and direction respectively.

ACKNOWLEDGEMENTS

RD is thankful to Prof. Rajesh Pandey, Emeritus Scientist, Mohanlal Sukhadia University, Udaipur for his valuable suggestions and comments during collection of data and his constant encouragement throughout the research work. We would like to acknowledge the Land Processes Distributed Active Archive Centre (LPDAAC) for providing the MODIS

aerosol and atmospheric water vapour online. We are also thankful to the Reviewers for their useful comments and suggestions.

Compliance with Ethical Standards

The authors declare that they have no conflict of interest and adhere to copyright norms.

REFERENCES

Altaratz, O., Bar-Or, R.Z., Wollner, U. and Koren, I., 2013. Relative humidity and its effect on aerosol optical depth in the vicinity of convective clouds, Environ. Res. Lett., 8(3), article id. 034025.

Andreae, M.O., 2009. Correlation between cloud condensation nuclei concentration and aerosol optical thickness in remote and polluted regions, Atmos. Chem. Phys., 9, 543–556.

Bellouin, N, Boucher, O., Haywood, J. and Reddy, M.S., 2005. Global estimate of aerosol direct radiative forcing from satellite measurements, Nature, 438(7071), 1138-1141

Carlo L., Otto P.H. and Omar T., 2017. Direct radiative effect of aerosols based on PARASOL and OMI satellite observations, J. Geophys. Res., 122(4), 2366–2388.

Engström, A. and Ekman, A.M.L., 2010. Impact of meteorological factors on the correlation between aerosol optical depth and cloud fraction, Geophys. Res. Lett., 37(18), L18814.

Jethva, H., Satheesh, S.K. and Srinivasan, J., 2005. Seasonal variability of aerosols over the Indo-Gangetic basin, J. Geophys. Res., 110, D21204, doi: 10.1029/2005JD005938.

Kaufman, Y.J., Gitelson, A., Karnieli, A., Ganor, E., Fraser, R.S., Nakajima, T., Mattoo, S. and Holben, B.N., 1994. Size distribution and scattering phase function of aerosol particles retrieved from sky brightness measurements, J. Geophys. Res., 99, 10341-10356.

Kohil, E.E., Saleh, I.H. and Ghatass, Z.F., 2017. A study of atmospheric aerosol optical properties over Alexandria city- Egypt",XXIII International Conference on Spectral Line Shapes IOP Conf. Series: J. Phy. Conf. Series, 810.

Koren, I., Remer, L.A., Kaufman, Y.J., Rudich, Y. and Martins, J.V., 2007. On the twilight zone between clouds and aerosols, Geophys. Res. Lett., 34(8), L08805.

Marshak, A., Platnick, S., Varnai, T., Wen, G.Y. and Cahalan, R.F., 2006, Impact of three-dimensional radiative effects on satellite retrievals of cloud droplet sizes J. Geophys. Res., 111, D09207.

Misra, A., Jayaraman, A. and Ganguly, D., 2008. Validation of MODIS derived aerosol optical depth over Western India, J. Geophys. Res. Atm., 113, D04203.

Moorthy K.K., Prabha R., Nair, Prasad, B.S.N., Muralikrishna, N., Gayatri H.B., Narsimhamurthy, B., Niranjan, K., Ramesdh Babu, V., Satyanarayan, G.V., Agashe, V.V., Ather, G.R., Singh, S., and Srivastava, B.N., 1993. Results from the MWR network of IMAP, Indian J. Radio Space Phys., 22, 243-258.

Moorthy K.K., Nair P.R. and Satheesh S.K., 1998. Global change studies, scientific results from ISRO-GBP, (eds. Subbaraya et al.), 45-66.

Morys, M., Mims III, F.M., Hagerup, S., Anderson, S.E., Baker, A., Kia, J. and Walkup, T., 2001. Design, calibration, and performance of MICROTOPS II hand-held ozone monitor and sun photometer. J. Geophys. Res. 106, 14573–14582.

Narasimhamurthy, B., Raju, N.V., Thukarama, M., Prasad, B.S.N. and Krishna Moorthy, K., 1998. MWR Studies of the temporal and spectral features of atmospheric aerosols over Mysore (12.3^{0}N), In Global change studies, scientific results from ISRO-GBP (eds. Subbaraya, B.H. et al.), 77-92.

Niranjan K., Thulasiraman S. and Satyanarayana G.V., 1998. Variation of aerosol spectral optical depths and size distribution at Visakhapatnam during 1987-96, In Global change studies, scientific results from ISRO-GBP (eds. Subbaraya, B. H. et al.), 67-76.

Pandey, R. and Vyas, B.M., 2004. Study of total column ozone, precipitable water content and aerosol optical depth at Udaipur, a tropical station, Curr. Sci., 86(2), 305-309.

Patrick, S., et al., 2015. MODIS Atmosphere L3 Monthly Product. NASA MODIS Adaptive Processing System, Goddard Space Flight Center, USA: http://dx.doi.org/10.5067/MODIS/MOD08_M3.006.

Raj, P.E., Devara P.C.S., Mahesh kumar, R.S., Pandithurai G., Dani, K.K., Saha S.K., Sonbawne S.M. and Tiwari, Y.K., 2004. Results of sun photometer–derived precipitable water content over a tropical Indian station, J. Appl. Meteorology, 43, 1452-1460.

Ramanathan V., Crutzen, P.J., Lelievld, J., et al., 2001. Indian ocean experiment: An integrated analysis of the climate forcing and effects of the great Indian ocean haze, J. Geophys. Res., 106, 28371-28398.

Ramachandran S., Sumita K. and Rohit S., 2012. Aerosol optical depth trends over different regions of India, Atmos. Env., 49, 338-347.

Ramachandran, S., 2013. Aerosol optical properties over South Asia from ground-based observations and remote sensing: a review, Climate, 1, 84-119.

Ranjan R.R., Joshi H.P. and Iyer K.N., 2007. Spectral variation of total column aerosol optical depth over Rajkot: a tropical semi-arid Indian station, Aerosol and Air Quality Res., 7, 33-45.

Rao, P.S.P., Momin, G.A., Safai, P.D., Ali, K., Naik, M.S. and Pillai, A.G., 2001, Aerosol and trace gas studies at Pune during INDOEX IFP-99. Curr. Sci. 80, 105-109.

Rosenfeld, D., 2006, Aerosols, Clouds and Climate. Science, 312, 1323-1324.

Srivastava, A.K., Devara, P.C.S., Rao, Y.J., Bhavanikumar, Y. and Rao, D.N., 2008. Aerosol optical depth, ozone and water vapor measurements over Gadanki, A tropical station in peninsular India, Aerosol and Air Quality Res., 8(4), 459-476

Zhang, J.L., Reid, J.S. and Holben, B.N., 2005, An analysis of potential cloud artifacts in MODIS over ocean aerosol optical thickness products, Geophys. Res. Lett. 32, L15803.

Received on: 12.1.18; Revised on: 5.2.18; Accepted on: 15.4.18

J. Ind. Geophys. Union (July 2018)
v.22, no.4, pp: 450-454

Study and analysis of weather parameters during avalanche for Bahang region, Manali (Himachal Pradesh)

Neha Ajit Kushe* and Ganesh M. Magar

P.G. Department of Computer Science, S.N.D.T. Women's University, Juhu Road, Mumbai-49

*Corresponding Author: neha.kushe@hotmail.com

ABSTRACT

Snow avalanche has been an integral part of the natural hazards in the mountainous region. In India, avalanches are mainly observed in the north and north-eastern zone of the country, which mainly comprises of Himalayas and their surrounding areas. The Himalayan region is broadly classified into Upper, Middle and Lower Himalaya Zones. However, due to the varied nature of meteorological and environmental conditions, the avalanche climatology is not the same for the whole Himalayan range and the environmental factors that lead to avalanche in all these zones, are different. This paper presents the study and analysis of the weather parameters during avalanche, to find influencing range of the weather parameters for avalanche occurrence in Bahang region of Manali, Himachal Pradesh, which falls in the Lower Himalaya Zone.

Keywords: Avalanche, Bahang region, Himalayas, Meteorological parameters, Snow.

INTRODUCTION

Avalanche is considered one of the most hazardous phenomena occurring in the mountainous terrain throughout the world. It has been observed in every continent which boasts of an area having snow covered mountains. Though normally considered a natural disaster, an avalanche can also be caused due to other factors, like skiers, snowmobilers, animals or explosives. Avalanche consists of snow masses, mainly containing of ice along with rocks, soil, vegetation, etc. which descend steep slopes at an accelerated rate (Schweizer et al., 2003). They are said to be naturally triggered when the force of the snow exceeds the strength of the snowpack, leading to a mechanical failure in the snowpack. Because of this, the snow breaks and starts sliding down the mountain slope. The main factors contributing to avalanche danger are terrain, fresh precipitation, wind, temperature and snowpack stratigraphy (Schweizer et al., 2003). However, the most important terrain factor dominating the avalanche release is slope of the terrain (Schweizer et al., 2015). This is because the slope is the only factor which remains constant over time and normally a slope angle >30° is required for avalanches (Schweizer et al., 2003). The Avalanche Path mainly consists of three main zones, namely starting zone, track and runout zone (International Association of Hydrological Sciences. International Commission on Snow and Ice, 1981). Starting zone is where the initial snow mass releases, track consists of the path traced by the avalanche and runout zone is where avalanche decelerates and snow is deposited.

In India, avalanches are observed majorly in the north and north-eastern zone of the country, which mainly comprises of Himalayas and their surrounding areas. It is considered the third largest deposit of ice and snow in the world, after Antarctica and the Arctic. It encompasses about 15,000 glaciers (PBS, 2011). Further the higher regions of the Himalayas are snowbound throughout the year and it boast of a permanent snow line of around 5,500 metres, which is the highest in the world (Ya-feng et al., 1980). However due to such environmental factors, numerous number of avalanches have hit the Himalayas. In India, Snow & Avalanche Study Establishment (SASE) was setup in Manali in the year 1969 to study the snow and avalanche problems in the snowbound belt of Indian Himalayas (Sharma, 2000). Indian Himalayan region experience such a wide diversity in climatic and precipitation patterns that the snow properties and related avalanche activity assume a wide variation. Accordingly, the Western Himalayas has been classified into Lower Himalaya zone or Subtropical zone, Middle Himalaya zone and the Upper Himalaya zone or High Latitude zone (Sharma and Ganju, 2000). Further in order to obtain snow-meteorological data from these various parts of Indian Western Himalayas, 46 manned observatories and 16 Automatic Weather Stations (AWS) were installed (Ganju and Singh, 2004). However, algorithms and parameters influencing the avalanche activity for each zone of the Himalayas at any given time are different (Sharma and Ganju, 2000). As a result, the parameters that are normally considered to find avalanche probability for a region in Upper Himalaya zone, may not be the same as the factors affecting the avalanche occurrence for a region in Lower Himalaya zone. Hence individual study of the climatic conditions for each region is required for formulating an accurate avalanche prediction model. A similar observation station was installed in

Figure 1. Location of the study area of Bahang region in Himachal Pradesh.

Table 1: List of Parameters Considered

S.no	Variable	Characteristics Period/Time	Unit
1	Maximum Temperature	Day x	°C
2	Minimum Temperature	Day x	°C
3	Dry Temperature	0830 h (x)	°C
4	Wet Temperature	0830 h (x)	°C
5	Pressure	0830 h (x)	millibar
6	Average Wind Speed	0830 h (x-1)-0830 h (x)	kmph
7	Humidity	0830 h (x)	%
8	Sunshine	0830 h (x-1)-0830 h (x)	hrs: min

Bahang Region of Manali, Himachal Pradesh. Present study is to find the ranges of the meteorological parameters in which avalanches have occurred in Bahang. Figure 1 presents the location of the Bahang Region.

STUDY AREA AND DATA CHARACTERISTICS

Observation station was installed at Bahang (2192 m) in Manali, which falls in the Pir Panjal Range of Lower Himalayas (Gusain et al., 2014). Weather trends for Bahang from the year 1976 to 2011 showed an increasing trend for maximum and minimum temperature and decreasing trend for snowfall. Snow and meteorological data from this observatory was used to find the relation of parameters to the avalanche activity. The past records corresponding to 22 snow meteorological variables from the period from Jan 2005 to March 2013(covering the months from Jan to March in each winter), was archived in the database with respective dates of observation. The list of the parameters used for this study are given in Table 1.

A total of 812 days was considered for this study, which comprised of 1624 records which were taken at 0830 hrs and 1730 hrs (both IST (GMT + 5.30)). For each record, the associated avalanche information was also stored in the database and used for this study. The relation between wet temperature, dry temperature and humidity was used to find the missing values in either of these three columns (Stull, 2011). The rows that still consisted missing values were discarded and thus a total data of 805 days was used for the present study.

Table 2. Probability of Avalanche Occurrence for each parameter in each range

Range	Max Temp	Min Temp	Dry Temp	Wet Temp	Pressure	Avg Wind Speed (24 hrs)	Humidity	Sunshine (24 hrs)
0.0-0.1	0.4783	0	0	0	0	0.108	0	0.12
0.1-0.2	0.0566	0	0	0	0.111	0.0269	0	0
0.2-0.3	0.1607	0	0.063	0	0.086	0	0	0
0.3-0.4	0.0444	0.0458	0.106	0.058	0.087	0	0	0
0.4-0.5	0	0.128	0.006	0.093	0	0	0	0
0.5-0.6	0	0	0	0	0.016	0	0	0.015
0.6-0.7	0	0	0	0	0.017	0	0	0
0.7-0.8	0	0	0	0	0.054	0	0	0
0.8-0.9	0	0	0	0	0	0	0.0367	0
0.9-1	0	0	0	0	0	0	0.1679	0

METHODOLOGY

The values for all the parameters were normalized so that all the values belonged to a common scale by using the equation:

$$X_{norm} = \frac{X - X_{min}}{X_{max} - X_{\min}} \quad \text{..... (1)}$$

where X_{norm} gives the normalized value between 0 to 1 for each record and X_{min} and X_{max} are the minimum and maximum values for each parameter respectively. The values were then categorized into 10 equal groups. Further the probability of avalanche occurrence, p(A) for each group was calculated by the following equation:

$$p(A) = \frac{d_i}{D_i} \quad \text{..... (2)}$$

where d_i were the days when avalanche had occurred in the i^{th} range and D_i were the total days in the i^{th}range (Joshi and Ganju, 2009). The probability of Avalanche occurrence for the various parameters for Bahang region, is summarised in Table 2 and plotted in Figure 2.

RESULT AND DISCUSSION

The aim of the present study was to find the behaviour of different weather parameters in case of an Avalanche. The analysis of avalanche condition for Bahang region, mainly led to the fact that avalanche activity is not a frequently happening natural disaster in Bahang. As a result, it is necessary to have accurate predictions of avalanche activity, so that proper warning can be given to people staying in the surrounding region and necessary precautions can be taken by them to protect them from exposure from an avalanche. The avalanche influencing conditions for each parameter are given as follows:

Present study reveals that a maximum temperature of 0°C to 2.8°C has a major impact on occurrence of avalanche. In fact, almost 40% of avalanches have occurred in the said temperature range. The rest of the avalanche activity was found between the range of 2.8°C to 11.2°C. Hence, if the maximum temperature exceeds 11.2°C, the chances of avalanche activity are slim. A major avalanche activity was found when minimum temperature was between the range -0.9°C to 1°C. The avalanche activity was almost 77%, when the minimum temperature was between the said range. The remaining 20% avalanches have occurred when the minimum temperature had fallen between -2.8°C to -0.9°C.

For dry temperatures, 66% avalanche had occurred when the dry temperature was between 0.05°C to 2.4°C, whereas almost 70% of avalanches happened when the wet temperature was between 0.3°C to 2.25°C. In case of dry temperatures, almost 27% avalanches had occurred when the dry temperature was in the range of -2.3°C to 0.05°C. However, for wet temperature same percentage of avalanche had occurred in the range of -1.65°C to 0.3°C.

Though the maximum number of avalanches have occurred in the range of 794.4 mb to 796.2 mb with regards to pressure, it can be seen from the results no particular range of pressure has a clear effect on the avalanche occurrence. This can be seen as the avalanche activity is fairly divided between the pressure range from 790.8 mb to 803.4 mb. Further this is also seen from the probabilities of avalanche occurrence, where six out of ten ranges have shown an avalanche probability in the range of 0.01 to 0.1. In case of wind speed that had been averaged over 24 hrs, around 70% avalanches have occurred when the total average wind speed over a full day is less than 1.46 kmph. In fact, no avalanche activity is seen if the average wind speed is above 2.93 kmph.

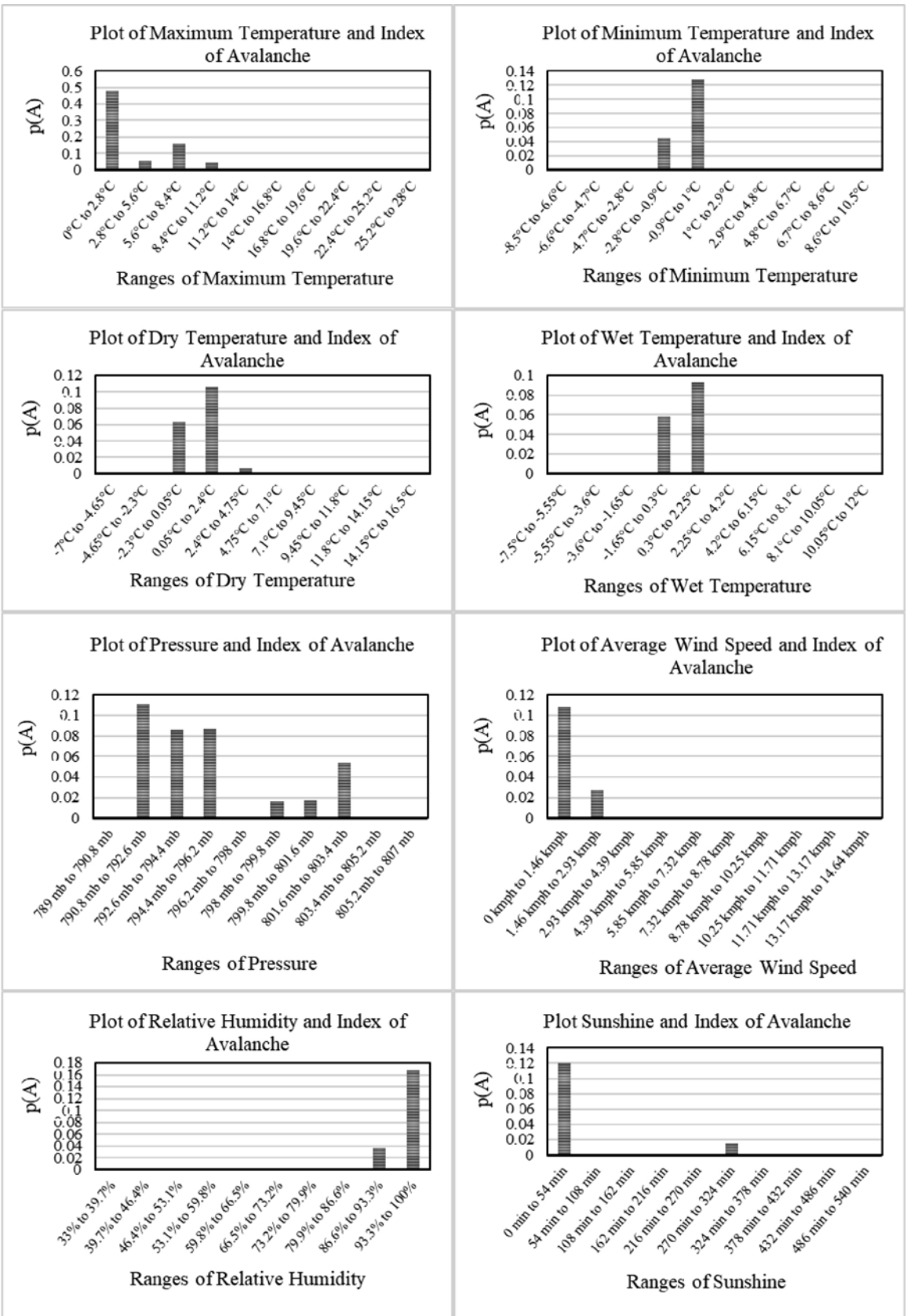

Figure 2. Probability of avalanche occurrence for the various parameters for Bahang region of Manali (Himachal Pradesh)

For humidity, it was observed that the avalanche normally occurs when the amount of water vapour present in the air is on a higher side. The maximum number of avalanches were observed when the humidity was more than 93.3%. The rest of the avalanches have occurred when the humidity was more than 86.6%. Similarly, the results show that less the amount of sunshine in 24 hrs, higher is the probability of avalanche occurrence as almost 96% avalanches have occurred when the sunshine has been less than 54 mins.

Hence, overall it can be seen that rate of avalanche occurrence is high for low ranges of maximum temperature, average of wind speed over 24 hours and amount of sunshine for a full day. Similarly, for minimum temperature, dry temperature and wet temperature, avalanches are observed in the intermediate range of considered parameter. Likewise, avalanches are mainly observed when the humidity present in the atmosphere is high. Pressure does not show any major influence on the formation of avalanche for the Bahang region of Manali.

CONCLUSION

The analysis of the various weather parameters for Bahang region has been presented in the current study. The range for each parameter were found which had led to avalanche and the major conditions that had influence on the avalanche activity. By observing the results, the effect of meteorological parameters on avalanche occurrence was observed and the avalanche prone ranges were obtained for all the weather parameters. This study can help us to understand the climatic condition for Bahang region of Manali and thus could be used to create an avalanche prediction model for the said region.

ACKNOWLEDGEMENTS

The Authors are thankful to Director, SASE (Snow Avalanche Study Establishment) for providing us with the snow and meteorological data for Bahang, Manali for our research study purpose. We would also like to thank Dr. Amreek Singh for kind support.

Compliance with Ethical Standards

The authors declare that they have no conflict of interest and adhere to copy right norms.

REFERENCES

Ganju, A. and Singh, A., 2004. A new approach to avalanche forecasting and disaster management for Western Himalaya. World congress on Natural Disaster Mitigation, 19-21 February 2004.

Gusain, H.S., Mishra, V.D. and Bhutiyani, M.R., 2014. Winter temperature and snowfall trends in the cryospheric region of north-west Himalaya. Mausam, 65(3), 425-432.

International Association of Hydrological Sciences. International Commission on Snow and Ice, 1981. Avalanche atlas; illustrated international avalanche classification. UNESCO, Paris, France: UNESCO.

Joshi, J.C. and Ganju, A., 2009. Analysis of maximum and minimum temperature in view of avalanche activities over north-west Himalayas. Mausam, 60(3), 368-371.

PBS, 2011. The Himalayas, Himalayas Facts, Nature, http://www.pbs.org/wnet/nature/the-himalayas-himalayas-facts/6341/

Schweizer, J., Jamieson, J.B. and Schneebeli, M., 2003. Snow avalanche formation. Rev. Geophy., 41(4).

Schweizer, J., Bartelt, P. and Herwijnen, A.V., 2015. Snow avalanches. In: Snow and Ice-related hazards, risks, and disasters, Elsevier, 395-436.

Sharma, S. and Ganju, A., 2000. Complexities of avalanche forecasting in Western Himalaya—an overview. Cold regions science and technology, 31(2), 95-102.

Sharma, S.S., 2000. An overview of snow and avalanche research in Indian Himalaya, Proceedings of the 2000 Int. Snow Sci. Workshop, October 1-6, Big Sky, Montana 558-565.

Stull, R., 2011. Wet-Bulb Temperature from relative humidity and air temperature, J. Appl. Meteorol. and Climate, 50(11), 2267-2269.

Ya-feng, S., Tze-chu, H., Pen-hsing, C. and Chi-chun, L., 1980. Distribution, features and variations of glaciers in China. World glacier inventory, IAHS-AISH, Publication no. 126, pp: 111-116.

Received on: 12.2.18; Revised on: 4.6.18; Accepted on: 11.6.18

ANNOUNCEMENT

of

55th Annual Convention

on

"CHANGING WATER CYCLE AND WATER RESOURCES"

December 5-7, 2018

at
Rabindranath Tagore University (RNTU)
Madhya Pradesh, Bhopal

Honorary Secretary
Indian Geophysical Union
CSIR-NGRI Campus, Uppal Road
Hyderabad- 500007, India
Email: igu123@gmail.com

ANNOUNCEMENT FOR IGU CONVENTION - 2018

Abstracts are requested for the 55th Annual Convention of IGU to be held at Rabindranath Tagore University, Bhopal during December 5-7, 2018. Nominations (hard and soft copies) for the following Five Award/Prize/Medal of IGU are invited in the prescribed proforma (available at www.iguonline.in) so as to reach the IGU office on or before **31-8-2018**. Nominator must be a member of IGU and should be past recipients, fellows or executive council members of IGU or any distinguished Earth Scientist/Professor

IGU-Hari Narain Lifetime Achievement Award to an eminent Senior Scientist for exceptional contribution to the causes of Indian Earth Sciences.

Decennial Award to a Senior Scientist for outstanding contribution in establishing a school of Earth Sciences in India.

IGU Krishnan Medal to a Young Scientist (below 40 yrs. of age as on 31-01-2018) for significant contribution to Indian Earth Sciences.

IGU-Anni Talwani Memorial Prize to meritorious Scientist (below 60 yrs as on 31-01-2018) for outstanding contribution to Earth Sciences covering land and/or offshore of India.

IGU-JG Negi Young Scientist Award to a Geophysicist/Geologist whose age does not exceed 35 years (as on 31-01-2018) for his/her outstanding contribution to Geosciences.

IGU Best Oral Presenter Award: Cash prizes are given to two Research Scholars (registered for Ph.D.) who are pursing quality research in the field of Geosciences under "Young Researcher Program" and selected based on the merit of full paper submitted to the Annual Convention of IGU.

Anni Talwani Memorial Grant for Women Researchers: Indian women researchers/students below 30 years of age (as on 31-01-2018) are encouraged to participate in the Annual Convention of IGU. The selection will be based on the merit of a full paper submitted to the Annual Convention, certified by the Head of the Department/ Organization. 3rd AC train fare, accommodation and registration fee waiver will be provided to four grantees.

Honorary Secretary,
Indian Geophysical Union
NGRI Campus, Uppal Road
Hyderabad- 500 007
Email: igu123@gmail.com

GUIDE FOR AUTHORS

The Journal of Indian Geophysical Union (J-IGU), published bimonthly by the Indian Geophysical Union (IGU), is an interdisciplinary journal from India that publishes high-quality research in earth sciences with special emphasis on the topics pertaining to the Indian subcontinent and the surrounding Indian Ocean region. The journal covers several scientific disciplines related to the Earth sciences such as solid Earth geophysics, geology and geochemistry, apart from marine, atmosphere, space and planetary sciences. J-IGU welcomes contributions under the following categories:

- Research papers and short notes reporting new findings.
- Review articles providing comprehensive overview of a significant research field.

In addition, J-IGU also welcomes short communications, after communications and report on scientific activity, book reviews, news and views, etc.

The manuscript should be submitted electronically as a single word format (.doc file) including the main text, figures, tables, and any other supplementary information along with the signed "Declaration Letter". The manuscript should be submitted by email (jigu1963@gmail.com) to the Chief Editor.

After acceptance of the manuscript the corresponding author would be required to submit all source files (text and Tables in word format) and figures in high resolution standard (*.jpg, *.tiff, *.bmp) format. These files may be submitted to J-IGU as a single *.zip file along with the "Copyright Transfer Statement".

IMPORTANT INFORMATION

Ethics in publishing
J-IGU is committed to ensuring ethics in publication and takes a serious view of plagiarism including self-plagiarism in manuscripts submitted to the journal. Authors are advised to ensure ethical values by submitting only their original work and due acknowledgement to the work of others used in the manuscript. Authors must also refrain from submitting the same manuscript to more than one journal concurrently, or publish the same piece of research work in more than one journal, which is unethical and unacceptable. Editor of J-IGU is committed to make every reasonable effort to investigate any allegations of plagiarism brought to his attention, as well as instances that come up during the peer review process and has full authority to retract any plagiarized publication from the journal and take appropriate action against such authors if it is proven that such a misconduct was intentional.

Similarly, Editor and Reviewers are also expected to follow ethical norms of publishing by ensuring that they don't use any unpublished information, communicated to them for editorial or review purpose, in their own research without the explicit written consent of the author. They are also expected to keep manuscript/ data/ observations/ any other information related to the peer review confidential to protect the interest of the authors. Reviewers should refrain from reviewing the manuscripts in which they have conflicts of interest resulting from competitive, collaborative, or other relationships or connections with any of the authors, companies, or institutions connected to the manuscript.

Conflict of interest
All authors are requested to disclose any actual or potential conflict of interest including any financial, personal or other relationships with other people or organizations within three years of beginning the submitted work that could inappropriately influence, or be perceived to influence, their work.

Submission declaration
Submission of a manuscript implies that the work has not been published previously and it is not under consideration for publication elsewhere, and that if accepted it will not be published elsewhere in the same or any other form, in English or in any other language, without the written consent of the publisher. It also implies that the authors have taken necessary approval from the competent authority of the institute/organization where the work was carried out.

Copyright
After acceptance of the manuscript the corresponding author would be required to sign and submit the "Copyright Transfer Statement".

MANUSCRIPT PREPARATION

The corresponding author should be identified (include E-mail address, Phone/Mobile number). Full affiliation and postal address must be given for all co-authors.

Abstract:
An abstract of not more than 300 words must be included.

Text:
The manuscript should be structured to include a front page containing the title, Author(s) name, affiliation and address of the institute, where the work was carried out, a short title, and 5-to-6 Key words. Author(s) present address, if different from the above mentioned address, may be given in the footnote. The corresponding author should be identified with an asterisk and his/her email ID should be provided. This page should be followed by the main text consisting of Abstract, Introduction, Methods/ Techniques/ Area description, Results, Discussion, Conclusions, Acknowledgements, and References. Tables and Figures with captions should be inserted at the end of main text. It should not be inserted in the body of the text.

Figures/ Illustrations:
All figures should be provided in camera-ready form, suitable for reproduction (which may include reduction) without retouching. Figures in high-resolution (at least 300 dpi) standard formats (*.jpg, *.tiff, *.bmp) are acceptable. Figures should be numbered according to their sequence in the text. References should be made in the text to each figure. Each figure should have a suitable caption.

Tables:
Authors should take note of the limitations set by the size and layout of the journal. Table should not exceed the printed area of the page. They should be typed on separate sheets and details about the tables should be given in the text. Heading should be brief. Large tables should be avoided and may be provided as supplementary information, if required.

Equations:
Equations should be numbered sequentially with Arabic numerals and cited in the text. Subscripts and Superscripts should be set off clearly. Equation writing software that presents each equation as an object in MS Word will be accepted. Style and convention adopted for the equations should be uniform throughout the paper.

References:
All references to publications cited in the main text should be presented as a list of references in order following the text and all references in the list must be cited in the text. References should be arranged chronologically, in the text. The list of references should be arranged alphabetically at the end of the paper.

References should be given in the following form:
Kaila, K.L., Reddy P.R., Mall D.M., Venkateswarlu, N., Krishna V.G. and Prasad, A.S.S.S.R.S., 1992. Crustal structure of the west Bengal Basin from deep seismic sounding investigations. Geophys. J. Int., 111,45-66.

REVIEW PROCESS:

All manuscripts submitted to the journal are peer-reviewed. It is advisable to send the contact details of 4 potential reviewers along with the manuscript to expedite the review process. Editor has the option to select reviewers from the list or choose different reviewers. The review process usually takes about 3 months. All enquiries regarding the manuscript may be addressed to the Editor.

GALLEY PROOF:

Technical editing of manuscripts is performed by the editorial board. The author is asked to check the galley proof for typographical errors and to answer queries from the editor. Authors are requested to return the corrected proof within two days of its receipt to ensure uninterrupted processing. The editor will not accept new material in proof unless permission from the editorial board has been obtained for the addition of a "note added in proof". Authors are liable for the cost of excessive alterations to galley proof.

PUBLICATION CHARGES:

There are no page charges for publication and printing charges for b/w figures. However, in view of substantial cost involved in printing of color figures, author will be charged for printing of pages containing color figures @ Rs. 2,500/- per page. The charges may be revised at any time based on cost of printing and production. Author will receive an estimate/ invoice of the color figures reproduction cost along with the galley proof. It is the responsibility of the author to remit the color figures reproduction cost within one month of the receipt of the estimate/invoice.

The corresponding author will receive a soft copy (pdf format) of his/her published article. Should the author desire to purchase reprints of his/her publication, he/she must send the duly signed Reprint Order Form (accompanies the galley proof and contains price details) along with the corrected galley proof to the Editor. The reprint charges must be paid within one month of sending the Reprint Order Form.

Any payment related to printing of color figures and/or purchase of reprints should be made in the form of a Demand Draft in the name of Treasurer, Indian Geophysical Union, payable at Hyderabad.

You may download the pdf file from: http://www.j-igu.in/IGU-Guide-forAuthors.pdf